UNIVERSITA' DEGLI STUDI DI PADOVA

Facoltà di Agraria

Corso di Laurea in Scienze Forestali e Ambientali

LARGE SCALE CHARACTERIZATION OF ARTIFICIAL DRAINAGE NETWORKS: NEW OPPORTUNITIES FROM HIGH RESOLUTION TOPOGRAPHY

Relatore:
Prof. Paolo Tarolli
Correlatore:
Dott.ssa Giulia Sofia

Laureando:
Massimo Prosdocimi
Matricola n.
1014948

Anno accademico 2011/2012

RIASSUNTO

Le recenti alluvioni che hanno colpito la pianura alluvionale veneta nell'autunno del 2010, hanno causato ingenti danni sia a persone che a infrastrutture. Questi disastri hanno spinto i politici e i responsabili della gestione territoriale, a considerare con maggiore attenzione il concetto di mitigazione del rischio idrogeologico a livello regionale. In questa prospettiva, il seguente lavoro vorrebbe dimostrare come una tecnologia per il remote-sensing, quale il laser scanner montato su aeroplano (LiDAR) e l'ampia diffusione di sistemi informativi geografici (GIS), siano in grado di facilitare la raccolta e gestione di dati idrogeomorfologici ad una scala regionale, offrendo in questo modo nuove opportunità nel campo dell'idrologica, geomorfologia e della gestione integrata di bacini idrografici. Questa tesi si focalizza su un approccio semi automatico basato su dati topografici ad alta risoluzione (modelli digitali del terreno derivanti da LiDAR), sviluppato da Cazorzi et al. (2012), per identificare il reticolo idrografico minore in un tipico ambiente agrario. Poiché ci si aspetta che il reticolo idrografico minore influenzi la risposta idrologica durante gli eventi alluvionali, la sua localizzazione e la quantificazione della capacità di invaso che lo caratterizza, sono aspetti fondamentali per la gestione integrata dei bacini. Secondo tale metodologia, è possibile stimare anche alcune statistiche relative al reticolo quali la lunghezza, larghezza dei canali, la densità di drenaggio e la capacità di invaso. Un altro obiettivo del seguente lavoro è quello di analizzare gli effetti della capacità di invaso del reticolo idrografico minore sul deflusso superficiale prodotto dall' importante evento di precipitazione verificatosi tra Ottobre e Novembre 2010 in Veneto. Questo tipo di analisi viene eseguita per valutare la presenza di aree che potrebbero essere a rischio di alluvione già solo semplicemente per il deflusso prodotto direttamente dall'apporto meteorico. L'obiettivo di quest'ultima valutazione è in primis quello di testare l'operativa della metodologia proposta a scala regionale, e poi di verificare, se i cambiamenti di uso del suolo (considerando l'evoluzione durante gli ultimi anni), possano influenzare il deflusso superficiale e quindi, l'effetto attenuante operato dal reticolo idrografico minore nei confronti delle alluvioni. Questa analisi preliminare, che richiede sicuramente un approfondimento, possibile solo se si hanno a disposizione dataset storici più ampi, può essere uno strumento utile ai fini gestionali specialmente in aree soggette ad alluvioni.

ABSTRACT

The recent major flood affecting the Veneto floodplain in autumn 2010, caused significant damages to both people and infrastructures. These disasters have driven policy makers and land managers to a greater concern for the hydrogeological safety of regional territory. In this perspective, this work would like to demonstrate how a remote sensing technologies such as airborne LiDAR, and the wide distribution of geographical information softwares (GIS), are able to facilitate the collection of hydrogeomorphological data at regional scale, offering new opportunities and advances in hydrology, geomorphology and integrated watershed management. In detail, this thesis focuses on a semi-automatic approach based on high-resolution topographic data (LiDAR-derived DTMs), developed by Cazorzi et al. (2012) to identify the minor drainage network system in a typical agrarian landscape. Since the minor drainage network is expected to affect hydrological response during floods, its recognition and the quantification of the water storage capacity within the channels are crucial for watershed planning. According to such semi-automatic approach, it is also possible to estimate some network statistics such as channels length, width, drainage density and storage capacity. Another purpose of this work is also to analyze the effects of drainage network storage capacity on the direct surface runoff, produced by the main rainfall event happened between October and November 2010 in Veneto. This, in order to evaluate the presence of areas that may be already risky simply for the runoff directly produced by the local rainfall. The purpose of the latter evaluation firstly, is to test the suitability of the methodology, and then to notice if changes in land use (considering the evolution during years) might affect the direct runoff and therefore, the attenuating effect performed by the minor drainage system towards floods. This preliminary analysis, that absolutely has to be enlarged with a wider historical dataset, can be a useful tool for management purposes especially in flood prone areas.

INDEX

1 INTRODUCTION

1.1 ANTHRPOCENE, ANTHROPOGENIC LANDSCAPE AND HYDROGEOLOGICAL RISK

The Anthropocene defines Earth's most recent geologic time period as being human-influenced, or anthropogenic, based on global evidence that atmospheric, geologic, hydrologic, biospheric and other earth system processes are now altered by humans (Ellis E. 2008). The word combines the root "anthropo", meaning "human" with the root "-cene", the standard suffix for "epoch" in geologic time. The term was proposed in 2000 by Nobel Prize winning scientist Paul Crutzen. The word quickly entered the scientific literature as a vivid expression of the degree of environmental change on Earth caused by humans, and it is currently under discussion as a potential formal unit of the geological time scale (Zalasiewicz *et al*., 2008). Geologic epochs are distinguished from one another based on geological observations, such as the composition of sediment layers and other tools of paleoclimatology. To justify the identification of a new Anthropocene epoch, it must therefore be demonstrated that evidence of anthropogenic global change, is present at such a level that it can be distinguished using geologic indicators (Ellis E. 2008).

The most commonly cited and readily measured global change associated with humans is the rise of greenhouse gases, especially carbon dioxide and methane, around the beginning of the Industrial Revolution, together with the associated rise in global temperatures and sea level caused by this global warming. Other key indicators include massive global increases in soil erosion caused by land clearing and soil tillage for agriculture, massive deforestation, and massive extinctions of species caused by hunting and the widespread destruction of natural habitats. The originator of the Anthropocene terminology, Paul Crutzen, favors the beginning of the Industrial Revolution as the starting point for the Anthropocene. Zalasiewicz *et al*. (2008) are in general agreement with Crutzen that the Anthropocene is best identified at the beginning of the Industrial Revolution, though they also propose the beginning of the nuclear era in the 1960s as a useful date.

A central point for any understanding of the long term relations between humans and their environment is how humans are conceptualized versus the rest of natural world. A recent and thought provoking contribution in the field of mapping global environments is the launching of the concept of *anthropogenic biomes* (Ellis & Rammankutty 1998). They argue that "human-dominated ecosystems now cover more of the Earth's land surface than do "wild"

ecosystems"; the conclusions is that nature is now embedded within human systems. It is therefore no longer possible to ignore the human influence that affects any kind of technical research or approach. Historically, biomes have been identified and mapped based on general differences in vegetation type associated with regional variations in climate (Udvardy 1975; Matthews 1983; Prentice *et al*., 1992; Olson *et al*., 2001; Bailey 2004). Now that humans have restructured the terrestrial biosphere, global patterns of species composition, land-surface hydrology and the biogeochemical cycles of carbon, nitrogen and phosphorus, have all been substantially altered (Matson *et al*., 1997; Vitousek *et al*., 1997; Foley *et al*., 2005). In this perspective, Ellis and Rammankutty (1998) have presented an alternate view of the terrestrial biosphere, based on an empirical analysis of global patterns of sustained direct human interaction with ecosystems, yielding a global map of "*anthropogenic biomes*" (Fig. 1.1).

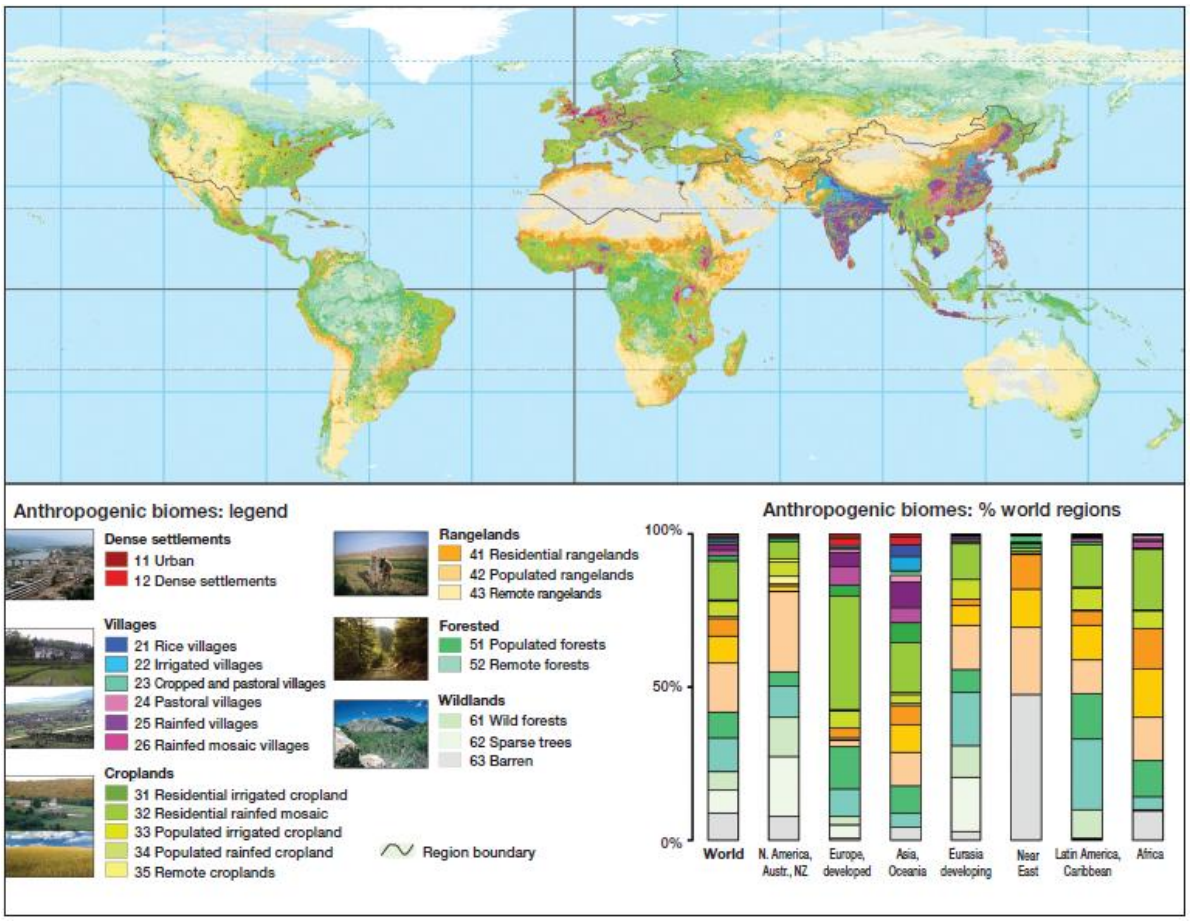

Fig. 1.1 Anthropogenic biomes: world map and regional areas. Biomes are organized into groups (Tab 1.1), and in order of population density. Map scale = 1:160000000 (Ellis and Ramankutty, 1998).

Table 1.1 Anthropogenic biome descriptions (Ellis and Ramankutty, 1998).

Group	Biome	Description
Dense settlements		*Dense settlements with substantial urban area*
11	Urban	Dense built environments with very high populations
12	Dense settlements	Dense mix of rural and urban populations, including both suburbs and villages
Villages		*Dense agricultural settlements*
21	Rice villages	Villages dominated by paddy rice
22	Irrigated villages	Villages dominated by irrigated crops
23	Cropped and pastoral villages	Villages with a mix of crops and pasture
24	Pastoral villages	Villages dominated by rangeland
25	Rainfed villages	Villages dominated by rainfed agriculture
26	Rainfed mosaic villages	Villages with a mix of trees and crops
Croplands		*Annual crops mixed with other land uses and land covers*
31	Residential irrigated cropland	Irrigated cropland with substantial human populations
32	Residential rainfed mosaic	Mix of trees and rainfed cropland with substantial human populations
33	Populated irrigated cropland	Irrigated cropland with minor human populations
34	Populated rainfed cropland	Rainfed cropland with minor human populations
35	Remote croplands	Cropland with inconsequential human populations
Rangeland		*Livestock grazing; minimal crops and forests*
41	Residential rangelands	Rangelands with substantial human populations
42	Populated rangelands	Rangelands with minor human populations
43	Remote rangelands	Rangelands with inconsequential human populations
Forested		*Forests with human populations and agriculture*
51	Populated forests	Forests with minor human populations
52	Remote forests	Forests with inconsequential human populations
Wildlands		*Land without human populations or agriculture*
61	Wild forests	High tree cover, mostly boreal and tropical forests
62	Sparse trees	Low tree cover, mostly cold and arid lands
63	Barren	No tree cover, mostly deserts and frozen land

When viewed globally (Fig. 1.1), anthropogenic biomes clearly dominate the terrestrial biosphere, covering more than three quarters of Earth's ice-free land and incorporating nearly 90% of terrestrial NPP (Net Primary Productivity) and 80% of global tree cover.

Connected to the Anthropocene and the development of anthropogenic biomes, there is also the development of the concept of *engineered landscape* (Lansing, 1991; Earle and Doyel, 2008). This concept, focuses on the specific type of domesticated landscape, characterized by the presence of facilities such as terraces, canals, dams and reservoirs for agriculture, but also roads, buildings, monuments, villages and cities. It is therefore almost synonymous with *the built environment* which David Harvey sees as a "humanly created resource system, comprising use values embedded in the physical landscape" (Harvey 1982). The concept of "domestication of landscapes", as proposed by Clark Erickson (DATA?), refers to the intentional and unintentional activities that transform environments into productive landscapes.

In this perspective, population density is a useful indicator of the form and intensity of these interactions, as increasing population have long been considered both a cause and a consequence of ecosystem modification to produce food and other necessities (Boserup 1965, 1981; Smil 1991; Netting 1993). Great differences in population density help to distinguish situations in which humans may be considered merely agents of ecosystem transformation, from situations in which human populations have grown dense enough to cause significant and, sometimes permanent, changes in the ecosystem processes (Ellis and Ramankutty, 1998). According to the same authors, furthermore, human-ecosystem interactions may be categorized into four classes, based on major differences in population density: high population density ("dense", >100 persons per km^2), substantial population intensity ("residential", 10 to 100 persons per km^2), minor population ("populated", 1 to 10 persons per km^2), and inconsequential population ("remote", <1 person per km^2). Considering the Italian situation, it should be pointed out that our Country average population density is about 200 inhabitants/ km^2; this makes Italy one of the highest populous countries, if compared to the European mean (Ue27 in Fig. 1.2) of 114 inhabitants per km^2 (Eurostat demography – regional data, 2010) (Fig. 1.2).

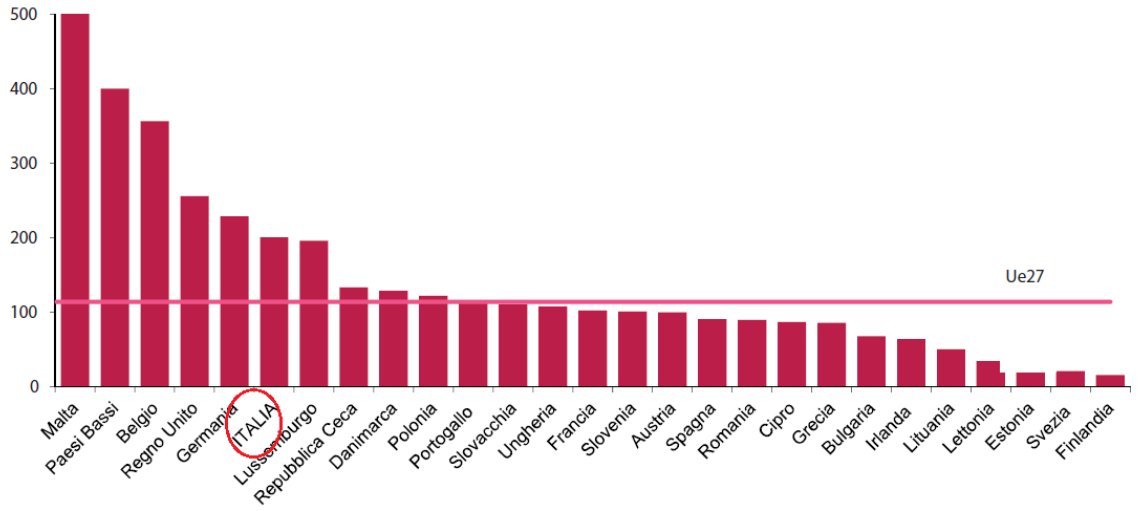

Fig. 1.2 Human population density in the European Union countries in 2010 (inhabitants per Km^2). The pink line (Ue27) represents the European average density. (Eurostat, Demography – Regional data, 2010).

Despite the fact that dangerous events (i.e. landslides and floods) that might occur are generally driven by geomorphological and climatic settings, over the last 50 years there has been a growing body of evidence pointing to the effect of human behavior on the global natural environment, and on the possibility that certain types of natural disasters, such as floods, may be increasing as a direct consequence of human activity. Floods and landslides

are natural events that have always been occurring, but the increasing in population number and human pressure led to two main consequences: i) the modification in the hydrologic regimes, and ii) an increasing of the elements at risk, and therefore an increasing of damages.

Numerous authors investigated the human contribution to change in the hydrologic regimes. Two studies, made by Min *et al*. and Pall *et al*. in 2011, conclude that climate warming is already causing extreme weather events that affect the lives of millions. These researchers directly links rising greenhouse-gas levels with the growing intensity of rain and snow in the Northern Hemisphere, and the increased risk of flooding in the United Kingdom. The latter study states that anthropogenic climate change may have almost doubled the risk of the extremely wet weather that caused the floods. The rise in extreme precipitation in some Northern Hemisphere areas, has been recognized for more than a decade (Oppenheimer, 2011). In addition, an earlier study conducted by Scott *et al*. in 2004, found, with a confidence level > 90%, that global warming has at least doubled the likelihood of extreme events such as the 2003 European heatwave, which has been probably the hottest in Europe since at least AD 1540.

Together with the increasing of events, there is also to consider the increasing of exposure, that contributes to the increasing of risk and damages. Concerning this, a significative image showing the population density together with flood occurrence, is reported in Fig. 1.3.

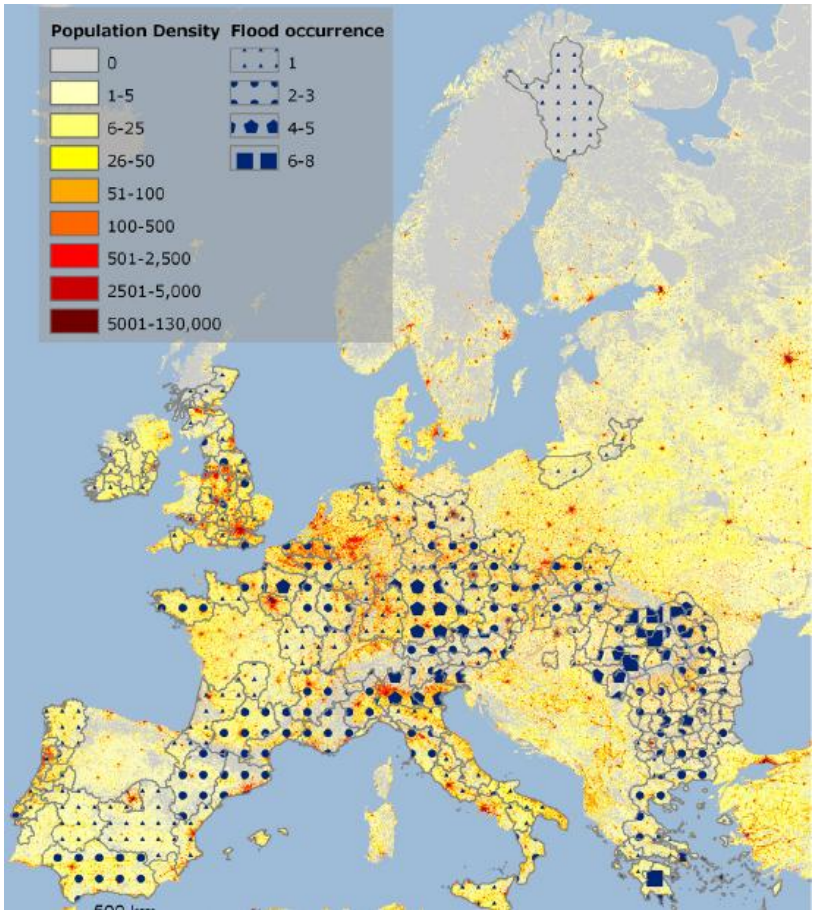

Fig. 1.3 Flood occurrence in the EU27 from 2000 to 2009 on administrative boundary level and population density. Sources: EM-DAT, LandScan ("Health impacts of floods in Europe" – A MICRODIS Report, November 2010).

In Europe, several regions with high-income, have areas with a high population density and have been flooded more than once. In the lower-income countries, population density in general is lower, especially in the most often flooded regions in Romania and Greece. Focusing on the Italian situation, it is possible to notice that areas with high population density are mainly located in the Northern part, in correspondence of the Po Valley, and along the shorelines. However, the floodplain areas are the ones more affected by floods event, and the Veneto Region is a clear example of such critical situation.

Focusing on the increasing of exposed elements, floods and landslides are events of annual occurrence in many locations. They become 'disasters' when they are of unusual proportion, occur in unusual places, or they occur unexpectedly, thus exceeding the ability of the affected community or society to cope with the events. It is in fact important to remember that the severity of flood disasters, for example, is not solely linked to the intensity of the natural hazard, but also to many human-driven factors that contribute to increasing the risk for flooding and magnifying the impacts, such as soil degradation, deforestation, urbanization,

and poor urban drainage. UNESCO defines a disaster as "*an event, concentrated in time and space, in which a community undergoes severe danger and incurs such losses to its members, their property and belongings that the social structure is disrupted and the fulfillment of all or some of the essential functions of the society is prevented*" (United Nations Disaster Relief Organization - UNDRO). Natural disasters are greatly increasing and nowadays, there is also a well-visible increase in the number of hazardous events reported due to significant improvements in information access, but also due to population growth (Centre for Research on the Epidemiology of Disasters – CRED, 2005). According to what reported in the "Annual Disaster Statistical Review", in 2011, 332 natural disasters were registered, less than the average annual disaster frequency observed from 2001 to 2020 (384). However, the human and economic impacts of the disasters in 2011 were massive. Natural disasters killed a total of 30 773 people and caused 244.7 million of victims worldwide (Fig. 1.4).

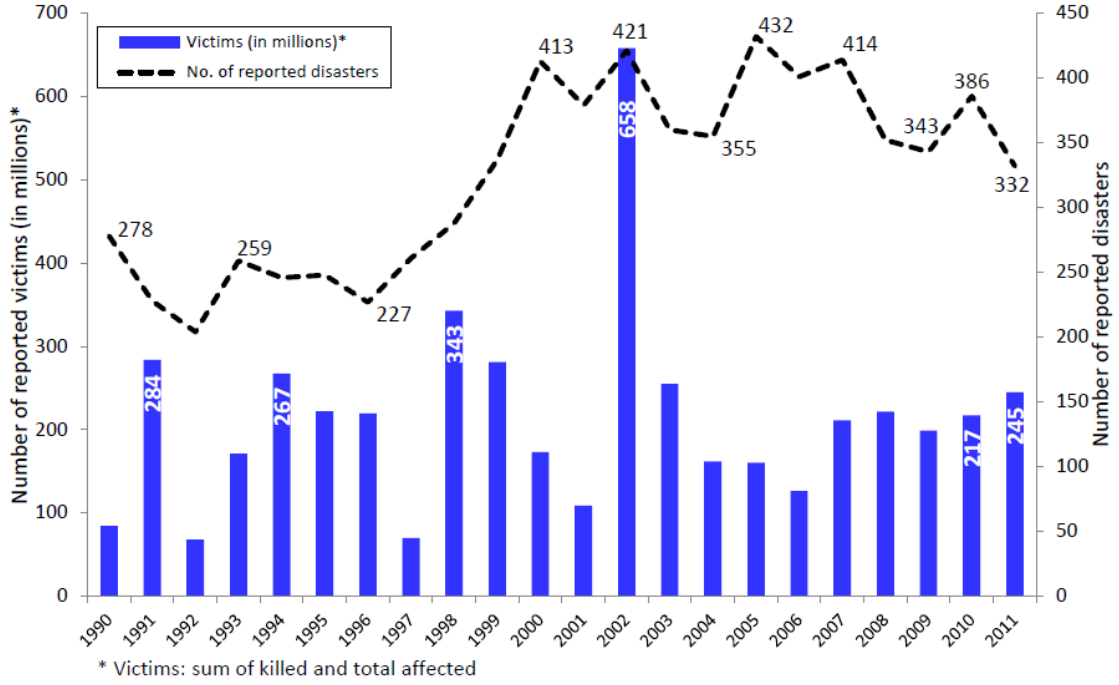

Fig. 1.4 Trends in occurrence and victims, considered as the sum of killed and total affected, from 1990 to 2011 (Annual Disaster Statistical Review 2011 – The number and trends).

Although some of the increase in reported number of natural disasters is undoubtedly the result of better data collection, particularly in comparison with the earlier years of the twentieth century, there does seem to be evidence that the number and severity of hydrometeorological events are increasing, and among these, floods more than the other ones (Fig. 1.5).

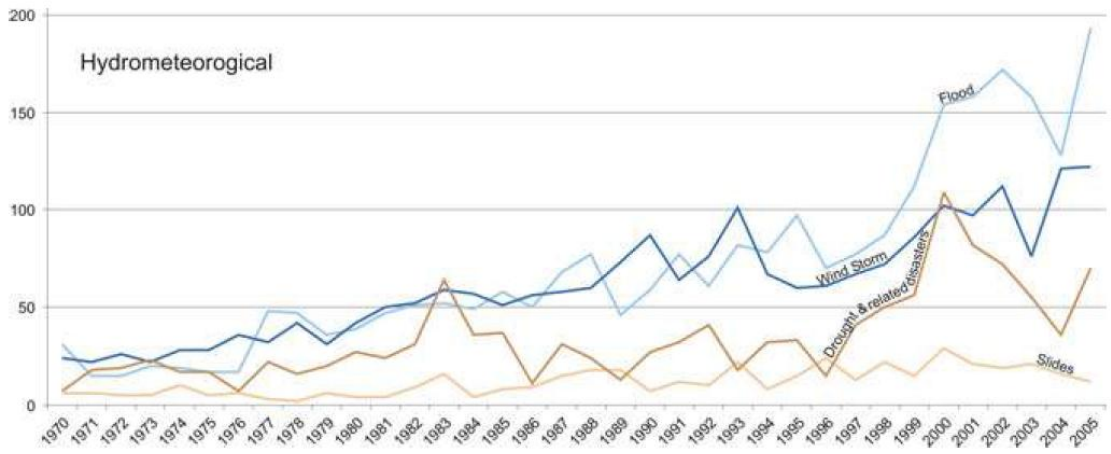

Fig. 1.5 Increase of Hydrometeorological events, especially floods registered in the span of time 1970-2005 (Centre for Research on the Epidemiology of Disasters - CRED, 2005).

Still according to the "Annual Disaster Statistical Review", floods result to be the most common natural disasters in the top ten rank of natural disasters by number of victims in 2011 (Tab. 1.2).

Table 1.2 Top 10 natural disasters by number of victims (Annual Disaster Statistical Review 2011 – The numbers and trends).

Event	Country	Victims (in millions)
Flood, June	China P Rep	67.9
Drought, January-May	China P Rep	35.0
Storm, April	China P Rep	22.0
Flood, September	China P Rep	20.0
Drought	Burundi, Djibouti, Ethiopia, Kenya, Somalia, Uganda*	14.0
Flood, August-December	Thailand	9.5
Flood, August-October	India	5.5
Flood, August-November	Pakistan	5.4
Cold Wave, January	China P Rep	4.0
Flood, August-September	China P Rep	3.8
	Total	**187.2**

*Ethiopia (4.8 million), Kenya (4.3 million), Somalia (4.0 million), Uganda (0.7 million), Djibouti (0.2 million), Burundi (0).

Making a comparison between the natural disaster impacts occurred in 2011 and those ones in 2001-2010 time period, by disaster sub-group (climatological, geophysical, hydrological and meteorological), emerges that the lower number of reported natural disasters in 2011 was mainly due to a smaller number of hydrological and meteorological disasters (Fig. 1.6).

However, the higher number of victims in 2011 is explained by the larger impact from hydrological disasters compared to the decade's average.

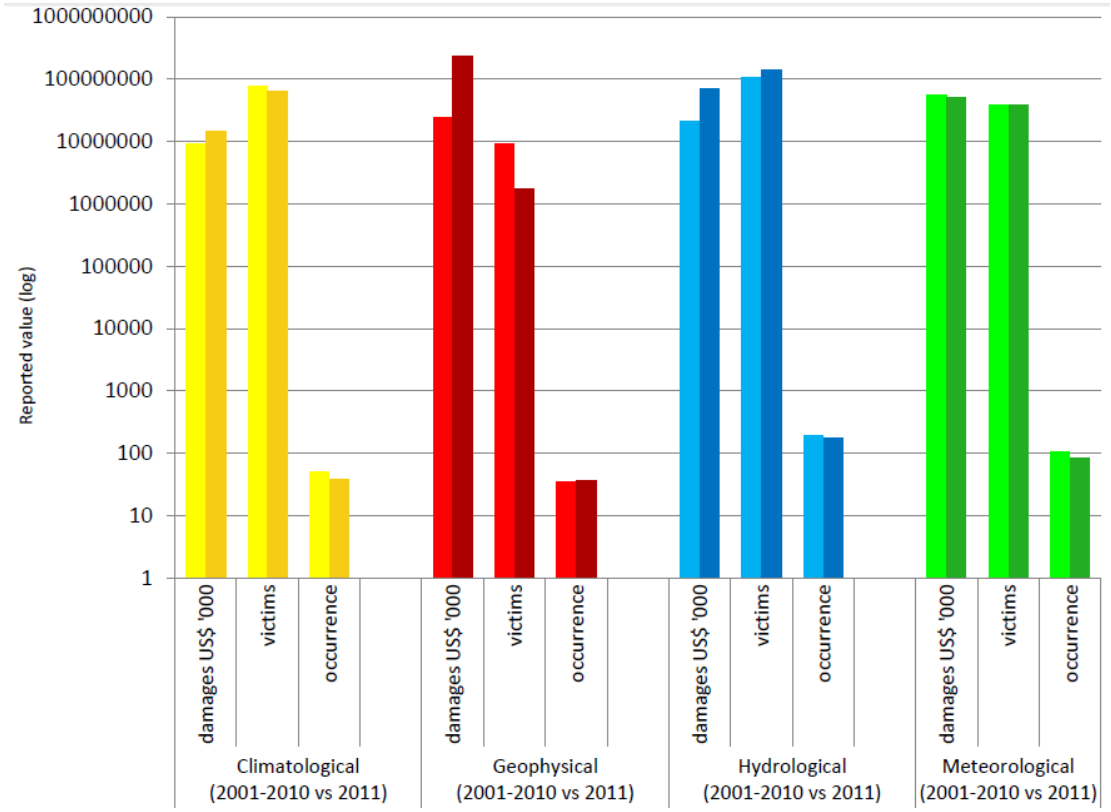

Fig. 1.6 Natural disaster impacts by disaster sub-group: 2011 versus 2001-2010 annual average (Annual Disaster Statistical Review 2011- The numbers and trends).

Focusing on our Country, Italy spends each year more than 1 billion of Euro to repair damages caused by landslides and floods, and it is considered the highest hydrogeological-risk country of Europe, and the fourth of the world after China, Japan and Central-Southern America (C.N.G., 2010).

According to the "*Ministero dell'Ambiente e della Tutela del territorio e del Mare*", (Ministry of Environment and Territory of the Sea - METS) the national surface characterized by high hydrogeological risk is equal to 29 517 km^2 (about 10% of the whole surface), including 89 % of the municipalities, and of these areas at risk, 58.4 % is interested by risk caused by landslides and 41.6 % by floods (AA. VV., 2008a). According to the study conducted by the National Council of Geologists (C.N.G.) in 2010, about 6 million of people live in the 10% of the national surface characterized by high hydrogeological risk, and of this endangered population, about 19 % live in Campania, 14 % in Emilia Romagna and the rest are located in the three widest Italian Northern regions: Piedmont, Lombardia and Veneto. From the post-

World War II period up to now, the hydrological disasters have cost 213 billion of Euro, and 27 billion of Euro have been invested in the period from 1996 to 2008. The Ministry of Environment and Territory of the Sea, thanks to the work carried out by River Basin Authorities through the realization of Hydro-geological Structure Plans (PAI), has estimated a financial requirement of 40 billion of Euro to ensure hydrogeological safety over the whole national surface. Of this amount, 68 % would pertain to interventions in the twelve North Central regions, and the rest 32 % would be made available for the eight southern regions (C.N.G., 2010).

It is clear that floods and landslides are common phenomena in Italy and that, almost every year, they produce damages. Guzzetti *et al*., (2005) reported that in our Country, about 2580 floods and/or landslides happened and about 50 593 people died, were missing or were injured between 1279 and 2002 (Fig. 1.7). These data, anyway, suffered from the lacking of precision in the record of missing, homeless, evacuate or injured people in the historical database, therefore they probably underestimate the real numbers of casualties. A precise estimation about the number of the single landslide or flood events, anyway, is not easy: such events are common all over the national territory and sometimes they are triggered by the same large meteorological event at the same time over different locations.

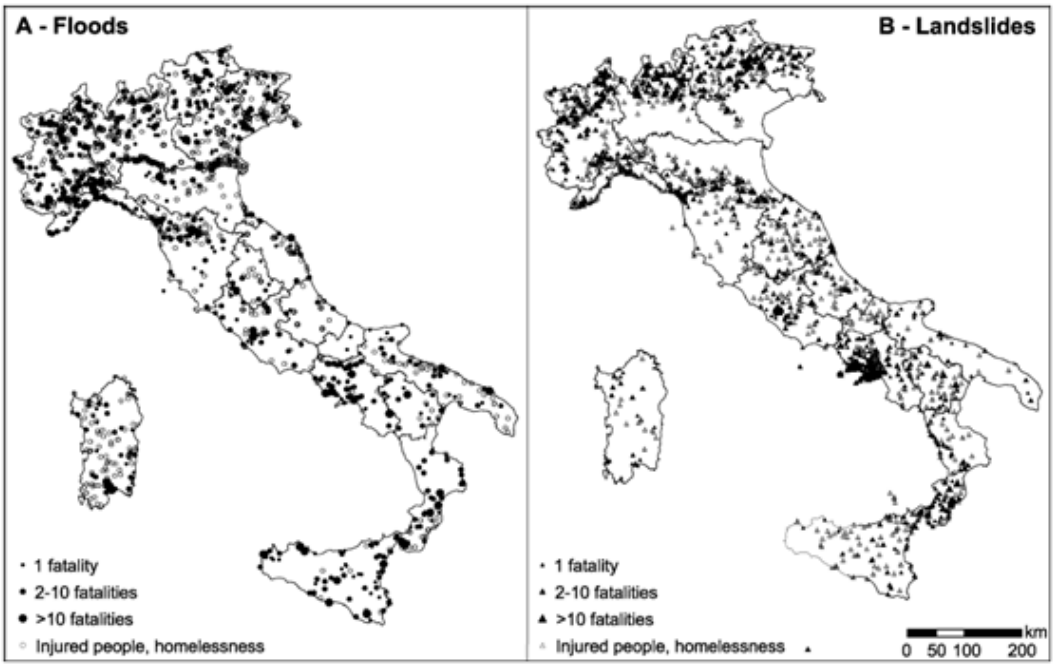

Fig. 1.7 Map showing the distribution of floods (circle) and landslides (triangle) with human consequences in Italy for the 1300 to 2002 period. The size of the symbol indicates the magnitude of the event (Guzzetti et al., 2005).

Guzzetti *et al*., (2005) also demonstrated how the three most catastrophic landslides and floods events in the 20th century, were all caused by or were associated with the presence (Vajont 1963) or the failure (Gleno 1923) of a dam or a man-made embankment (Stava 1985). These catastrophic events indicate the potentially destructive effect of artificial structures, and that poor planning in the design and management of man-made structures can result in numerous casualties. Harmful flood and landslide events were recorded for the 26.3 % of the Italian municipalities. Fatal events were more frequent in the Alpine regions of northern Italy. In southern Italy, fatal landslides were more numerous in Campania and particularly in the area between Naples and Salerno. Analysis of the seasonal distribution of harmful events has also been carried out and has revealed that landslide and flood fatalities were more numerous in the autumn. In addition, a quantitative estimate of flood and landslide risk to people in Italy has been attempted, and the individual risk through the calculation of mortality rates has been estimated. The results showed that, for the post-World War II period, the landslide mortality rate (0.15) was higher than the flood mortality rate (0.12) (Guzzetti *et al*., 2005).

Focusing on the last 50 years, some examples of disasters that occurred in our Country, can be mentioned: Polesine 1951, Florence 1966 (35 causalities), Genoa 1970, Piedmont 1994 (70 causalities), Versilia 1996 (14 causalities), Sarno 1998 (160 causalities), Soverato 2000 (12 causalities), Piedmont and Aosta Valley 2000 (25 causalities), Messina 2009 (35 causalities), and more recently Veneto 2010 and Marche 2011(Fig. 1.8).

This peculiar configuration, brought a series of laws and regulation to be applied and respected, to improve land management and protection (Box 1).

Fig. 1.8 Some floods occurred over the past years

THE REGULATORY FRAMEWORK

The victims and infrastructural damages caused by these events sped Italy up to enact laws to prevent, reduce and limit injuries. To make the hydrogeological risk prevention more efficient, the regulatory framework must be strengthened and right and feasible measures must be available. The consequences of these disasters in Italy become so significant to represent a really socio-economic issue, hence the attention must be shifted from a setting based on damage compensation to a real culture of prevention and prevision, focused on risk conditions detection.

The rules for the actions needed to guarantee the hydrogeological land planning, suitable to the safety of the population, the protection of the cultural heritage, the environment and human activities have been fixed by the Law for the "soil protection" in 1989 (*Legge quadro n. 183 del 18 maggio 1989*). These measures are still identified and coordinated within the *River Basin Plan* which encompasses a wide area, putting itself at a higher level than provincial and regional administrations planning. This *Plan* considers the *river basin* (or watershed) as the basic geographical unit for developing the proper land management in an integrated, multi-sectorial way and trough consultation. Hence, a watershed approach can be defined as an integrated framework for environmental and natural resources management that coordinates public and private efforts for decision making and planning. Watershed boundaries almost never follow administrative boundaries and that is why, modern planning methods require to seek the involvement of all the stakeholders in a given planning unit. Another significant innovation introduced by the above-mentioned Law is the institution of the *River Basin Authority*, an organization with planning and programming functions, which locates itself in an intermediate position between the national and regional levels.

As a consequence of the disasters occurred in 1998 and 2000 in Campania and Calabria regions, the *Sarno* Decree has been enacted. This Decree, after few months, turned out into a Law, and it aims to precisely spot the highest hydrogeological risk areas along all the country with the drafting of *Hydro-geological Structure Plans* (PAI). These PAI identify the principal structural and non-structural measures, evaluate their costs and plan their realizations according to a priority order, to make the high-risk areas as much safe as possible.

Shifting from the national to the European scale, two directives require great attention and must be mentioned: the "*Water Framework Directive 2000/60/EC*" and "*Floods Directive 2007/60/EC*".

The *Water Framework Directive* is a legal framework to protect and restore clean water across Europe and ensure its long-term, sustainable use. Its approach for water management is based on the *river basins*, and sets specific deadlines for Member States to protect aquatic ecosystems. The Directive addresses all waters: inland surface waters, transitional waters, coastal waters and groundwater. It precisely gives definitions of many terms and it introduces the main unit for management of river basins: the "*River Basin District*", made up of one or more neighboring river basins together with their associated groundwaters and coastal waters. Legislation focuses also on the need for international collaboration for certain river basins which cross Member State boundaries and specifies three planning cycles of six years each up to the year 2027.

On the other hand, the *Floods Directive* has the purpose to establish a framework for the assessment and management of flood risk, aiming at the reduction of the adverse consequences to human health, the environment, cultural heritage and economic activity associated with floods in the Community. The Directive covers all type of floods, both along rivers and in coastal areas; there are also other risks, such as urban floods and sewer floods, which need to be take into account as well. The main requirements under the Directive are:

- Preliminary flood risk assessment (Art. 4,5);
- Flood hazard maps and flood risk maps (Art. 6);
- Flood risk management plan (Art. 7,8, Art. 10 on public consultation and Annex).

Flood hazard maps cover the geographical areas which could be flooded according to three probability scenarios (low, medium, high); the maps must show the flood extent, water depths and flow velocity.

Flood risk maps show the potential adverse consequences associated with the probability flood scenarios and are expressed in terms of the indicative number of inhabitants potentially affected, type of economic activity within the area potentially affected and other information which Member States consider useful.

Flood risk management (FRM) plans focus on the reduction of potential adverse consequences of flooding for human health, environment and economic activity. FRM plans must take into account costs and benefits, flood extent, soil and water management, spatial planning, land-use and nature conservation. They have to focus on prevention, protection, preparedness, including flood forecasts and early-warning systems. They may also include the promotion of sustainable land-use practices and improvement of water retention.

Box 1 The Regulatory framework in Italy.

1.1.1 FLOODS, SOIL CONSUMPTION AND NETWORK CHARACTERIZATION

Among the natural hydrogeological instabilities, this thesis focuses on floods. Based on the *Floods Directive*, a flood can be defined as the "*temporary covering by water of land not normally covered by water*" (Floods Directive 2007/60/E, Art. 2). Flooding is generated when landscape runoff delivered to the channel network exceeds its capacity to convey runoff to the catchment outfall, leading to the inundation of rural and/or urban riparian/floodplain areas. The European interest of floods is very high, especially concerning the impact of floods on public health. In recent years, Europe has witnessed some of the largest flooding events in its history. Indeed, seven out of the twenty most important floods ever recorded in Europe (in terms of the total reported number of affected people) occurred during the 2000-2009 decade. Recent major flooding events include the 2007 floods in the United Kingdom and the Elbe and Danube river floods during the summer of 2002. Over the last 10 years, floods in Europe have killed more than 1000 people and affected over 3.4 million others (Jakubicka *et al*., 2010). Concerning this, Fig. 1.9 shows the occurrence of floods recorder in EM-DAT (Emergency Events Database) from 2000 to 2009 at a sub-national level.

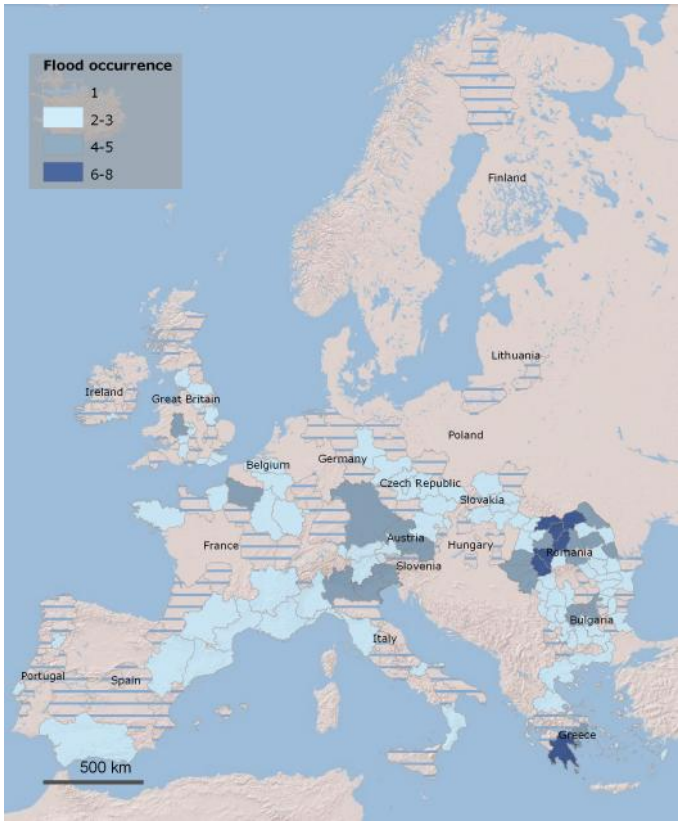

Fig. 1.9 Flood occurrence in the EU27 from 2000-2009. Source: EMDAT (Jakubicka *et al*., 2010).

Fig. 1.9 shows how floods are concentrated to certain regions within Europe, and that are hit very frequently, in some cases almost every year. On the top rank of this list, there are the regions in Romania that were affected up to eight times, meaning a flood almost every year, followed by Peloponnesse in Greece, which was affected 6 times in the last 10 years (Jakubicka *et al*., 2010). Focusing on Italy, it is possible to notice that the flood occurrence in Veneto, Lombardia and Friulia-Venezia Giulia regions is much higher than the one registered in the rest of the country.

Significant changes in land-use happened over the last few centuries in all European countries and whether the floods experienced in these recent years are triggered or exacerbated by human activities, has been the subject of much debate (e.g. Bronstert, 1996; Bronstert *et al*., 1999; Kundzewicz and Takeuchi, 1999; Longfield & Macklin, 1999; Kundzewicz and Kaczmarek, 2000). Anthropogenic activities that might lead to increased flood risk include river regulation measures, intensified land-use and forestry, and anthropogenic climate change (Bronstert *et al*., 2001).

During the last years, changes in agricultural techniques and the simultaneous increase of urbanization and industrialization, causing the so-called soil sealing, increased the extent of impervious areas. As reported by Leopold (1968), volume of runoff is governed primarily by infiltration characteristics and is related to land slope and soil type as well as to the type of vegetative cover. Passing from a permeable soil type (i.e. grassland) to a less permeable one (i.e. urbanized area), a faster and higher response of the watershed in generate runoff is expected and thus, a clear modification in hygrograph's shape. Raising limb will be steeper and will move backwards, while peak flow will reach higher values (Fig. 1.10).

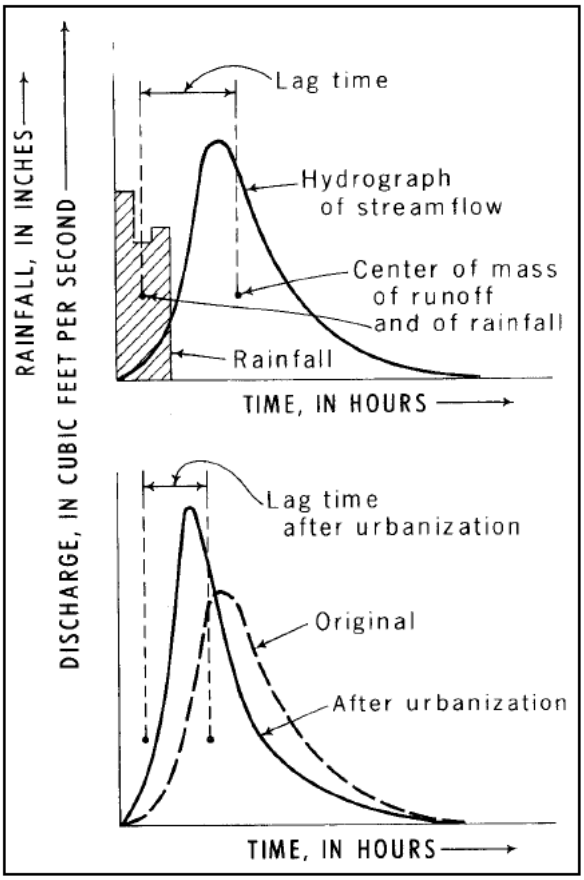

Fig. 1.10 Changes occur on hydrograph shape after urbanization (Leopold, 1968).

The analysis of effects of land-use change phenomena on floods and runoff generation requires deep assessments. Flood runoff may be generated due to rainfall either when the infiltration capacity of the land surface is exceeded or when infiltrating rainwater induces a subsurface flow response and/or saturated conditions in the riparian zone. Infiltration excess is bound to poor infiltration conditions and high rainfall intensities while subsurface stormflow, on the other hand, is supported by good infiltration conditions and the presence of preferential pathways and high groundwater levels (Bronstert *et al.*, 2001). Near-stream saturated areas may contribute to flood runoff either by producing saturation-excess overland flow or by exfiltrating directly into the stream bed. The appearance of the soil surface plays therefore a key role for the infiltration process. This element is influenced by a variety of factors including crusting, compaction and sealing at the soil surface, the extent type of vegetation cover, and surface as well as the micro-topography. Bronstert *et al.* (2001), for example, focused on the influence of land-use practices on storm runoff generation (Tab. 1.3), underlining how change in land use can influence runoff production and other important components of the hydrological cycle.

Table 1.3 Potential impact of land-use changes on surface and near-surface hydrological processes and relevance for components of the hydrological cycle (Bronstert et al., 2001).

Process	Potential impact of land-use changes and relevance for components of the hydrological cycle
Interception storage	Greatly affected by vegetation changes (e.g. crop harvest, forest cutting); relevant for evapotranspiration/energy balance
Litter storage	Affected by vegetation changes, in particular forest cutting; relevant for evapotranspiration/energy balance
Root zone storage	Affected by management practices like tilling method, etc.; relevant for evapotranspiration and storm runoff generation
Infiltration-excess overland flow	Affected by crop cultivation and management practices; relevant for storm runoff generation in the case of high rainfall intensities and low soil conductivity; may be enhanced by soil siltation and crusting
Saturation-excess overland flow	Only slightly affected by land-use changes (process is controlled by topography and subsurface conditions)
Subsurface stormflow	Only slightly affected by land-use changes (process is controlled by topography and subsurface conditions)
Runoff from urbanized areas	Highly affected by sewer system and sewage retention measures; relevant for storm runoff *from urban areas*
Decentralized retention in the landscape	Affected by landscape structuring and agricultural rationalization of arable land; relevant for storm runoff concentration *from arable land*

Local surface runoff can also increase as a result of modern farm management practices such as increased stocking densities on grasslands (Heathwaite *et* al., 1989; Heathwaite *et* al., 1990), the increase in maize crops, the production of fine seedbeds (Speirs and Frost, 1985), and trafficking on wet soils (Davies *et* al., 1973; Young and Voorhees, 1982). Reduced infiltration and increased surface runoff associated with modern practices is quite widespread (Hollis *et* al., 2003; Palmer, 2002; Palmer, 2003a; Palmer, 2003b; Soucher *et* al., 1998). Enhanced surface runoff generation in consequence of some of the above modern farming practices, can generate local-scale flooding. For example, long-term studies in small catchments in the South Downs of South-East England show that there is a significant relationship between the presence of autumns-sown cereal fields and local 'muddy floods' in autumn (Boardman *et* al., 2003). The frequency of these floods can be reduced by appropriate arable land management practices (Evans and Boardman, 2003). Similar conclusions have been drawn for France (Papy and Douyer, 2001; Souchere *et* al., 2003) and Belgium (Bielders *et* al., 2003; Verstraeten and Poesen, 1999).

Therefore, an evaluation of land-use-use changes impacts on flooding requires an identification of the relevant storm runoff generation mechanisms for the specific catchment characteristics and precipitation conditions (Bronstert *et al*., 2001). The same authors, to investigate the effects of urbanization on flood generation, designed spatially distributed scenarios of possible future land-use and land surface conditions with the help of a land-use

change modelling tool (Fritsch *et al*., 1999). In their study, urban areas are considered to have a portion of asphaltic surface, often connected to a sewer system and a fraction of greens, parks where better infiltration and soil storage conditions can be found. Therefore, to take into account this form of heterogeneity within grid cells, each grid cell is divided into a sealed and an unsealed part according to the degree of sealing of the cell's actual land-use type (Fig. 1.11).

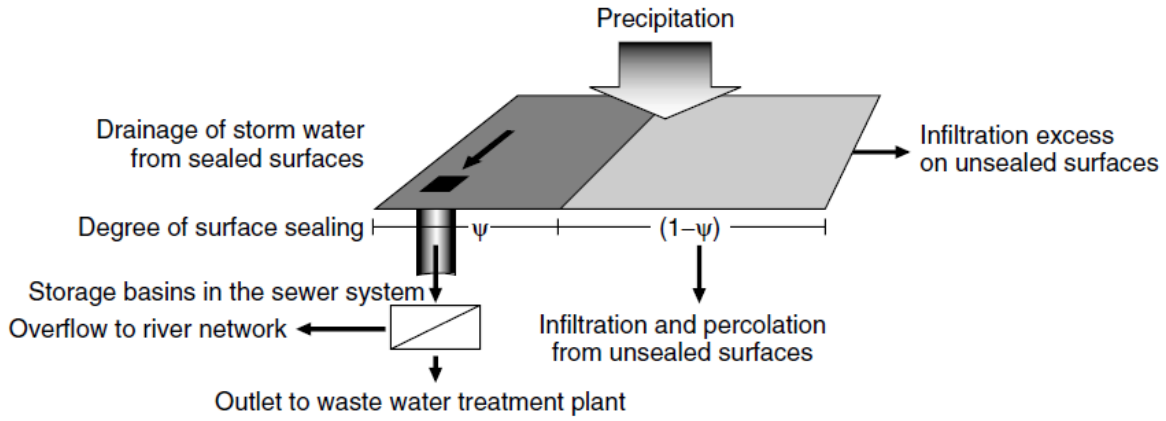

Fig. 1.11 Model concept for sealed surfaces within a grid cell and their connection to the sewer system (Bronstert *et al*., 2001).

The results of the study show that for high precipitation intensities, an increase in settlement area leads to markedly higher peak flows and flood volumes, whereas the influence of urbanization on advective rainfall events with lower precipitation intensities and higher antecedent soil moisture is much smaller. The pronounced increase in storm runoff for the convective event is mainly due to an increase in sewer overflow in settlement areas and infiltration-excess overland flow on farmland (Bronstert *et al*., 2001).

As outlined by Bronstert *et al*. (2001), both runoff generation and discharge conditions can be altered by human activities. In general, field drainage, wetland loss and urbanization result in increased 'flashiness' of runoff, more rapid downstream transmission of flood waves, and less floodplain storage (Newson *et al*., 2000). Pfister *et al.* 2003 focused on changed discharges linked to land-use changes in the Rhine and Meuse basins, underlining how different anthropic alteration brought to changes in the discharge regimes. These authors retrieved land use changes that had already been assessed by other works: urbanization and impermeabilization increased during the years, as it has been happening in most river basins in western Europe (Cosandey and Robinson, 2000). Together with this increasing, they registered the implementation of artificial drainage systems (Robinson *et al*., 2000), and the

re-allocation of lands that induced a lot of modifications in land management and consequently on water management (Loucks and Avakyan, 1998). Finally, the two areas have been strongly modified by the construction of levees, dykes and other structures, changing the discharge regime and straightening the channels. No clear evidence existed from historical time series for the impact of land-use changes on flood frequency and magnitude, however the anthropic pressure led to an accelerated discharge during periods of peak flows and a delayed discharge during low flow periods (de Wit *et al*., 2001).

O' Connell (2005) investigated the significant changes in UK land-use and management practices driven by UK and EU agricultural policies. She highlighted how such anthropogenic interventions tend to generate the perception that the natural hydrological functioning of catchments has been altered, usually adversely. Whit her paper, she tested this perception against the available evidence to answer the question if a link between agricultural land-use change management and flooding actually exists. There is field evidence that agricultural change may cause local flooding, but an almost complete lack of evidence that local-scale effects aggregate, causing impacts at larger scales downstream.

Brath *et al*. (2005) aimed to assess the effects that land use change, which have affected a wide portion of Italy in the second part of the last century, have induced on the flood frequency regimes. By considering as study area the Samoggia River basin, located in the Apennines mountains, and by applying a spatially distributed rainfall-runoff model to generate synthetic river flow series for different land use scenarios (1955, 1980 and 1992), they were able to investigate variations of the peak flow regime, due to the increasing human activity. In addition, they also compared these such variations with the magnitude of the simulation uncertainty. The results indicated that the sensitivity of the floods regime to land use change decreased for increasing return period of the simulated peak flow. By considering peak flows with return period ranging from 10 to 200 years, the effects of human activity seemed to be noteworthy.

From this literature review, it is clear that human activities have a direct influence on floods, especially in engineered landscapes. In these contexts, direct human alteration on floods is also connected to the presence of artificial drainage networks (Robinson *et al*., 2000), that in Northern Italy consists generally of open main, sub-main, and lateral ditches, located on the field boundaries but also within the plots. The whole network is subdivided into different drainage districts, each managed and monitored by a Land Reclamation Consortium (LRC). Each LRC has the responsibility to control, maintain and modernize the drainage network, and to guarantee the hydraulic safety of the territory from flooding. Drainage networks, in

fact, influence groundwater hydrology (Dahes *et al*., 2009), but also overland flow paths (Duke *et al*., 2006; Gascuel-Odoux *et al*., 2011; Lavasseur *et al*., 2011). Considering agricultural ditch drainage networks, four effects are commonly accounted for: *i*) the interception of overland flow on hillslopes; *ii*) the drainage of groundwater by lowering the water table; *iii*) the infiltration from the ditch towards the groundwater, and *iv*) the conveyance of water towards downstream areas (Carluer and Marsily, 2004; Dunn and Mackay, 1996; Lavasseur *et al*., 2011). In addition, as the ditches follow the field limits, water flow does not necessarily follow the steepest slope of the catchment surface topography; thus ditches are expected to modify the average distance and slope between the fields and the catchment outlet (Moussa *et al*., 2002). These networks, also referred as 'minor network', can play a key role also in the control of floods generation (Gallart *et al*., 1994; Voltz *et al*., 1998; Marofi, 1999; Moussa *et al*., 2002). In addition, such artificial networks may act as conduits or short-circuits for the transportation of contaminants, either dissolved or sorbed on soil particles, by-passing some of the retardation mechanisms such as sorption in the soil, retention of surface runoff by grass verges and biodegradation in the unsaturated zone (Carluer and De Marsily, 2003). Moussa *et al*. (2002) tried to assess the role of human impact on flood events, focusing especially the existence of tillage practices and ditch networks. Through a simulation approach that uses the based on the hydrological model MHYDAS (Modélisation Hydrologique Distribuée des AgroSystèmes), he attempted to take into account the main characteristics of farmed catchments, in particular the hydrological response of a farmed catchment to different tillage practices and the role of the ditch network. The simulations showed the sensitivity of the model and the impact of both tillage practices and ditch network on hydrological processes. In particular for the latter, the results exhibited that the ditch network accelerated runoff by concentrating flow and avoiding natural obstacles.

It is clear that land use changes and soil consumption lead to changes in flood flows. Urbanization and soil consumption, reduced the extent of agrarian drainage networks (Cazorzi *et al*., 2012), and at the same time they caused an overall decrease in volumes of small reservoirs, with consequences on flood risks (Brath *et al.*, 2003). To provide a general context at the national scale, the soil consumption related to increasing of urbanization has been analyzed by ISTAT (Istituto Nazionale di Statistica – Italian National Statistics Institute) with the intention of showing progresses made by statistical informatics systems to support land-use strategic planning. The LUCAS (Land-use/Cover Area frame statistical Survey) project allowed to compare general characteristics of the land-use in 23 European countries in 2009,

and between our regions as well. This comparative analysis showed that Italy has soil consumption levels that are suitable with its demographic and economic characteristics, but it also highlights some negative peculiarities in land-use for residential and productive purposes. The portion of artificial surface is equal to 7.3%, versus 4.3% according to the European mean Ue23 (Eurostat, LUCAS analysis, 2009) (Fig. 1.12).

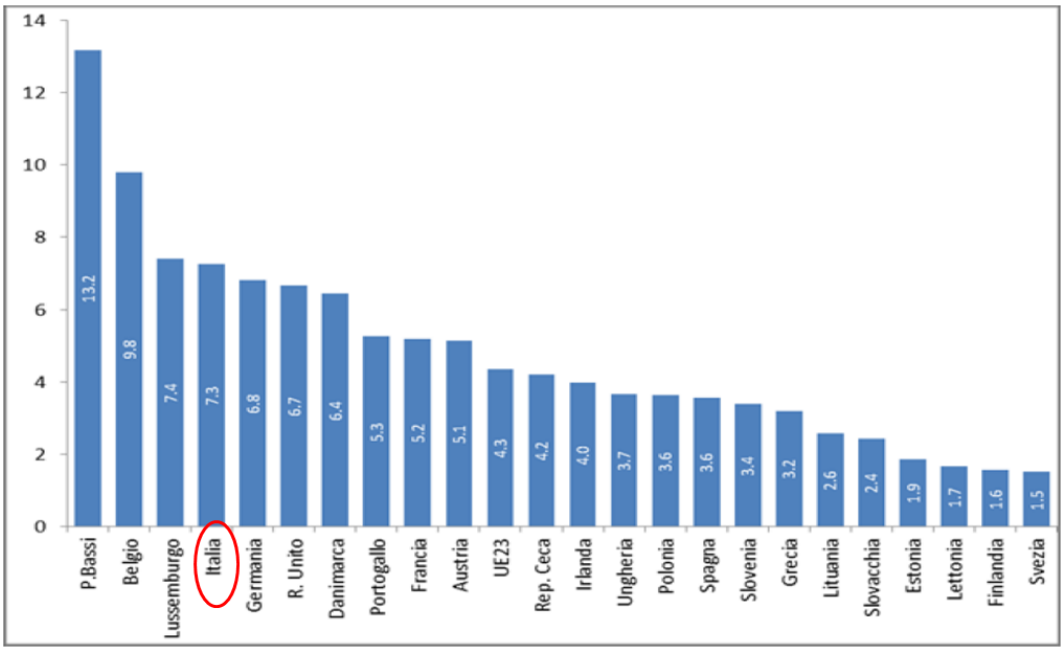

Fig. 1.12 Territory with artificial cover – Year 2009 (percentage incidence of the total surface) (Eurostat, LUCAS analysis).

From the point of view of land-use, the categories in which the soil consumption is more significant are those with "residential and services" purposes and with "high environmental impact", which gather the industrial, logistical and infrastructural land-uses. Italy ranks the ninth position with a percentage of 12.2%. (Eurostat, LUCAS analysis, 2009) (Fig. 1.13).

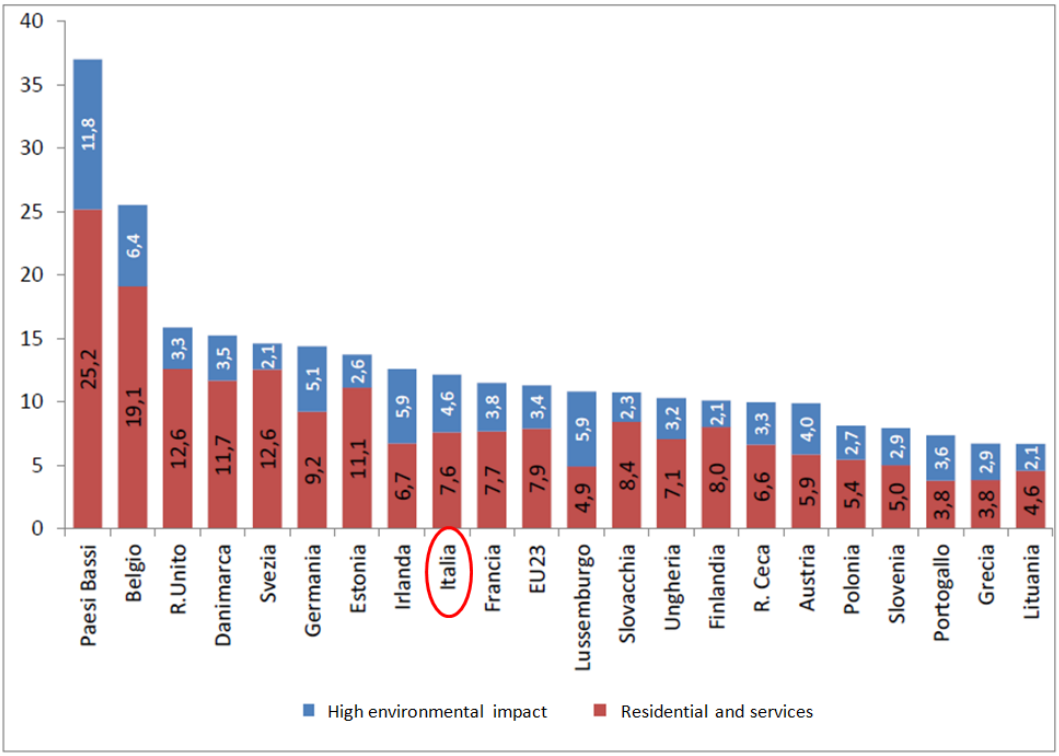

Fig. 1.13 Land-use in some European Union countries: portions of territory with "residential and services" purposes and with "high environmental impact" – Year 2009 (percentages) (Eurostat, LUCAS analysis).

The extension of Italian inhabited localities, which is an underestimation of the extension of urbanized areas, is around 20 000 Km^2, equal to 6.7% of the national surface. Compared to the situation registered in 2001, the increment of urbanized soil has been equal to 1639 Km^2, which corresponds to an increase of 8.8% and, if considered only the Veneto region, this increase is equal to 7.3% (Istat, census data 2001 and 2011) (Tab. 1.4).

Table 1.4 National and Veneto region surfaces according to different categories of inhabited localities – Years 2001 and 2011 (values and variations expressed in percentage).

REGIONI RIPARTIZIONI GEOGRAFICHE	Censimento 2001				Censimento 2011				Var. % 2001-2011		
	Totale località abitate (a)	*di cui: centri abitati*	Case sparse	Totale	Totale località abitate (a)	*di cui: centri abitati*	Case sparse	Totale	Totale località abitate (a)	*di cui: centri abitati*	Case sparse
Veneto	12.0	*10.5*	88.0	100.0	12.9	*11.2*	87.1	100.0	7.3	*6.9*	-1.0
Italia	**6.2**	***5.4***	**93.8**	**100.0**	**6.7**	***5.8***	**93.3**	**100.0**	**8.8**	***7.1***	**-0.6**

In addition, the analysis of data required for the territorial census shows how the soil consumption has not been homogeneous across the national territory. The urbanized land is, in general, greater in the Center-Northern part of the country, and in particular it reaches the 13% of the regional surface in Veneto and Lombardia regions.

This progressive loss of soil permeability and reduction of drainage networks represent a critical issue for the hydraulic safety of the lands, especially in floodplain contexts where management plans are already required to reduce the flood risk level to acceptable thresholds. Tools for a correct management and planning are therefore deeply needed. An example of these tools are the analysis of hydraulic compatibility and the application of the hydraulic invariance principle. The Veneto Region regulation, for example, defines that for all urban Master Plans that may cause transformations of the territory, and that would alter the existing hydraulic system, an hydraulic assessment of hydraulic compatibility must be submitted. Each project of land use transformation that causes a change of surface permeability should include compensatory measures, in order to maintain the previous runoff discharge (they should maintain a hydraulic invariance (Pistocchi, 2001) (Resolutions no. 1322, May 10, 2006 and no. 1841, June 19, 2007). In this perspective, network storage capacity assessment is therefore a crucial tool for flood management: low values of channel storage capacity can *i)* underline deficit in the network, and they can outline areas whose hydrological behavior is potentially critical during floods, where change in land use might increase the level of risk, and *ii)* they allow to identify storage areas already available on the surface, that can be considered to apply the hydraulic invariance principle.

In reclamation lands, such as the northern Italy floodplain, storage capacity within the network plays an important role also in the design of drainage channels and pumping stations, considering that a larger storage or retention capacity within the network system lowers the requirement for pumping capacity to achieve the same service objective (Malano and Hofwegen, 1999).

Drainage network recognition and quantification of water storage capacity within channels require accurate spatial information, but such information is usually lacking (Kothe and Bock, 2009), especially when dealing with large-scale applications. Ground-based geomorphological mapping is generally only performed on small areas (Burel and Baudry 2005), or with large investments in terrain surveys (Lagacherie *et al*., 2004). The official cartography (i.e. Regional Technical Map – RTM – at 1: 5000 scale) may be considered as a large-scale source of data, but the big limitation is its updating: in Italy this is supposed to be done approximately every 10-15 years, but no specific regulation exists. At the same time, for

map updating, new information about topography is needed. For the characterization of the network over large areas, problem arises in Italy for two main reasons: *i*) there are no technical manuals with precise indications regarding the suitable size and density of the in-field channel network; and *ii*) as in other European countries, each farm unit is very often not continuous. As a consequence, when scaling up from an agricultural plot scale to the LRC scale, the structure of drainage networks appears to be highly variable in space and hard to identify.

Concerning this, National or Local Mapping Agencies, especially in Europe, are moving towards the generation of digital topographic information. Remote sensing can therefore provide multiple options to support decision makers with accurate and up-to-date geoinformation in such environmental context. According to the purpose of the study and the prices/accuracy trade-off of the data required, different choices are available for the researchers who want to rely on remote sensing. Both Terrestrial Laser Scanner (TLS) and Airborne Laser Swath Mapping technology (ALSM), using LiDAR (Light Detection and Ranging, see Chapt. 3.1) technology, now provide high resolution topographic data. The most valuable peculiarity of these technologies is their capability to produce sub-meter resolution Digital Terrain Models (DTMs, see Chapt. 3.2), and high-quality land cover information (Digital Surface Models, DSMs) over large areas.

In addition to these high resolution technologies, the Shuttle Radar Topography Mission (SRTM) and the Advanced Spaceborne Thermal Emission and Reflection Radiometer (ASTER) topographic products have allowed detailed analyses in large regions. SRTM has collected data over nearly 80% of Earth's land surfaces, creating the first-ever near-global data set of land elevations (90m DTM) (Rabus *et al*., 2003; Farr *et al*., 2007). ASTER, on board the NASA's TERRA satellite, provides an opportunity to obtain high resolution (though less than TLS or LiDAR) terrain data from photogrammetric processing of stereo Visible Near Infrared (VNIR) sensor data. With this technology, it is possible to generate DTMs in heterogeneous terrain conditions, anywhere with coverage and with a spatial resolution of 30 m (Hirano *et al*., 2003; Fujisada *et al*., 2005).

The resolution of ASTER and SRTM DTMs, however, is not adequate to depict in-field network features, whose width spans from 0.5 up to a maximum of 5 or 6 meters, therefore it is necessary to focus on the LiDAR technology. LiDAR DTMs covering large areas are readily available for public authorities, and there is a greater and more widespread interest in the application of such information by agencies responsible for land management for the development of automated methods aimed at solving geomorphological and hydrological

problems (Cazorzi *et al*., 2012). Automatic feature extraction based on DTMs can offer large-scale applications and an accurate method that can help in improving topographic databases, and the aim of this thesis is to show an example of this application over large areas in engineered landscapes.

1.2 GOALS OF THE THESIS

This thesis focus on a wide area subjected to flooding, localized in the Veneto region and representative of an agrarian context within floodplain, where high resolution topographic data are available thanks to LiDAR flight realized within the "*Piano Straordinario di Telerivelamento Ambientale (PST-A)*" (Extraordinary Plan of Environmental Remote Sensing, EPRS-E) (Chapt. 4). The vulnerability of this territory to flood events can be explained by the presence of many artificial and highly-modified channels, as it will be better discussed in Chapt. 5.1. In this floodplain context, over the years, the natural river system has been in fact, deeply modified, through the artificial management of water levels and discharges. This resulted in an artificial drainage system, in which the flow occurs along a network of regular channels (larger channels and small ditches), often through water pumping. There is no doubt that this type of area is naturally exposed to the danger of floods, whose causes are multiple and often interacting with each other. The principal causes can be generally distinguished between problems related to large rivers unable to manage the incoming flows, and issues directly related to the inability of draining meteoric water through the smaller hydraulic network (ditches). While problems related to the large rivers are mainly connected to choices and actions applied in historical times, the problems of the smaller hydraulic network are due to small and relatively recent territorial changes: fast human settlement in floodplain, and the intense urbanization, have reduced the extent of the network while increasing at the same time impermeable surfaces, with the result that the remaining network drainage capabilities are no longer sufficient. As a consequence, situation of hydraulic crisis happen with increasing frequency and they affect the most urbanized districts, becoming particularly serious in conjunction with major floods, such as occurred in the Veneto region in 2010.

We deemed therefore important to focus on the minor drainage network system, considering that 1. Short time land use changes (such as urbanization plans) hardly modify large rivers: they mainly results in a reduction of the minor network; 2. Large rivers are historically subjects of hydraulic studies, therefore data are already available; 3. Information about the

minor network, on the other hand, are not available over large areas, and the size and density of the in-field channel network is highly variable in space and hard to characterize.

A semi-automatic approach has been applied to recognize and characterize agricultural ditches, (Cazorzi *et al*. 2012) (Chapt. 4.1). The mentioned methodology allows to compute some important network statistics, such as drainage density and storage capacity indexes that are generally not available but are crucial tools for flood management, because, as already reported, they can outline areas whose hydrological behavior is potentially critical during floods. The novelty is applying such methodology to a very wide area (180 000 ha). As a matter of facts, for the first time, this kind of analysis has been done at a regional scale.

To provide an overview of the relationship between the network and its derived indexes, the hydraulic behavior of the territory, and some recent land use change, we also evaluated how the land use changes occurred during the period from 1990 to 2006 have affected the propension of the land to produce surface runoff (Chapt. 4.2). The effects of drainage network storage capacity on direct runoff have been analyzed as well, through the application of a simple index named residual runoff (m^3), (difference between the direct runoff and the effective storage capacity). However, while it was possible to compute the variation in the propension of producing runoff over the years, considering the Curve Number maps, it was not possible to assess the variation of the minor drainage network system and hence, of the storage capacity. We are aware that the latter analysis should be a further information to provide, for a complete evaluation. However such information is lacking because: 1. The only available source for the characterization and the location of the minor network are field survey (cartography wouldn't provide information about network geometry), so this information is not available at a large scale for the past; 2. The only available large scale map to apply the procedure is the 2010 LiDAR DTM, because DTMs that are not derived from LiDAR, even when available, do not have a resolution that is sufficient to depict the small elements of the network. However, it is likely thinkable that variations of the drainage network system are related to land use changes as well, and, although the quantification of the water storage capacity for the past periods has not been possible, it could be very interesting and useful for future projects.

Going back to the analysis, the simple comparison between direct runoff and storage capacity, is provided to verify the effectiveness of the actual network on laminating the direct runoff produced during the November flood event. It must be underlined that in such kind of analysis, for a more complete evaluation, the upstream contributions should be also accounted for, but this simplified assessment aims to identify the presence of areas that may be already

in critical condition for the runoff directly produced by the input local rainfall. An efficient network should be able to drain 60-70% of the normal rainfall, but in some cases this is not true. This simplified analysis, however, is provided also to underline that change in land use (in this case considering the evolution during the years), should be also accounted in planning and managing procedures.

2 THE 2010 VENETO FLOOD

During 2010, two main flood events happened in Veneto, one in November and one in December, compromising the hydrological asset of the region and resulting in economic losses and damages. This thesis focus on the one that impacted the Veneto region from October 31th to November 2nd 2010. This because this event first impacted on the area, causing the highest number of damages and problems, and was directly influenced by the intensity of the rainfall event. The second event of December, instead, was also influenced by the diminished capacity of the area to cope with the flood, due to the damages caused by the previous events.

Considering the flood event occurred in November, a large, long-lived storm system, on the piedmont mountain range system of Veneto, produced hydrogeological instabilities along almost all the principal channels, causing the breakdown of embankments and the consequent flooding on large regional areas (140 Km^2 of territory affected) (Fig.2.1). Other than the intense rainfall, the permanence of the scirocco wind either on the coast and on the mountains, made the pre-existing snow melt down.

Fig. 2.1 Suburbs of Padua affected by the flood event 2010 (Regione Veneto, "La Grande Alluvione", 2010).

From sampled and local rainfall data, registered by the monitoring network system (raingauges) and downloaded from the ARPAV (Agenzia Regionale per la Prevenzione e Protezione Ambientale del Veneto) website, a regional rainfall distribution can be obtained through an Inverse Distance Weighting interpolation method (Fig. 2.2).

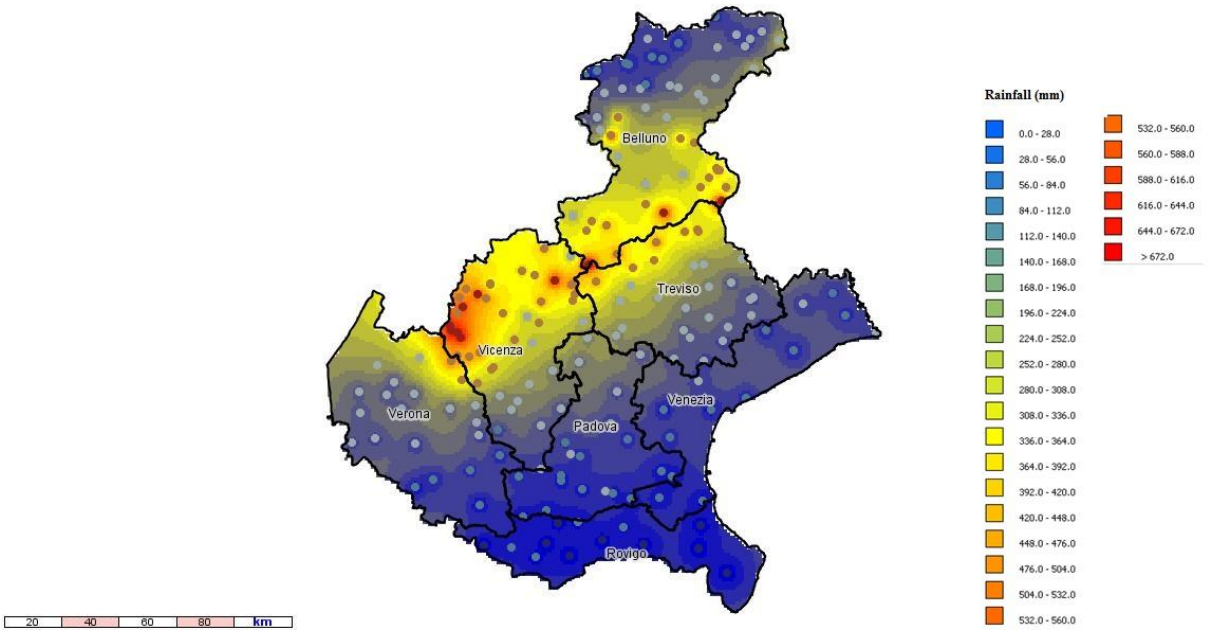

Fig. 2.2 Regional rainfall distribution map obtained through a IDW interpolation method using the following parameters: maximum distance 1000000 m and exponent 2. The colored dots correspond to the raingauges which constitute the regional monitoring network system.

From Fig. 2.2, what comes out is that heavy rainfall is especially located along the provincial boundary between Belluno and Treviso and in the Northern part of Vicenza. These areas are therefore, those ones that are much affected by the rainfall event but, bad repercussions have been also registered downstream, where the residential and industrial areas are mostly distributed. It is therefore important to point out that the actual break of embankments, registered in the considered section (see Chapt. 5.1.1, Fig. 5.21), was not caused only by the local precipitation occurred in the floodplains, but was mainly due to the combination of upstream runoff and the incapacity of the minor drainage network to laminate the local surface runoff.

According to what reported by ARPAV (Agenzia Regionale per la Prevenzione e Protezione Ambientale del Veneto), considering the event broadly, it should be pointed out that very high maximum local rainfall values have been recorded (in the mountainous part of the region),

and that mean areal rainfall values have been significant over various areas, witnessing in such way that abundant precipitations have affected not only single localities but larger areas too. It must also be stated that these elevated totals of precipitation were not due to a high rainfall intensity, that has always been minor than 25/30 mm/hour instead, but to the prolonged duration of the event.

This event has also been compared to two other significant flood events occurred in October 1992 and in November 1966 (figures 2.3 and 2.4). The comparison has been made according to the available pluviometric data, recorded in two days for each event (ARPAV, 2010).

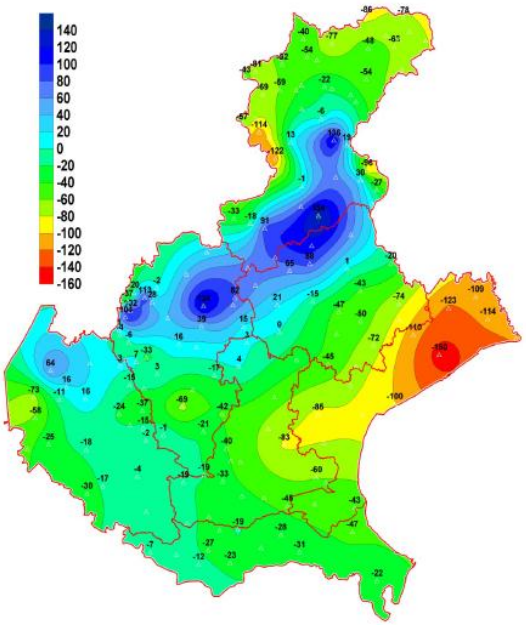

Fig. 2.3 Map showing the differences in precipitation values (mm) recorded in two days, between the 31st October – 1st November 2010 event and the 4th-5th October 1992 event. Positive values correspond to a greater magnitude of the former event cited, while negative values stand for a greater magnitude of the latter event cited. In the floodplain context, all the values are negative, witnessing in that way that in the 1992 event, it rained much more than in the 2010 one. The situation is exactly the opposite in the mountainous portions (ARPAV, 2010).

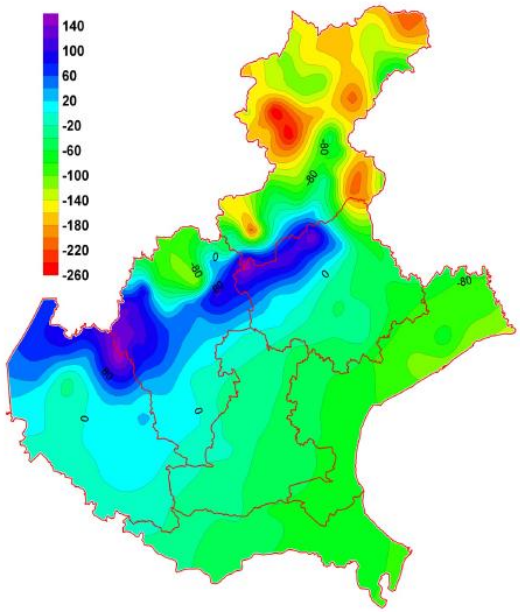

Fig. 2.4 Map showing the differences in precipitation values (mm) recorded in two days, between the 31st October – 1st November 2010 event and the 4th-5th November 1966 event. Positive values correspond to a greater magnitude of the former event cited, while negative values stand for a greater magnitude of the latter event cited. As already assessed in Fig. 2.3, in the floodplain context, most of the values are negative, witnessing in that way that in the 1966 event, it rained more than in the 2010 one. On the opposite, the mountainous regions have been affected by more precipitations in 2010. (ARPAV, 2010).

Still based on the available data made by ARPAV, the attention now shifts from pluviometric to hydrometric data. In succession, hydrometric heights recorded by the monitoring network system spread over the Veneto region are reported. We will mainly focus on the Brenta and Bacchiglione rivers, because they are the main ones that converge on our study area (see Chapt. 5, Fig. 5.3 and 5.4). The map showing the localization of hydrometric stations along the cited river basin, is reported in Fig. 2.5.

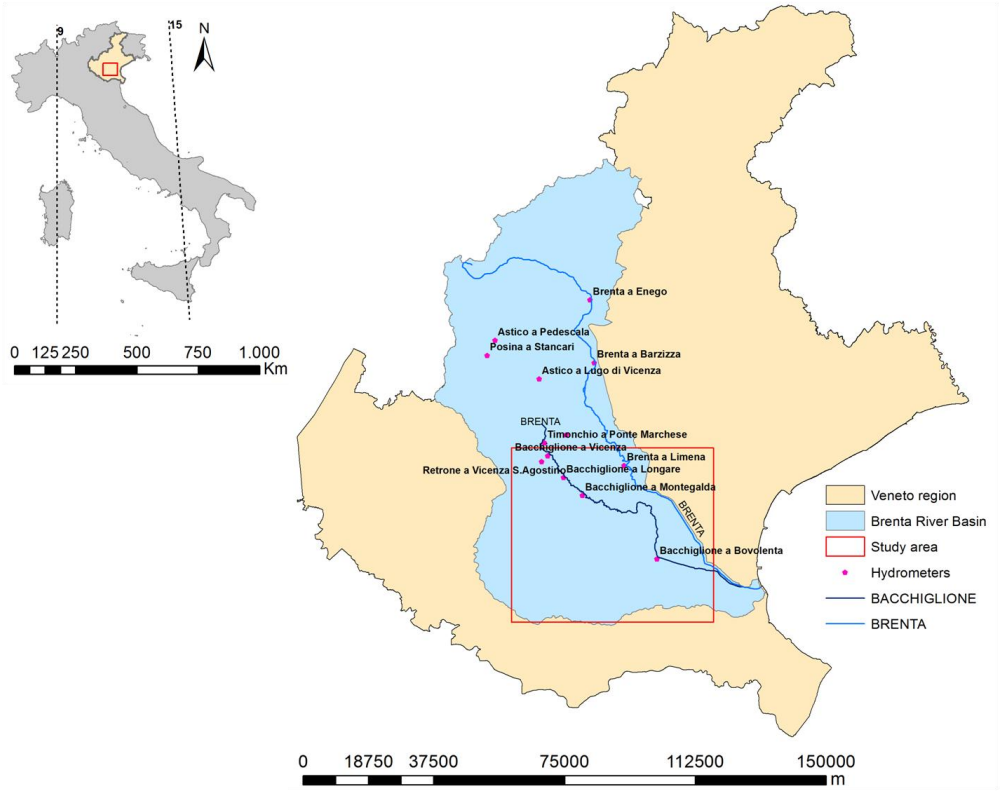

Fig. 2.5 Map showing the distribution of the hydrometric stations over the river basin of interest. In the map are also reported the Bacchiglione (in dark blue) and Brenta (in light blue) rivers. The red rectangle corresponds to the study area as will be better described in Chapt. 5.

Bacchiglione river

The flood of Bacchiglione river caused numerous problems during the event: all the river sections monitored exceeded the maximum historic level registered. In Fig. 2.6, the reaction of the hydrometers in correspondence to the breaking of embankment, is well evident. It must be noted that the hydrometer of Montegalda (Fig. 2.6), went out of order in correspondence of the presumable peak flow (ARPAV, 2010).

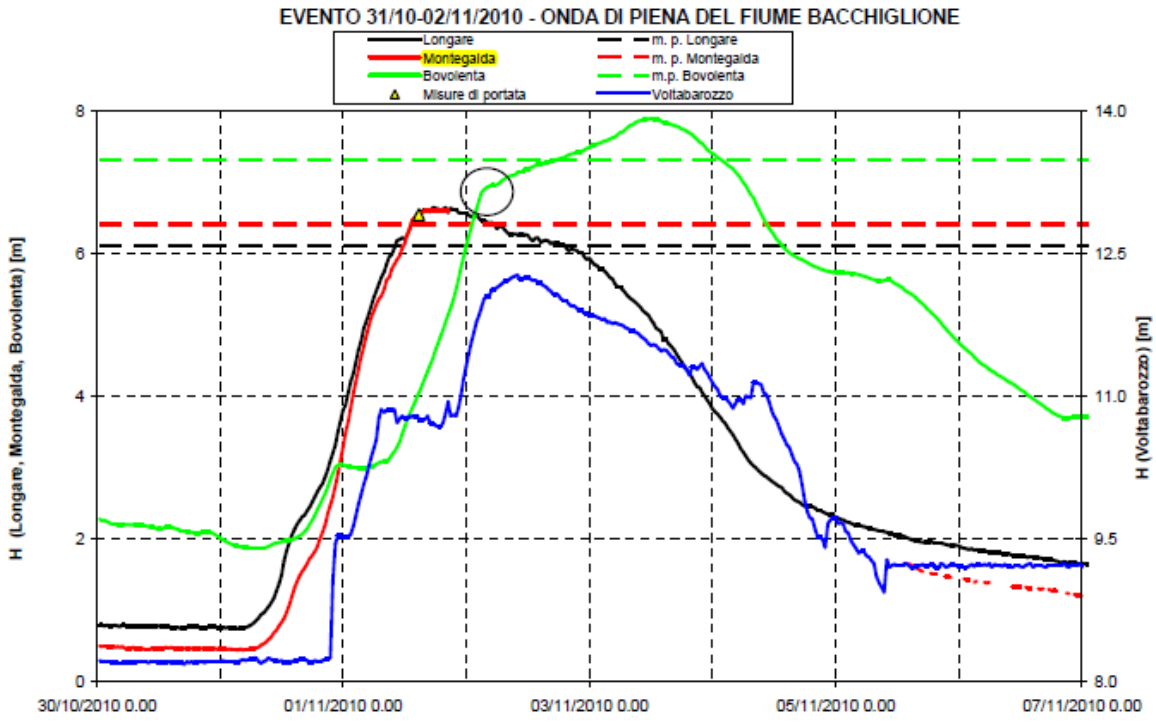

Fig. 2.6 Variation of the hydrometric levels along the Bacchiglione river during the 30/10 – 5/11 2010 flood event. The circle corresponds to the break of embankment occurred in correspondence of Roncaiette, within the municipality of Ponte San Nicolò (ARPAV, 2010).

All the maximum hydrometric level values, recorded by the monitoring network system for such flood event are reported in Tab. 2.1. The table also reports the maximum hydrometric level recorded by each station during some flood events in the past (ARPAV, 2010). What emerges is that all the maximum hydrometric values registered for the 2010 flood event result to be greater than the historical ones.

Table 2.1 Maximum hydrometric levels reached during the 2010 flood event and compared to some historical ones (ARPAV, 2010).

River Basin	River	Hydrometric station	31/10-04/11/2010 event			Historic events		
			Date-Time	H (m)	Position in hist. serie	n° yrs hist. serie	yr of max disch.	Hmax (m)
BACCHIGLIONE	TIMONCHIO	P.te MARCHESE	01/11/2010 07.30	3.70	1	11	2000	3.47
BACCHIGLIONE	BACCHIGLIONE	VICENZA	01/11/2010 19.00	6.18	1	16	1994	5.67
BACCHIGLIONE	RETRONE	S. AGOSTINO	02/11/2010 13.00	3.50	1	15	1997	3.13
BACCHIGLIONE	ASTICO	PEDESCALA	01/11/2010 08.00	2.02	-	-	1999	2.64
BACCHIGLIONE	POSINA	STANCARI	01/11/2010 08.30	3.81	-	-	1999	3.78
BACCHIGLIONE	ASTICO	LUGO DI VICENZA	01/11/2010 13.00	2.15[2]	-	-	1999	2.62[2]
BACCHIGLIONE	TESINA	BOLZANO VICENTINO	01/11/2010 13.30	5.56	1	15	1999	5.38
BACCHIGLIONE	BACCHIGLIONE	LONGARE	01/11/2010 17.30	6.64	1	16	2002	6.10
BACCHIGLIONE	BACCHIGLIONE	MONTEGALDA	01/11/2010 20.30	6.60	1	13	1996	6.40
BACCHIGLIONE	BACCHIGLIONE	BOVOLENTA	03/11/2010 12.00	7.89	1	11	2009	7.32

Discharge measures computed in correspondence of some hydrometers are also reported in Tab. 2.2.

Table 2.2 Discharge measures computed along the Bacchiglione river during the 2010 flood event (ARPAV, 2010).

River Basin	River	Hydrometric station	Date	Hour	H_{MEDIA} (m)	Disch. (m^3/s)
Bacchiglione	Bacchiglione	Montegalda	1-nov-10	14.45	6.54	330
Bacchiglione	Tesina	Bolzano Vicentino	2-nov-10	11.55	3.73	265
Bacchiglione	Bacchiglione	Ponte S.Nicolò	3-nov-10	15.50	6.93Ast	302

Brenta river

Although the Brenta river did not reach maximum flow peaks, it anyway showed high hydrometric levels (Fig. 2.7 and Tab. 2.3).

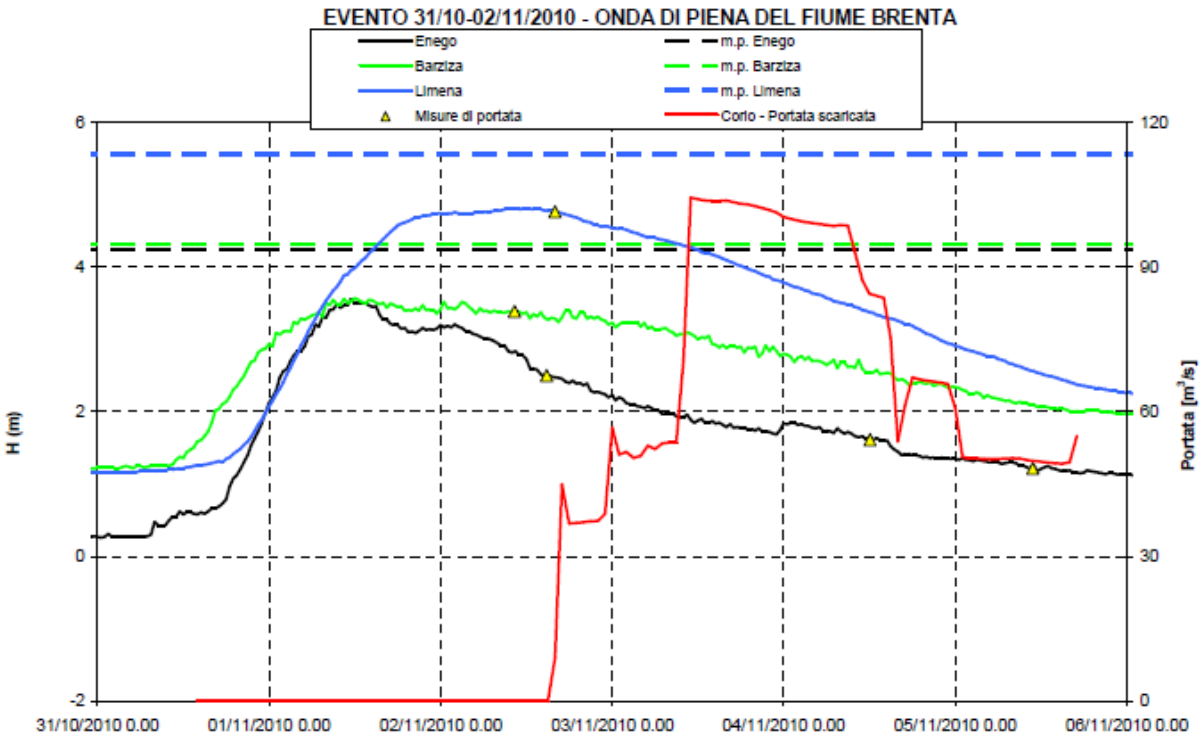

Fig. 2.7 Variation of the hydrometric levels along the Brenta river during the 30/10 – 5/11 2010 flood event (ARPAV, 2010).

As already done for the Bacchiglione river, also for the Brenta one all the maximum hydrometric level values recorded by the monitoring network system for such flood event, are reported in Tab. 2.3. The table also reports the maximum hydrometric level, recorded by each station during some past recent flood events (ARPAV, 2010). Differently from what has been seen in Tab. 2.1, all the maximum hydrometric values registered for the 2010 flood event, result to be lower than the historical ones.

Table 2.3 Maximum hydrometric levels reached during the 2010 flood event and compared to some historical ones (ARPAV, 2010).

River Basin	River	Hydrometric station	31/10-04/11/2010 event			Historic events		
			Date-Time	H (m)	Position in hist. serie	n° yrs hist. serie	yr of max disch.	Hmax (m)
BRENTA	BRENTA	ENEGO	01/11/2010 11.30	3.56	4	25	1993	4.25
BRENTA	BRENTA	BARZIZA	01/11/2010 12.00	3.57	4	26	1993	4.32
BRENTA	BRENTA	LIMENA	02/11/2010 12.30	4.81	3	15	1998	5.57

Discharge measures computed in correspondence of some hydrometers are reported as well in Tab. 2.4.

Table 2.4 Discharge measures computed along the Brenta river during the 2010 flood event (ARPAV, 2010).

River Basin	River	Hydrometric station	Date	Hour	H_{MEDIA} (m)	Disch. (m^3/s)
Brenta	Brenta	Barziza	2-nov-10	10.20	3.39	727
Brenta	Brenta	Curtarolo	2-nov-10	16.00	4.77	667
Brenta	Brenta	Enego	2-nov-10	14.52	2.51	126
Brenta	Brenta	Enego	4-nov-10	12.05	1.62	57
Brenta	Brenta	Enego	5-nov-10	10.50	1.22	34

In addition, the attenuating effect operated by the dam of Corlo Sul Torrente Cismon contributed to mitigate the Brenta runoffs downstream and to keep the hydrometric levels lower, also after the passage of the peak flow in correspondence of the Barzizza section (Fig. 2.8).

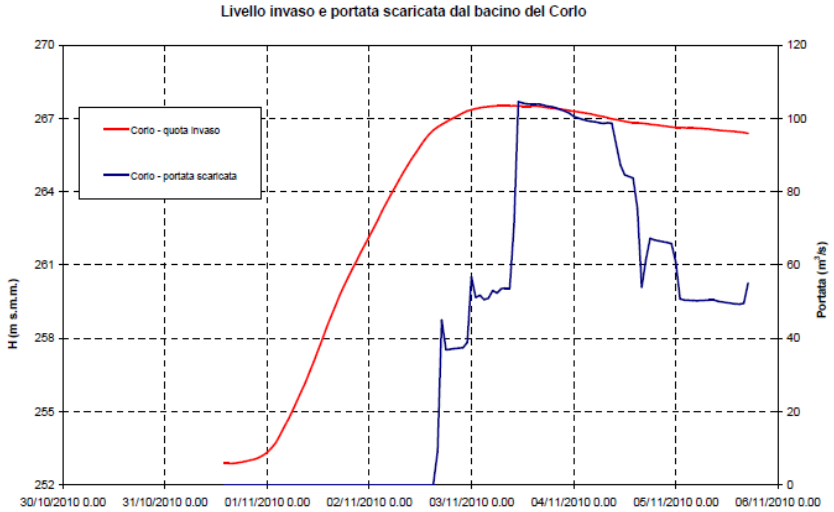

Fig. 2.8 Variation of the hydrometric level and of the discharge drained during the 2010 flood event by the Corlo reservoir (ARPAV, 2010).

3 GENERAL BACKGROUND

This chapter discusses the research that provides materials and methods for this study. It provides a theoretical basis of LiDAR technology (Chapt. 3.1) and it describes one of its main products: Digital Terrain Models (DTMs) (Chapt. 3.2). The section then focuses on the morphological representation of land surfaces (Chapt. 3.3), and on procedures for feature extraction from LiDAR DTMs (Chapt. 3.4). Finally, it gives a detailed description of the methodology applied in the present work (Chapt. 4).

3.1 LiDAR TECHNOLOGY

Light Detection And Ranging (LiDAR) is an optical remote sensing technology that can measure the distance to, or other properties of a target by illuminating it with light, using pulses from a laser. It is made of a laser telemeter that can be either held on the ground (TLS – Terrestrial Laser Scanner) or brought by an airborne (airborne LiDAR). In both cases, the working principle is the same. The electric impulse, created by a generator, emits a beam of infrared light; the emitted signal is then backscattered and reflected by the objects, and the measurement mechanism is able to provide some of the properties (e.g. traveling time, signal intensity) of the reflected pulse (Wehr and Lohr, 1999). The traveling time (Δt) spent by the laser pulse to reach the target and come back to the sensor, is computed trough a quartz clock. The distance (D) is a function of the traveling time Δt ad it is computed as:

$$\boldsymbol{D = \frac{\Delta t \cdot c}{2}} \qquad 1$$

where c is the speed of light ($3 \cdot 10^8$ m/s) (Watkins, 2005; Weitkamp, 2005).
The telemeter measures the travelling time in a discrete way, and this implies that also the distance is obtained as the sum of infinitesimal distances (Casella, 2003). The resolution in time δt, thus the shortest measurable lapse time, is in inverse proportion to the frequency of the generator:

$$\boldsymbol{\delta t = \frac{1}{f}} \qquad 2$$

while the resolution in distance is given by:

$$\delta D = \frac{\delta t \cdot c}{2} \qquad 3$$

The fundamental result of a LiDAR survey is the restitution of x, y, z coordinates of each measurement. In order to exactly know the coordinates of the targets, it is also required to know the correct position and orientation of both airborne and sensor. For this purpose, a Global Positioning System (GPS) receiver and an Inertial Measurement Unit (IMU) are both installed on the LiDAR system (Habib *et al*., 2005; Reutebuch *et al*., 2005; Webster and Dias, 2006; Pfeifer and Briese, 2007). The GPS receiver is used to record the aircraft trajectory and position in absolute coordinates, while the IMU unit measures the altitude of the aircraft (roll, pitch and yaw or heading) (Webster and Dias, 2006). Therefore, by synchronizing the information derived by the scanner, the IMU and the GPS, it is possible to determine the target location with high accuracy in three dimensional spaces (Liu, X. *et al*., 2007).

The three main components that typically compose an airborne LiDAR system are shown in Fig. 3.1: a laser scanner unit, a GPS receiver and a IMU (Habib *et al*., 2005; Reutebuch *et al*., 2005; Webster and Dias, 2006; Pfeifer and Briese, 2007).

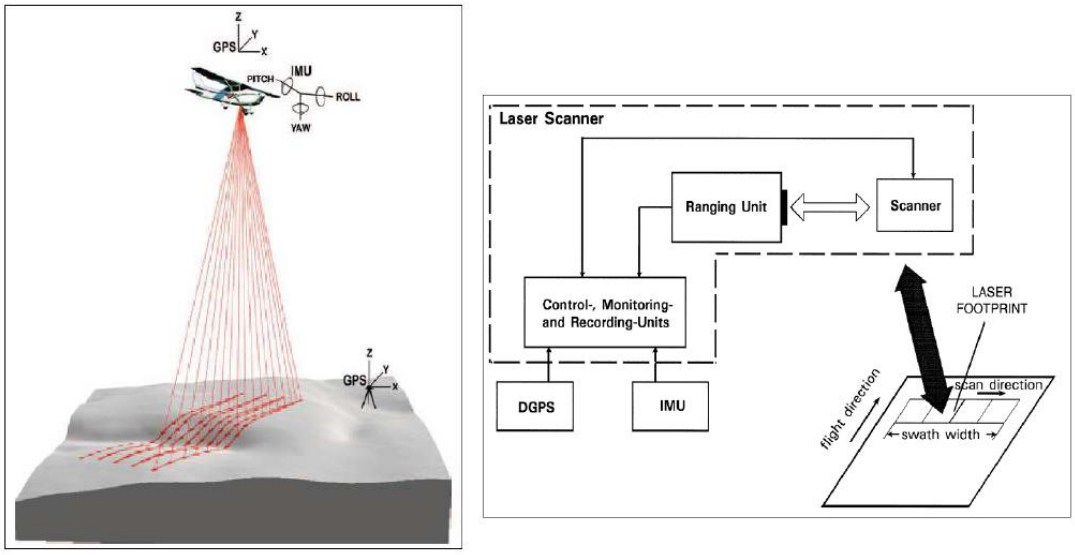

Fig. 3.1 LiDAR schematic, showing scanning laser unit and scan patterns on the ground (red), and aircraft positioning and altitude measurement systems (Carrier-phase DGPS for aircraft position and an inertial measurement unit –IMU- for recording pitch, yaw, and roll of the aircraft) (Reutebuch *et al*., 2005; Wehr and Lohr, 1999).

The laser scanner unit consists of a pulse generator of laser with a wavelength in the range of 0.8 μm to 1.6 μm and a receiver to get the signal of scattered and reflected pulses from targets (Wehr and Lohr, 1999; Mukai *et al*., 2006; Pfeifer and Briese, 2007).

Several types of lasers exist according to different wavelength ranges in which they operate. The 600-1000 nm lasers, are the most common for non-scientific applications. They are inexpensive, but since they can be focused and easily absorbed by the eye, the maximum power is limited by the need to make them eye-safe. A common alternative, 1550 nm lasers, are eye-safe at much higher power levels since this wavelength is not focused by the eye, but the detector technology is less advanced and so, these wavelengths are generally used at longer ranges and lower accuracies. They are also used for military applications as 1550 nm is not visible in night vision goggles, unlike the shorter 1000 nm infrared laser. Airborne topographic mapping LiDARs generally work at 1064 nm frequency, while bathymetric systems generally use 532 nm frequency, because 532 nm penetrates water with much less attenuation than does 1064 nm (Cracknell, Arthus P.; Hayes, Ladson 2007). The overall vertical system accuracy is usually in the dm order and is related to the accuracy of GPS and IMU. Airborne GPS is able to yield results in 5 cm horizontally and 10 cm vertically, while IMU can generate attitude with accuracy within a couple of centimeters (Liu, 2008). Some laser scanning systems provide, in addition to range, information on the intensity of the recorded signal (range, and in some cases, also amplitude) for multiple echoes within one pulse (Wehr and Lohr, 1999; Charaniya *et al*., 2004; Reutebuch *et al*., 2005). Recording multiple returns is quite useful for the topographic mapping in forested areas or for the description of forest stand and structure (Sheng *et al*., 2003), and it is of great advantage in mountainous environments.

Another improvement of this technology is given by the integration of a high-resolution digital camera or video camera with a LiDAR system (Ackermann, 1999; Ahlberg *et al*., 2004). This combination constitutes an effective fusion with photogrammetry, from a methodical and technological point of view.

The high measuring rate of laser scanning is of particular importance. Present measuring rates lie between 2 kHz and 25 kHz. Accordingly, from 1000 m flying height, the sampling densities on the ground range from about 1 point per m^2 up to 20 points to m^2 (Ackermann, 1999).

LiDAR technology has application in geomatics, archaeology, geology, seismology, forestry and especially in geomorphology. In fact, LiDAR data have become a major source of digital terrain information (Raber *et* al., 2007), and terrain modeling has been the primary focus of

most LiDAR surveys (Hodgson *et al*., 2005). The most valuable characteristic of this technology, in fact, is its capability to produce sub-meter resolution Digital Terrain Models (DTMs), and high-quality land cover information (Digital Surface Models, DSMs) over large areas, providing new tools for earth surface processes analysis (Tarolli *et al*., 2009).

3.2 DIGITAL TERRAIN MODELS

An accurate representation of landscape morphology is a strategic tool in the analysis of natural processes, environmental planning, landscape evolution and support to environmental political decisions.

There has been a significant increase in the use of LiDAR data for Digital Elevation Models (DEM) generation over the last decade, as more reliable and accurate LiDAR systems are developed (Sithole and Vosselman, 2003). Lohr (1998) and Kraus and Pfeifer (1998) are pioneers who demonstrated the suitability of using airborne LiDAR for the generation of DEMs.

Digital elevation models have been developed to represent the terrain surface: the most common ones are the regular grid, usually square grid (DTM in raster format), the triangular irregular network (TIN), and the contour line model (Ramirez, 2006). The form of DEM used for this entire work is that of the regular grid Digital Terrain Model (DTM).

A DTM is a topographic model of the bare earth that can be manipulated by computer programs. In its simplest form, the raster format, it consists of a matrix of cells (or pixels) organized into rows and columns where each cell contains a constant elevation value. Vegetation, buildings and other man-made (artificial) features are removed digitally, leaving just the underlying terrain. On the other hand, Digital Surface Models (DSMs) are digital representations of a surface which include whatever is present on the bare ground (Fig. 3.2).

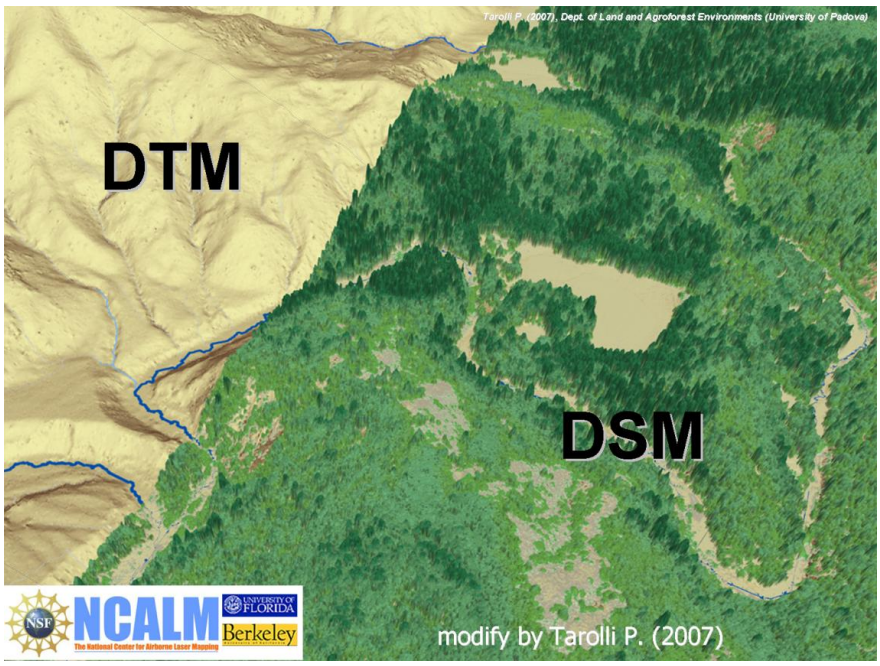

Fig. 3.2 Differences between DTM and DSM (Tarolli, 2008c).

DTMs are mostly represented in Cartesian coordinate system – i.e. x, y, z, though there are some DTMs presented in geographic coordinate system – i.e. angular coordinates of latitude and longitude. An important characteristic of DTMs is that they are geo-referenced. The geo-referentiation is defined by the ordering of elevation values within the matrix, whose structure implicitly records topological relations between data points (El-Sheimy *et al*., 2005). The widespread use of such grid models for morphological quantification is mainly due to the fact that the matrix form is the simplest and the most efficient approach in terms of storage and manipulation (El-Sheimy *et al*., 2005; Ramirez, 2006; Ziadat, 2007). In fact, the main advantages of storing data as a raster are as follows:

- a simple data structure;
- a powerful format for advanced spatial and statistical analysis;
- the ability to represent continuous surfaces and perform surface analysis;
- the ability to perform fast overlays with complex datasets.

On the other hand, TIN are a form of vector-based digital geographic data and are constructed by triangulating a set of vertices (points). The vertices are connected with a series of edges to form a network of triangles. There are different methods of interpolation to form these triangles, such as Delaunay triangulation or distance ordering.

The edges of TINs form contiguous, non overlapping triangular facets and can be used to capture the position of linear features that play an important role in a surface, such as

ridgelines or stream courses. Because nodes can be placed irregularly over a surface, TINs can have a higher resolution in areas where a surface is highly variable or where more detail is desired, and a lower resolution in areas that are less variable. The input features used to create a TIN remain in the same position as the nodes or edges in the TIN. This allows a TIN to preserve all the precision of the input data while simultaneously modeling the values between known points. However, TIN models are less widely available than raster surface models and tend to be more expensive to build and process. The cost of obtaining good source data can be high, and processing TINs tends to be less efficient than processing raster data because of the complex data structure. TINs are typically used for high-precision modeling of smaller areas, such as in engineering applications, where they are useful because they allow calculations of planimetric area, surface area, and volume. The maximum allowable size of a TIN varies relative to free, contiguous memory resources. Ten to 15 million nodes represents the largest size achievable under normal operating conditions with Win32. Regardless, it's strongly recommended to cap the size at a few million for the sake of usability and performance.

Returning to DTM description, it is important to focus the attention on its quality assessment because it strictly influences the quality of spatial analysis (Burrough and McDonnell, 1998). Generic quality if a DTM can consist of many factors, as for example in the accuracy of the DTM in respect to the input points (interior quality), or its accuracy related to external control data (exterior quality) (Briese, 2010). The common techniques for quality assessment are based on the statistical comparison of small reference areas of higher quality with the created DTM in order to find outliers. More specifically, the features which have an impact on DTMs accuracy are the point density and terrain slope (Karel and Kraus, 2006), the ratio of point resolution to grid resolution and the distance between each point and its nearest neighbor (Briese, 2010). Concerning this, interpolation methods try to make the DTM accuracy as high as possible in relation also to the kind of surface in consideration. Interpolation is made of a set of spatial analyst functions that predict values for a surface from a limited number of sample points, creating a continuous raster. The assumption that makes interpolation a viable option is that spatially distributed objects are spatially correlated; in other words, things that are close together tend to have similar characteristics. There is a variety of available interpolation methods and researchers have tried to evaluate which of them is the most appropriate and accurate. (Zimmerman *et al.*, 1999). Figure 3.3 shows (in profile) different examples of ways in which adjacent grid values can be used to imply a continuous surface.

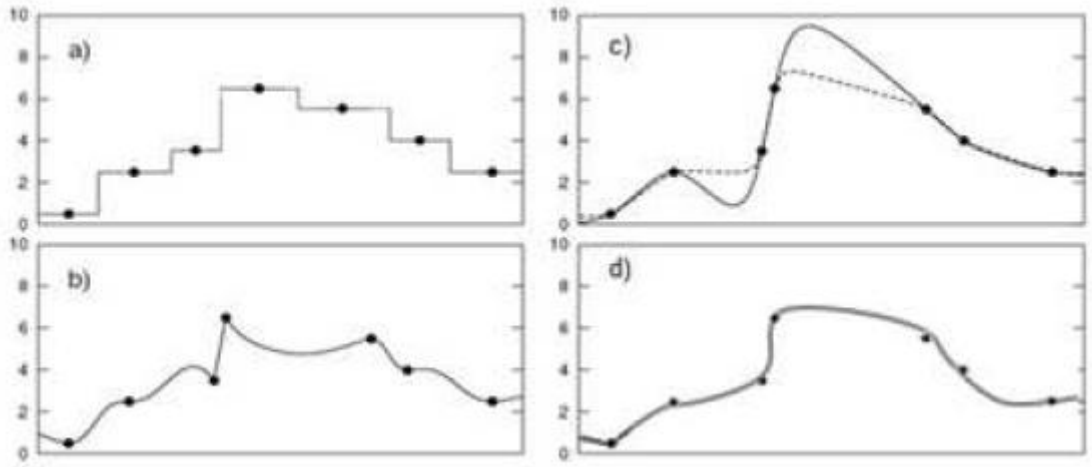

Fig. 3.3 Comparison of different interpolation methods for a one-dimensional example: (a) Proximal interpolation; (b) inverse distance squared; (c) spline interpolation; (d) quadratic interpolation (modified by Grayson and Bloschl, 2001).

Some of the most common interpolation methods are reported in succession.

Natural neighbor interpolation technique (Sibson, 1981) is, for example, an appropriate method for calculating a grid of values from data which can be both regular, clustered or random combinations of distributions of points. The first step is a triangulation of the data by Delauney's method, in which the apices of the triangles are the sample points in adjacent Thiessen polygons. The triangulation is unique except where the data are on a regular rectangular grid. To estimate the value of a point, it is inserted into the tessellation and then, its value is determined by sample points within its bounding polygons. For each neighbor, the area of the portion of its original polygon that became incorporated in the tile of new point, is calculated. These areas are scaled to sum to 1 and are used as weights for the corresponding samples (Webster and Oliver, 2001). Then, inverse distance weighting (IDW) technique (Shepard, 1968) is a method that estimates the values of an attribute at unsampled points using a linear combination of values at sampled points, weighted by an inverse function of the distance from the point of interest to the sampled points. The assumption is that sampled points closer to the unsampled point, are more similar to it than those further way in their values (Li J. and Heap D.A., 2008). Weights diminish as the distance increases, so nearby samples have a heavier weight and have more influence on the estimation (Isaaks and Srivastava, 1989).

The splines consist of polynomials that describe pieces of a line or surface and are fitted together so that they join smoothly (Burrough and McDonnell, 1998; Webster and Oliver, 2001), and the local trend surfaces (LTS) fit a polynomial surface for each predicted point,

using the nearby samples (Venables and Ripley, 2002). In the end, kriging technique (Matheron, 1960) is a method of interpolation which predicts unkown values from data observed at known locations. It uses variograms to express the spatial variation and it minimizes the error of predicted values which are estimated by spatial distribution of the predicted values.

Although a great variability of interpolation methods exists, there seems to be no single interpolation method that is universal for all kinds of data sources or purposes. For example, linear interpolation of contour lines can create ramps (Hutchinson, 1988), spline interpolation can create deep pits (Wood, 1996), and inverse distance weighting interpolation can create terraces (Burrough and McDonnell, 1998).Focusing again on DTM, another important point to consider is that there is also an implicit scale of analysis implied by the grid resolution. The bigger is the cell size, the more general is the approximation of the terrain surface representation, and so, the lower is the resolution (Ramirez, 2006). The general idea is to select a resolution that produces best predictive properties without giving computational constraints. In general a grid DTM is commonly over-sampled in low relief areas and under-sampled in high relief areas (Hengl *et al*., 2003). In order to increase the details of the terrain representation, the sample point density must be raised while the cell size reduced. Another loss in the quality of DTM is caused by the automatic filtering processes applied to LiDAR raw data (Jones *et al*., 2007; James *et al*., 2007; Cavalli *et al*., 2008a). This fact greatly influences the representativeness of the derived DTM for morphological characterization of processes, in fact, small errors in elevation may produce large errors in derived values, especially second-order derivatives such as curvature (Florinsky, 2002; Wise, 1998).

3.3 MORPHOLOGICAL REPRESENTATION OF SURFACES

DTMs are most valuable as a basis for the extraction of terrain-related attributes and features. Information may either be deduced by visual analysis through visualization, or by quantitative analysis trough interpretation. The objective of DTMs interpretation is the derivation of geomorphometric parameters. The procedures required to extract hydrogeomorphic or anthropogenic features are continuously implemented by commercial geographic information systems (GIS). Morphometric analysis of surfaces has been widely applied in order to relate morphology to hydrological processes at different scales. It is absolutely unthinkable to quantitatively represent topography and processes, without taking into account the scale-

dependence of such phenomena. Both hydrology and geomorphology deal with nature through processes, interactions and implications on a variety of scales (Sivapalan, 2005), and the concept that "scale matters" has been highlighted by a lot of studies both in hydrology (e.g. Bloschl and Sivapalan, 1995; Vogel and Roth, 2003; Sivapalan, 2005) and geomorphology (e.g. Evans 1972, 1979; Dodds and Rothmnan, 2000; Shary *et al*., 2005). Processes that are important at one scale are not necessarily important at other scales (Sivakumar, 2008), and dominant processes change within changing scales (Grayson and Bloschl, 2001). Several studies have revealed how different physical factors exert dominant controls in different geomorphic regions that can be addressed ad local scale, hillslope scale and catchment scale (Fig. 3.4).

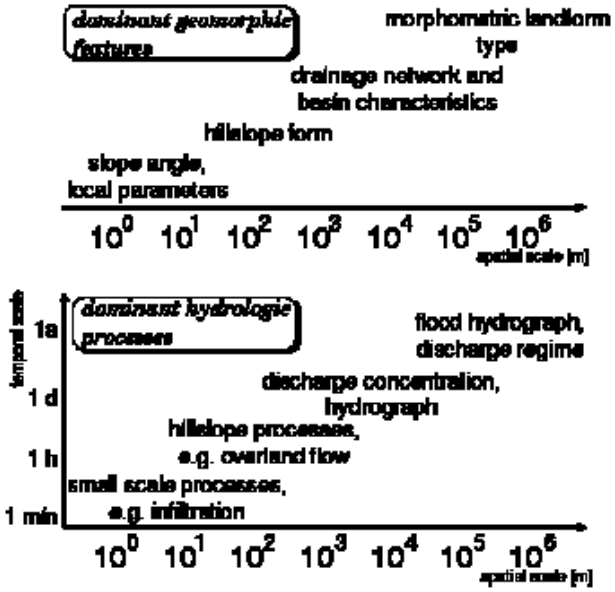

Fig. 3.4 Scales in hydrology and geomorphology: dominant features of each discipline in a spatial and temporal context (Anderson and Burt, 1978)

The main tool for morphometric analysis is the approach to topographic attributes. Moore *et al*., (1991, 1993) described terrain attributes and divided them into categories: primary and secondary or compound attributes (Tab. 3.1). Primary attributes are directly computed from elevation data and include variables such as elevation, slope, aspect, curvature etc. Secondary or compound attributes involve combinations of the primary attributes such as upslope area accumulation, wetness index etc.

Table 3.1 Geomorphometric parameters and objects on different scales (Moore *et al.*, 1991).

Primary morphometric parameters	Simple primary morphometric parameters	Slope Angle β Vertical Curvature ω_v Horizontal Curvature ω_h
	complex primary morphometric parameters	Flowlength l Flowaccumulation a Slope of downslope flowpath
	compound primary morphometric parameters	$ln(a/tan\beta)$ $ln(tan\beta/l)$ $a \cdot tan\beta \cdot \omega_h$
Morphometric objects	linear objects	flowpaths thalweg networks slopes
	areal objects	form elements catchments landform units
representative morphometric parameters	dimension parameters	object length or width, object area circularity elontation ratio
	relief parameters	statistic measures of primary parameters slope of 63ong est flowpath hypsometric integral portion of high curvature average height index of relief thickness (average height/area)

Questions as in what the optimum scale is to apply to evaluate parameters have been raised (Pirotti and Tarolli, 2010; Tarolli *et al.*, 2010; Sofia *et al.*, 2010), and the question is still open, as in if these indicators can also be suitable in anthropogenic landscapes.

3.3.1 MORPHOMETRIC INDICATORS

3.3.1.1 Slope

Slope is the first surface derivative of terrain elevations (DTM), and for this reason it falls among the primary topographic attributes.

The DTM surface can be approximated through a bivariate quadratic function (Evans, 1979), where x, y, and Z are local coordinates, and *a* to *f* are quadratic coefficients (Eq. 4):

$$z = ax^2 + by^2 + cxy + dx + ey + f \quad (4)$$

The topographic slope can be identified as:

$$slope = \sqrt{\left(\frac{\delta z}{\delta x}\right)^2 + \left(\frac{\delta z}{\delta y}\right)^2} \quad (5)$$

This formula assumes that a plane surface can be placed at any point on the surface z(x,y) in such a way that it only just touches the surface: it is a tangential plane and relies on the notion of infinitesimally small distances. However, surfaces within GIS are typically modeled as grids, with a finite resolution. Therefore slope calculations will use approximations to the formula above depending on the surface model used, which is itself an appropriate representation of the true surface. Topographic slope coincides with the Standard Slope Function which is also known as the "*Horn method*", due to the researcher's name who developed it (Horn, 1981). The function calculates, for each cell, the maximum rate of change in value from that cell to its neighbors. Basically, the maximum change in elevation over the distance between the cell and its eight neighbors, identifies the steepest downhill descent from the cell. Conceptually, the Slope function fits a plane to the z-values of a 3 x 3 cell neighborhood around the processing or center cell. The direction the plane faces is the aspect for the processing cell. The lower is the slope value, the flatter is the terrain; the higher is the slope value, the steeper is the terrain. If there is a cell located in the neighborhood with a NoData z-value, the z-value of the center cell will be assigned to the location. At the edge of the raster, at least three cells (outside the raster's extent) will contain NoData as their z-values; to these cells will be assigned the center cell's z-value. The result is a flattening of the 3 x 3 plane fitted to these edge cells, which usually leads to a reduction in slope. The output slope raster can be calculated in two types of units, degrees or percent (Fig. 3.5).

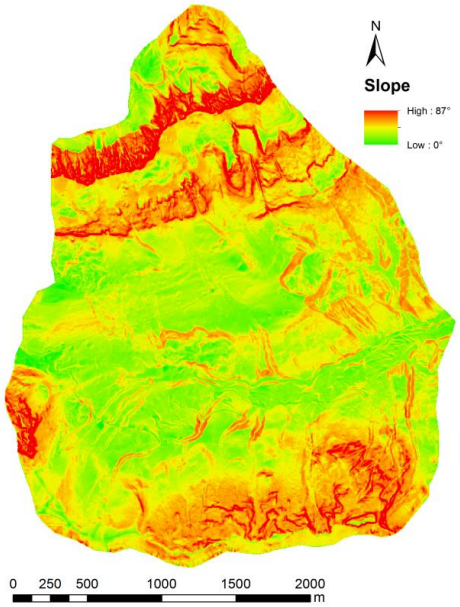

Fig. 3.5 Slope map of the Vizza watershed, a 8 km^2 river basin located in the Belluno province. The watershed is not included within the boundaries of the study area, but it has been reported only to show an example of a slope map. Darker red values correspond to higher values and thus, to steeper slopes.

3.3.1.2 Curvature

Curvature is a second spatial derivative of the terrain elevations and is a useful measure for the interpretation of dominant sediment transport processes on the landscape (Lashermes *et al*., 2007; Istanbulluoglu *et al*., 2008; Tarolli and Dalla Fontana, 2009). Total curvature is defined as the sum of both plan and profile curvature (Eq. 6). The expression is given as follows:

$$\nabla^2 z = \left(\frac{\delta^2 z}{\delta x^2} + \frac{\delta^2 z}{\delta y^2}\right) \qquad \mathbf{6}$$

The two most frequently calculated forms of curvature are profile and plan curvature (Gallant and Wilson, 2000). Plan curvature represents the degree of divergence or convergence perpendicular to the flow direction. Profile curvature represents the convexity or concavity along the flow direction. In general terms, divergent-convex landforms (Curv < 0) are associated with the dominance of hillslope/diffusion processes, while concave-convergent (Curv > 0) landforms are associated with fluvial-dominated erosion.

Considering the definition of curvature as a direct surface derivative, its computation requires the local surface to be approximated by some representative functions, with reference to a

coordinate system (x,y,z) (Evans, 1972; Horn, 1981; Zevenbergen and Thorne, 1987; Mitasova and Hofierka, 1993; Shary et al., 2002). Curvature is then found by differentiating the surface equation. In general, the most appropriate curvature form depends partly on the nature of the surface patch being modeled. Among the available approaches, Evans' (1979) method is one of the most suitable at least for first-order derivatives (Shary et al., 2002), it performs well in the presence of elevation errors (Albani et al., 2004; Florinsky, 1998), and it has been recently generalized by Wood (1996) to allow multi-scale characterization of curvature.

According to Evans (1979), differentiating Eq. 4 (Chapt. 3.3.1.1) it is possible to derive two measures of maximum (convexity) and minimum (concavity) curvature (terms between brackets in Eq. 7 and 8 respectively), and Wood (1996) proposed the generalization of these formulae for different window sizes (Eq. 7, 8):

$$\boldsymbol{C_{max} = n * g(-a - b + \sqrt{(a-b)^2 + c^2})} \quad \textbf{7}$$

$$\boldsymbol{C_{min} = n * g(-a - b - \sqrt{(a-b)^2 + c^2})} \quad \textbf{8}$$

where *g* is the grid resolution of the DTM, and *n* is the size of the moving window.

The Eq. (7) and (8) have been used for multi-scale terrain analysis (Wilson *et al*., 2007), and for morphometric feature parameterization (Eshani and Quiel, 2008; Sofia et al. 2011; Tarolli et al. 2012). A mean curvature (C_{mean}) derived from these two formulas has been used by Pirotti and Tarolli (2010) for channel network extraction. Cavalli and Marchi (2008) applied the same generalization procedure to plan curvature formulation, for the characterization of surface morphology.

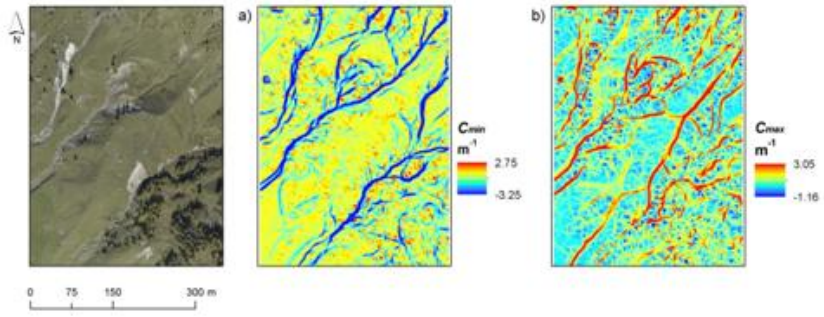

Fig. 3.6 Example of minimum (a) and maximum (b) curvature, and overview of the actual landscape on the area (Sofia, 2012).

3.3.1.3 Openness

A new approach recently developed is the DTM-based surface 'openness' by Yokohama *et al*., 2002, that expresses the dominance (exposure) versus enclosure of a location on an irregular surface. Positive openness is used to identify local convexities and it is equal to the mean zenith angle of all determined horizons while the negative one is based on nadir angles and is used to identify local concavities (Yokohama *et al*., 2002).

Topographic openness is computed as the average of either zenith (φ) or nadir (ψ) angles along eight azimuths D (0, 45, 90, 135, 180, 225, 270, and 315) within a radial distance L (Fig. 3.7, Yokohama *et al*., 2002). To perform terrain analyses maintaining homogeneity with curvature, openness can be evaluated considering an *n* x *n* moving window (Wood, 2009). Instead of a radial distance, pixels are processed if they belong to the considered neighborhood as a function of the window size.

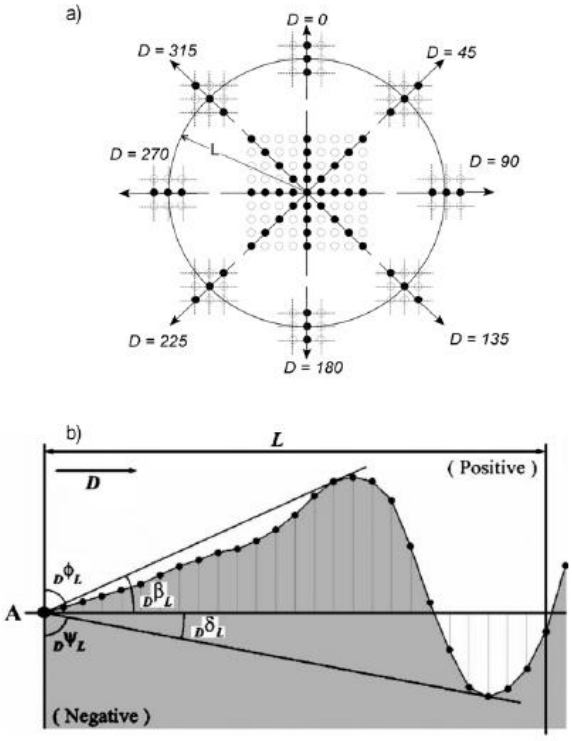

Fig. 3.7 a) Azimuths D (0, 45, 90, 135, 180, 225, 270 and 315) within a radial distance L; b) Openness for a location A, according to azimuth and nadir, considering a defined D. (modified from Yokohama *et al*., 2002).

Openness has also been used for surface characterization and visual assessment of landform (Prima *et al*., 2002; Cavalli *et al*., 2011) and for feature extraction (Sofia et al. 2011), because

it offers a clear vision of the landscape without constraints of the more classical hillshade (Fig. 3.8) (Sofia, 2012).

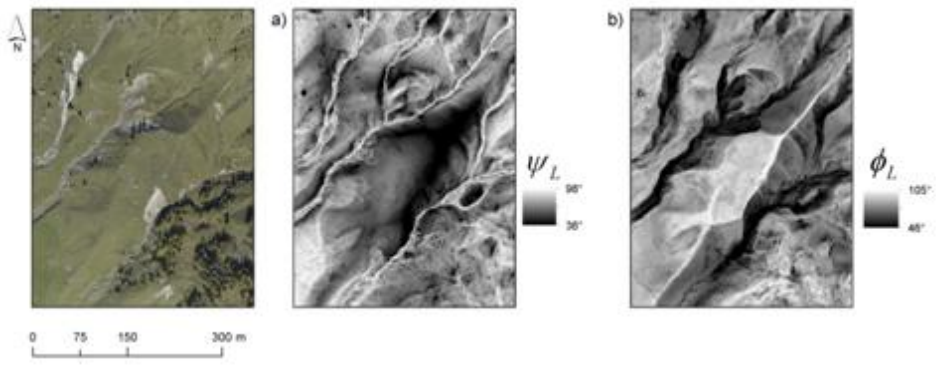

Fig. 3.8 Example of negative (a) and positive (b) openness (Sofia, 2012).

3.3.1.4 Elevation residuals

Sometimes, local variations in topography, such as changes in elevation from one cell to another, have an effect on the analyzed features. For this reason it is possible to consider the nature of each elevation point in relation to a wider context, as in the case of identifying elements that may have lower/higher values than their surroundings. This kind of approach does not take into account the hydrological connectivity of the surface topography, rather the relationship of a certain elevation point to the surrounding landscape (Wilson and Gallant, 2000). The mean elevation $\bar{z}$ is the element to consider as a reference against which to compare the elevation at the central point of the window:

$$\overline{z_w} = \frac{1}{n_w} \sum_{i \in w} z_i \qquad \textbf{9}$$

where n_w is the number of pixel within the considered neighborhood and z_i is the elevation at each pixel.

The difference between the elevation at the centre of the window and the mean elevation is a measure of the relative topographic position of the central point, and its range is influenced by the range in elevation within the size of the window. Using this terrain attribute for feature extraction means to apply a low-pass filter to the DTM, providing in this way a smoothed elevation model (Eq. 9) representing an approximation of the large-scale landscape forms. The difference between this smoothed map and the original DTM is an approximation of the local relief, where only small-scale topography features are preserved, in spite of large-scale

landscape forms. Concerning this, two models can be derived: the Relative Elevation Attribute (REA, Carturan *et al*., 2009) (Eq. 10, Fig. 3.9a), which represents a relative elevation map, and the other which represents a map of Residual Topography (Cavalli *et al*., 2008) (Eq. 11, Fig. 3.9b).

$$\boldsymbol{REA_w = \overline{z_w} - z_{DTMw}} \quad \textbf{10}$$

$$\boldsymbol{RT_w = z_{DTMw} - \overline{z_w}} \quad \textbf{11}$$

Where Z_{DTMw} is the elevation at the central pixel within the considered neighborhood (w) and $\overline{z_w}$ is the average elevation of cells within the same neighborhood according to Eq. 9 (Carturan *et al*., 2009; Humme *et al*., 2006; Hiller and Smith, 2008; Doneus and Briese, 2006; Cavalli *et al*., 2008).

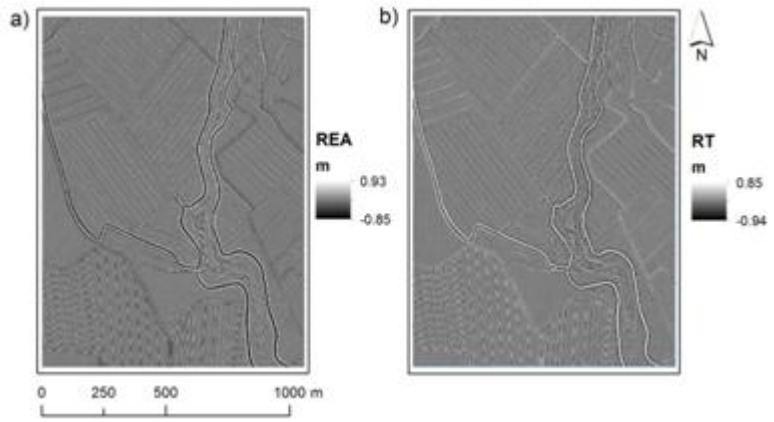

Fig. 3.9 Evaluation of REA (a) and Residual Topography (b) for a floodplain area (Sofia, 2012).

3.4 FEATURE EXTRACTION FROM LiDAR DTMs

Nowadays LiDAR DTMs covering large areas are readily available for public authorities, and there is a greater interest in the application of such information by agencies responsible for land management for the development of automated methods aimed at solving geomorphological and hydrological problems. Automatic feature extraction from LiDAR DTMs can greatly improve topographic databases and it is a useful tool for natural hazard mapping and environmental planning. In addition, it can solve some of the problems related to traditional mapping such as restrictions on access and time or cost issues.

For mountainous environments, the reliability of LiDAR data for the automatic extraction of features has been proven by numerous studies (Tarolli and Dalla Fontana, 2009; Passalacqua *et al*., 2010; Pirotti and Tarolli , 2010; Tarolli *et al*., 2010; Sofia *et al*., 2011). In engineered landscapes within floodplains, high resolution DTMs have mainly been used for hydrological modeling purposes (Cobby *et al*., 2001; French, 2003; Dal Cin *et al*., 2005). In particular, Cobby *et al*., 2001, for example, aimed to demonstrate the potential of LiDAR in improving flood modeling, with particular emphasis on river flooding. He focused on the application of the segmenter[1] to improve the data required by 2D hydraulic flood models, i.e. maps of topographic height which provide model bathymetry, and vegetation height, which can be converted to distributed floodplain friction coefficients. French 2003 considered the application of airborne LiDAR to the provision of elevation data accuracies and spatial densities commensurate with a numerical hydraulic model of a morphologically complex estuary in southeast England. His observations are consistent with the findings of Marks and Bates (2000) in their evaluation of airborne LiDAR as a means of characterizing the topography of river floodplains and the implications of improved topographic parameterization for the accuracy of flood prediction using hydraulic models. Dal Cin *et al*., 2005 argued about the importance of implemented airborne LiDAR data for the survey of valleys and floodplains.

Some other studies, rather focused on morphological aspects (e.g. Lohani and Mason, 2001; Challis, 2006; Challis *et al*., 2006; Nelson *et al*., 2006), but it remains a fact that anthropogenic feature extraction from DTM in such environments represents a challenge and is a relatively new field of application (Cazorzi et al. 2012). In this thesis, the feature extraction from DTM in mountainous environments is not applied, in that regard a general summary of the studies done, will be given in Chapt. 3.4.1. On the other hand, feature recognition in floodplains is tested for one type of feature: drainage networks, while levees and scarps are not considered, but a background context for both is presented (Chapt. 3.4.2).

[1] *The segmentation of LiDAR data is a crucial prerequisite for the modeling of surface objects. An advantage of segmentation is that allows different topographic and vegetation height extraction algorithms to be used in automatically delineated regions of different cover types.*

3.4.1 MOUNTAINOUS ENVIROMENTS

DTMs have been widely applied to derive hydrogeomorphic features by using primary topographic attributes such as slope, aspect, and curvature (Florinsky, 1998), and more recently a flourishing literature developed thanks to the availability of LiDAR DTMs (Passalacqua et al. 2010, Pirotti and Tarolli 2010, Sofia et al. 2011, Tarolli et al. 2012). One of the aims of Tarolli et al. 2012, for example, has been to automatically recognize landslides crowns and features related to bank erosion of debris-flow channels starting from a high-resolution LiDAR DTM. For this purpose, different methods introduced by Tarolli and Dalla Fontana (2009), Pirotti and Tarolli (2010), and Lashermes *et al*., (2007) have been tested and compared to different statistical analysis of variability to define objective threshold of landform curvature for feature extraction.

Considering drainage networks, their extraction from DTMs is one of the most important digital terrain analysis in mountainous environments. Traditionally, extraction methodologies are based on the flow routing model. There are numerous drainage algorithms which allow to compute drainage networks over the raster surface (O' Callaghan and Mark, 1984; Quinn *et al*., 1991; Tarboton, 1997; Orlandini *et al*., 2003). They generally follow the procedure of filling pits, computing flow directions, and computing the contributing area draining to each cell grid (Tarboton, 2003). Then, in order to convert a drainage flow path into a network, a unique contributing area or slope-area threshold can be used according to the so-called traditional approach (O' Callaghan and Mark, 1984; Band, 1986; Mark 1988; Tarboton *et al*., 1991; Montgomery and Dietrich, 1994; Dietrich *et al*., 2003; Dalla Fontana and Marchi, 2003). However, this approach seems not to manage to identify the actual channel head location, as it totally relies on the fact that flow direction is strictly dependent from the topographic surface (Orlandini *et al*., 2011). On the contrary, physical location of channel heads is not related just to topographic slope, but sometimes it also depends on other factors such as geomorphic processes involved, soil properties, climatic environment, land use, etc. (Montgomery and Dietrich, 1988; Prosser and Abernethy, 1996; Wemple *et al*., 1996; Beven and Kirby, 1979; McGlynn and McDonnel, 2003).

As a consequence of these mentioned observations, several studies emerged, pointing out that a robust delineation of stream networks cannot always be achieved by the popular steepest descent algorithm, and in some case studies, it should be based on direct detection of morphology in the DTM (e.g. Molloy and Stepinski, 2007; Lashermes *et al*., 2007; Tarolli and Dalla Fontana, 2009; Thonmeret *et al*., 2010; Pirotti and Tarolli, 2010; Passalacqua *et al*.,

2010 a,b; Sofia *et al*., 2011). At this regard, a large number of indexes, directly derived from LiDAR DTMs, exists to identify terrain convergences (Gallant and Wilson, 2000). Some of them have already been used for network characterization (Tarboton and Ames, 2011; Molloy and Stepinski, 2007; Lashermes *et al*., 2007; Tarolli and Dalla Fontana, 2009; Thrommeret *et al*., 2010; Pirotti and Tarolli, 2010; Passalacqua *et al*., 2010a,b; Sofia *et al*., 2011).

Tarboton and Ames (2001) proposed the use of a proxy of curvature deriving from the Peuker and Douglas (1975) algorithm to account for spatially variable drainage density. Upwards curved grid cells have been used by other authors to derive channel networks from DTMs (Band, 1986; Gallant and Wilson, 2000). In order to define valleys and portions of probable channelized areas within the valley, Lashermes *et al*. (2007) used Wavelet analysis to locally filter LiDAR data and to detect threshold of topographic curvature and slope-direction change. Curvature maps derived from LiDAR DTMs have been used by Tarolli and Dalla Fontana (200) and Pirotti and Tarolli (2010) to assess the capability of high resolution topography for the characterization of convergent hollow morphology of channel heads and for channel network extraction respectively.

The referenced studies dealt with a prior assessment of the input data (Thommeret et al., 2010), calibration of the kernel size by interactively testing its effectiveness related to the investigated features (Pirotti and Tarolli, 2010), fixed arbitrarily chosen scales to evaluate topographic parameters (Tarboton and Ames, 2001; Molloy and Stepinski, 2007; Tarolli and Dalla Fontana, 2009; Passalacqua et al., 2010a,b). Some open questions still remain, as in how to identify thresholds that are not data-driven and how to objectively select scale without calibrating it on results and without considering a previous analysis of the data and of the study area. At this regard, Sofia et al. (2011) proposed a methodology relatively independent of the input dataset or from the size of the analyzed features. The approach is based on normalized topographic attributes, such as openness (Yokoyama et al., 2002; Prima et al., 2006) and minimum curvature (Evans, 1979) as a weight for the upslope area. The identification of the optimum scale to use to evaluate topographic parameters is based upon distribution analysis and statistical thresholds.

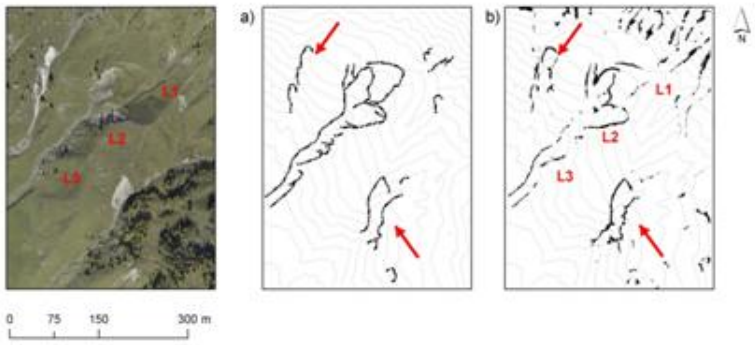

Fig. 3.10 Example of feature extraction from DTM in mountainous environments (modified from Tarolli *et al*., 2012).

3.4.2 ENGINEERED LANDSCAPES

Feature extraction from DTM in engineered landscapes is a relatively new field of application, considering that works in these areas are generally of a modelistic type.

A first method to identify artificial network reaches in agrarian landscape directly from the LiDAR point cloud has been assessed for example by Bailly *et al*., (2008). However, their approach had two main requirements:

- ditches are exclusively located at field boundaries;
- a geographic database of plot boundaries must be available.

These two requisites make the method not applicable for large scale applications in the Italian context, where a dense in-field network exists, the official cartography cannot be considered as a valid up-to-date network database, and field surveys are cost-prohibitive and time-consuming. In a floodplain context, problems for network extraction arise because the ability with which a DTM is able to detect a drainage network depends on the strength of the landscape gradient (i.e. flatness and/or slope changes). Low-relief areas are therefore, challenging even when high-resolution DTMs are available. For these contexts, drainage algorithms used on DTMs are unable to represent anthropogenically modified overland flow paths (Duke *et al*., 2006; Garcia and Camarasa, 1999). In such cases, the detection of the network benefits from morphological approaches, whereas channelized elements are defined by local morphologies, and hydrological connectivity is not accounted for.

This work applies the morphometric methodology based on high-resolution DTMs proposed by Cazorzi *et al*., 2011, in order to (1) detect the drainage networks, especially ditches and channels in agrarian contexts, and to (2) calculate some of the network summary statistics (i.e. network length, width, drainage density and storage capacity per unit of interest).

Other type of engineered feature (levees and scarps) can be found in floodplains: such features result to be hybrid objects, because they are man-made on one hand, and on the other hand, they are considered as belonging to the earth surface (Kruger and Meinel, 2008). A technique of extracting banks information from LiDAR DTMs has been investigated by Kruger and Meinel (2008). In their work, the authors proposed method to label pixels as banks when their height exceeds a certain threshold defined by flood alert levels considering dikes height. Kothe and Bock (2009) studied a way to post-processing DTMs in order to extract man-made features and rebuild the natural surface. In the work made by Sofia (2012), three different topographic parameters have been tested to verify their suitability for feature extraction in engineered landscapes. Both the parameter introduced by Tarolli *et al*., (2010), and an approach similar to the one proposed by Kruger and Meinel (2008), Kothe and Bock (2009), Carturan *et al*., (2009), Humme *et al*., (2006), Hiller and Smith (2008), Doneus and Briese (2006), have been applied. In addition, a new parameter based on a measure of randomness of surface has also been proposed.

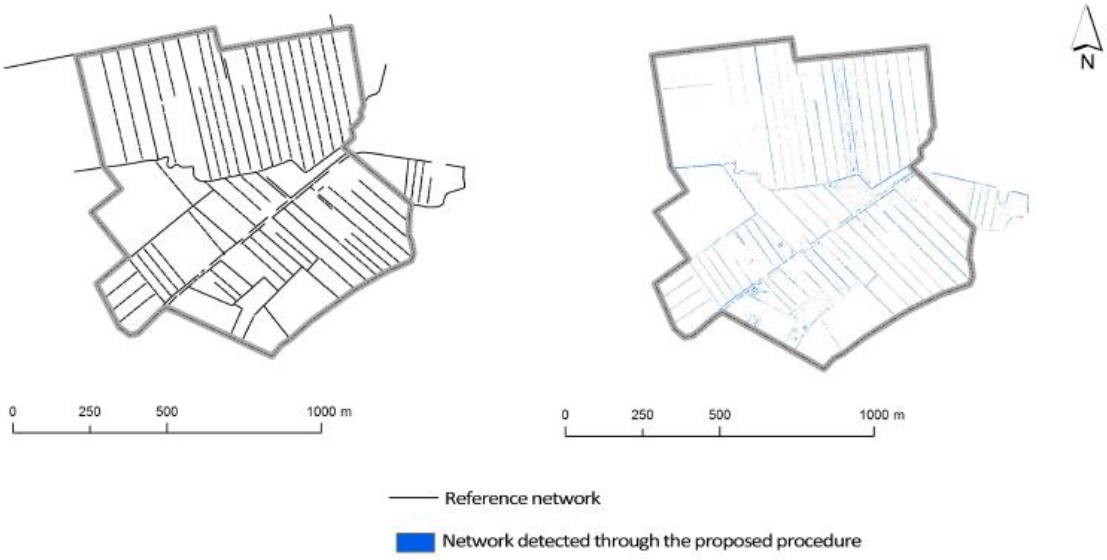

Fig. 3.11 Example of feature extraction from DTM in engineered landscapes (modified from Cazorzi *et al*., 2012)

4 METHODOLOGY

The chapter provides the detailed description of the methodology followed for this thesis. The whole procedure is based on a two-steps approach:

1) the application of the morphometric methodology developed by Cazorzi *et* al. (2012), relying on high-resolution DTMs in order to i) detect the drainage networks (ditches and channels) in agrarian/floodplain contexts, to ii) calculate some of the network summary statistics (network length, width, drainage density and storage capacity per unit of interest), and to iii) analyze them in relation to the areas that flooded during the flood event in Veneto from October, 31st to November, 2nd 2010 (See Chapt. 4.1.);
2) the application of the Soil Conservation Service Method (Chapt. 4.2) in order to i) compute the surface runoff produced by the main rainfall event considering three different land use and, to ii) evaluate the effect of the storage capacity of the drainage network system on the produced runoff.

The whole procedure starts from a LiDAR DTM (1m resolution) readily available for public authorities in Italy and it is applied to the study site described in Chapt. 5. This DTM has been realized within the "*Piano Straordinario di Telerivelamento Ambientale (PST-A)*" (Extraordinary Plan of Environmental Remote Sensing, EPRS-E) thanks to the cooperation of the Ministry of Environment and Territory of the Sea (METS), Chairperson of the Council of Ministers – Department of Civil Protection (DCP), the Ministry of Defense (MD), the Regions and Autonomous Provinces. The aim of this Plan is to undertake, for the first time, the establishment of a data base representative of national territory, with particular emphasis on its configuration, its relation to the environment. In particular, the project involves the acquisition by the Ministry of data produced by remote sensing technique with laser scanning LiDAR (by platform) and interferometric technique (by satellite) and the classification of these data in the database of National Geoportal (NG). The first aim of the EPRS-E is to create, as quickly as possible, a database to support decision making in all areas subject to hydrogeological risk and encourage the sharing of a "data set" off methodologies and results.

4.1 DRAINAGE NETWORK EXTRACTION AND CHARACTERIZATION

The first step of the approach can be divided in two parts:

1) from a high resolution DTM, the network is automatically detected and, always in an automatic fashion, a width and a length indexes are computed. From these indexes, network length and network drainage density are computed directly;
2) in a second step, by associating some characteristic cross-section areas to specific width ranges, it is possible to derive the network storage capacity.

While the first step is completely automatic, the second one requires the user to identify roughly some width ranges and cross section shapes. Once these are defined, the network storage capacity is evaluated automatically. The procedure does not consider a hydrological characterization: neither the connectivity of the network nor the flow directions are accounted for. The width and length indexes are evaluated directly from a raster map, without any skeletonization process. This because even if algorithm for such operations are available in many GIS, they usually produce highly irregular skeletons that are a poor representation of the channel itself (Cazorzi et al. 2012).

However, considering the DTM has a constraint all over the map due to the grid size (1m), two assumptions must be underlined: 1) this constraint makes inapplicable the reading of cross section geometry directly on the DTM, but it allows an approximation of the ditches widths, considering that their minimum width is about 1 m (equal to the DTM grid size); 2) an exact local characterization of the ditches is not expected, rather the purpose is a characterization of the network for each considered drainage unit (Cazorzi et al. 2012).

In agrarian landscapes, ditches and channels are usually linear and regularly distributed features, as it can be seen from figures 4.1 and 4.2.

Fig. 4.1 Example of the distribution of ditches in the Po Valley (Vittorio L., 2009).

Fig. 4.2 Other example of the distribution of ditches in the floodplain of the Veneto region (Google Earth, 2012).

They are commonly low 'amplitude' elements, considering amplitude as the difference in relief between low points on the ditch and height areas to either side. The main purposes are therefore to extract local small-scale, low-relief features from DTM avoiding as far as possible the large-scale landscape forms from data.

The considered parameter is the REA (Chapt. 3.3.1.4, eq. 10) (Carturan *et al.*, 2009) and such choice is done considering the various digital terrain analysis assessments made by Sofia (2012). In fact, in order to find out which topographic parameter was the one which best recognized the drainage network, she made a comparison between Maximum Curvature,

Entropy[2] and Residual Topography. The evaluation of the above-mentioned topographic attributes, has been made by comparing the automatically extracted features with the field surveyed ones, used as reference data, and by calculating some quality measures: Cohen's *k* index of agreement[3] (Cohen, 1960), Correcteness[4], Completeness[5], and Branching [6](Heipke *et al*., 2007; Lee *et al*., 2003). The results obtained make Residual Topography the most suitable topographic attribute for the floodplain context (Sofia, 2012).

In order to extract the drainage network based on relief control, prior to local relief evaluation, it is necessary to identify and mask some man-made terrain features on the original DTM, at least where their density is high (Cazorzi et al. 2012). These artificial elements i) may greatly affect the recognition procedure by increasing false detections and peak values on the relief index; ii) in the case of urban areas and mountains, they do not present a minor network and applying the computation to them would result only in an increasing computational time, without any significative results; iii) in case of roads, the presence of embankments and barriers would create bias due to peaks in the relief index; iv) major rivers are not considered because topographic information about them are generally available, and the presence of artificial embankments would result in bias for the extraction procedure.

At this purpose, once downloaded the land uses of the study area, those parts where man-made features were very dense such as urban, residential and industrial areas and roads have been selected according to the different level codes of land use (Corine land Cover codes 1, 4 and 5). The land-use data are updated to the year 2006 and have been produced by the CORINE land cover project. Such information is freely distributed by the Regione Veneto, through their geographic portal (http://idt.regione.veneto.it/app/metacatalog/). To these portions, the main rivers have been added. Finally, considering that i) the procedure is based on the identification of the local relief, ii) the procedure aims at the identification of the artificial drainage network, hilly or mountainous areas have been included in the mask (such as the area of the Regional Park of Colli Euganei). The mask obtained is shown in Fig. 4.3.

---

[2] *A further topographic parameter that can quantify attributes of terrain, offering a measure of the elevation organization and its degree of randomness (Sofia 2012).*

[3] *It is an index of agreement ranging from 0 (level of agreement due to chance alone) and 1 (perfect agreement).*

[4] *It is related to the probability of an extract linear piece to be indeed a scarp or a levee; it is a measure of the accuracy of the correctly extracted features. It ranges between 0 and 1, where 1 represents a perfect extraction.*

[5] *It expresses how much is missing of the features of interest. It ranges between 0 and 1, where 1 represents a perfect extraction.*

[6] *It offers a measure of the overestimation of the extractions. It ranges from 0 to + ∞, where 0 represents perfect extractions.*

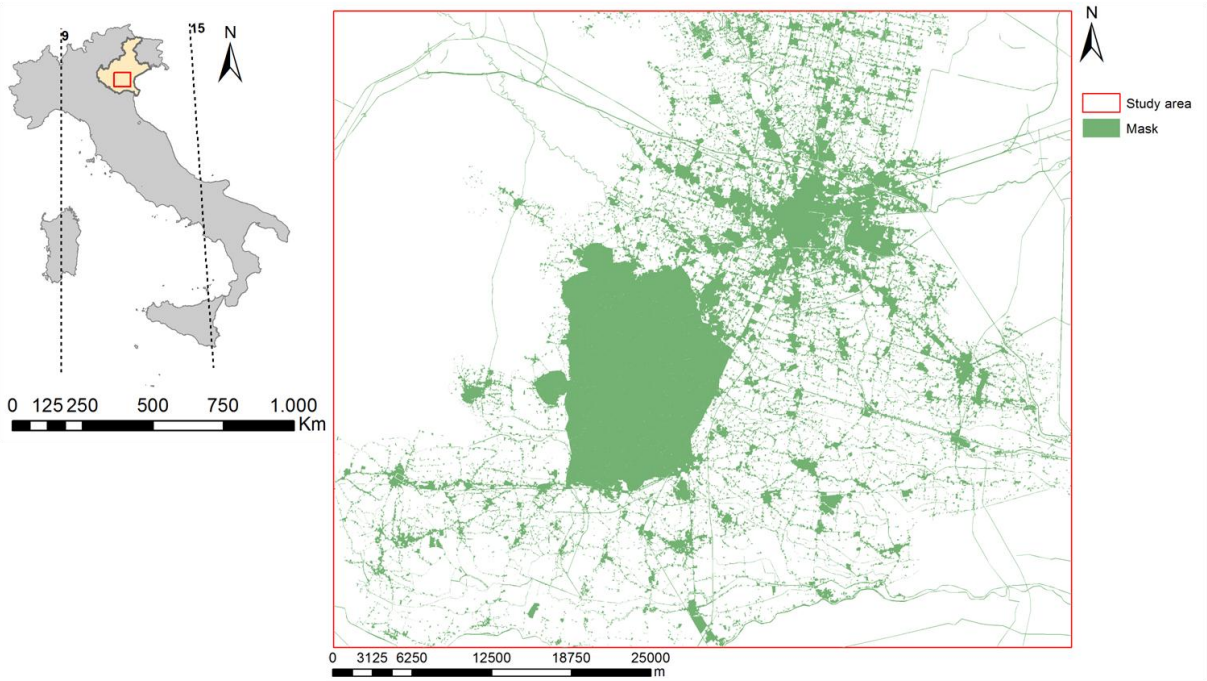

Fig. 4.3 Identification and mask of the areas where the man-made features are very dense. The big green polygon corresponds to the boundaries of the Regional Park of Colli Euganei.

Once created the mask, the available DTM (1m resolution) has been loaded and divided into numerous sub-areas of 500 x 500 m, in order to better highlight the variability of the drainage networks statistics and to increase the speed of the elaborations. The area covered by digital elevation data does not completely coincide with the borders of the study area (Fig. 4.4); because the DTM only covers those portions characterized by man-made ditches and highly modified channels. As all the analysis, that will be described in succession, require the support of elevation data, the effective study area ends up coinciding with the one where DTM is present. As already reported, the novelty of this thesis has been to apply the drainage network recognition methodology to a very wide area (180 000 ha). As a matter of facts, for the first time, this kind of analysis has been done at a regional scale

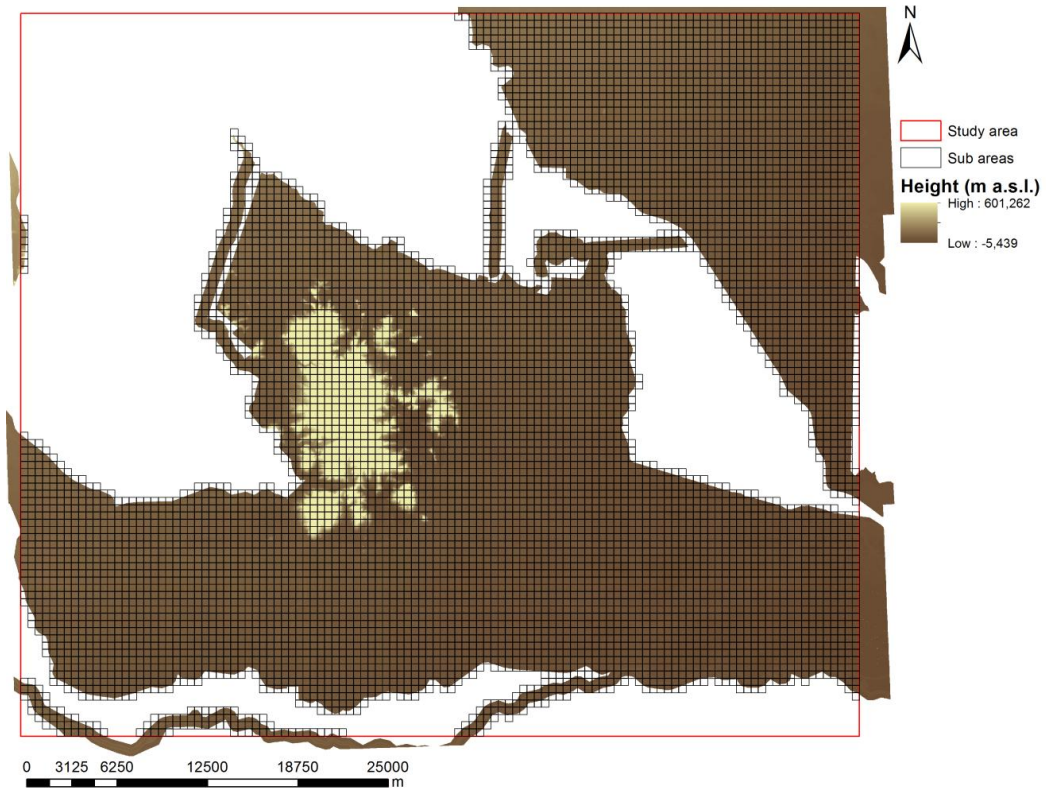

Fig. 4.4 Subdivision of the DTM into numerous sub-areas. The DTM does not entirely fill the study area

Once the DTM has been roughly masked, Eq. 9 and 10 are applied. Figure 4.5 shows an example of the procedure: the input DTM is shown in (a) and on it, some narrow linear elements corresponding to the drainage network system are visible. In fig. 4.5b, the derived REA map is presented highlighting the network features with higher values of the parameter. In order to further recognize the network, a thresholding approach has been applied to label the REA peak values. This approach is based on the fact that different processes leave their signature on the statistical properties of landform geometry, and by quantifying and labeling these signatures in detail, it is possible to identify a threshold to label where a process starts (Lashermes *et al*., 2007; Tarolli and Dalla Fontana, 2009; Passalacqua *et al*., 2010a,b; Tarolli *et al*., 2010; Pirotti and Tarolli, 2010; Sofia *et al*., 1022; Sofia 2012). In this case, the chosen threshold is the standard deviation of REA (Fig. 4.5). The result (Fig. 4.5c) is represented by a boolean map with features taking only binary values, 1 or 0 for network pixels and landscape

pixels respectively.

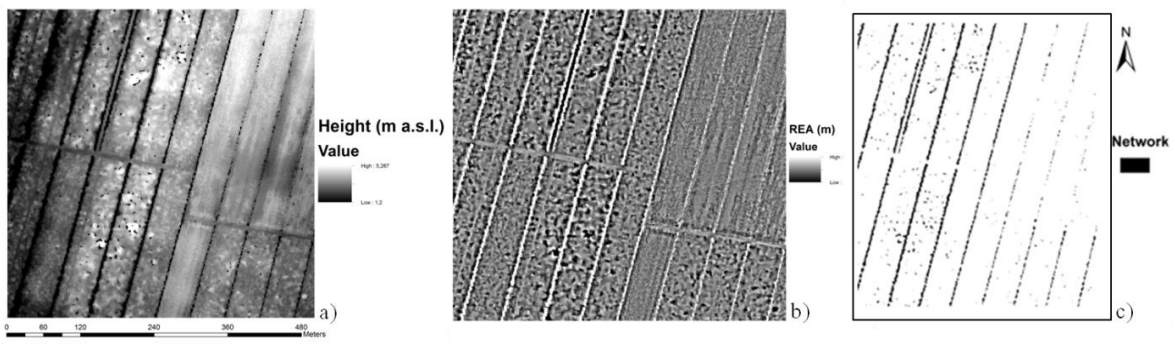

Fig. 4.5 Input DTM (a), derived REA map (b), and the boolean map detecting the drainage network derived after the thresholding approach (c)

Once the network is identified, the attention shifts to its geometrical characterization, thus to the calculation of some geometric parameters such as the network width index (W_{index}) and length index (L_{index}) (Cazorzi et al. 2012). The procedure starts from the Boolean map (fig. 4.5c). This map is composed by clusters of pixels (groups of connected cells having the same value). Each cluster does not necessarily correspond to a single network reach: multiple reaches with different geometries might be included as long as they're connected one to the other. Figure 4.6 shows an example of two different clusters: cluster B represents a single ditch with a specific and constant width, while cluster A includes two ditches with different widths.

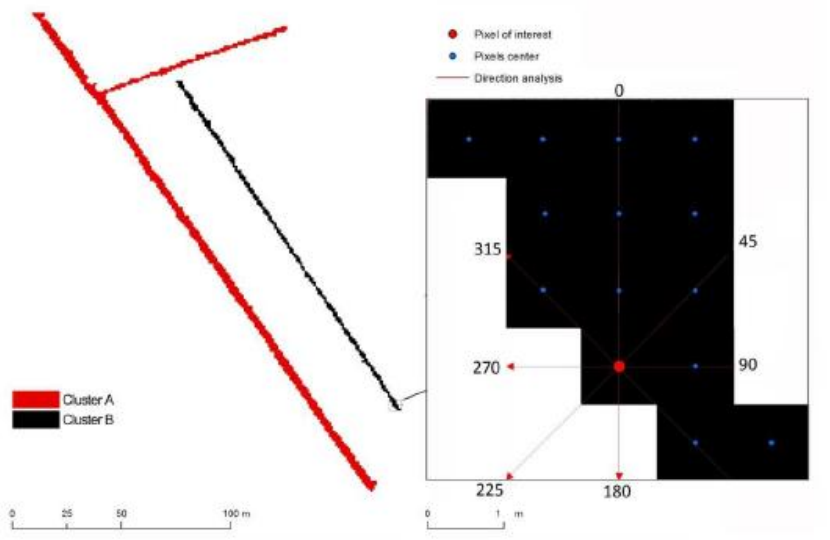

Fig. 4.6 Clusterization approach and cluster parameters evaluation. Cluster A is composed by reaches with different geometries, while cluster B is a single reach with constant width. On the overview, an example of the pixel width evaluation is shown: the red arrows show, for the considered pixel (red dot), the four directions D (0-180, 45-225, 90-270, 135-315) used for width evaluation (modified from Cazorzi *et al.*, 2012). In this case, the derived pixel width is 2.

For each cluster it is possible to calculate shape-related quantities such as area, width and length and, as the DTM grid size is known, the surface for each cluster (s_c) can be easily computed as the sum of the areas of pixels within the cluster.

The computation of the network width index for each cluster relies on the following steps. For each pixel of the cluster, the connected neighboring cells along four directions *D* (0-180, 45-225, 90-270, 135-315) are counted (Fig. 4.6), and the width w_{px} associated to each pixel is computed as:

$$\boldsymbol{w_{px} = \min\left({}_{0-180}\mathbf{count}_{\mathbf{px}}, {}_{45-225}\mathbf{count}_{\mathbf{px}}, {}_{90-270}\mathbf{count}_{\mathbf{px}}, {}_{135-315}\mathbf{count}_{\mathbf{px}}\right)} \quad \mathbf{12}$$

where ${}_{D}count_{px}$ is the number of pixels connected to the considered one (*px*) along the direction D (Cazorzi *et al*., 2012). In the case shown in Fig. 4.6, for the pixel of interest, the evaluated w_{px} is 2.

The width index W_{index} for each cluster is the computed taking into account the average value of the pixel widths:

$$\boldsymbol{W_{index} = \frac{\sum_{px=1}^{n} w_{px}}{n}} \quad \mathbf{13}$$

where w_{px} comes from Eq. (12) and *n* is the number of pixel within the cluster (Cazorzi *et al*., 2012).

The length index L_{index} is computed as the ratio between the cluster area (Sc) and the cluster width index W_{index} (Cazorzi *et al*., 2012).

$$\boldsymbol{L_{index} = \frac{s_c}{W_{index}}} \quad \mathbf{14}$$

The main advantage of this approach is that it does not require any skeletonization procedures to measure an actual length, avoiding common errors, such as loops or neckings, that are difficult to resolve through automatic procedures, and might require manual interpretation.

In Fig. 4.7, an example of the two indexes is provided.

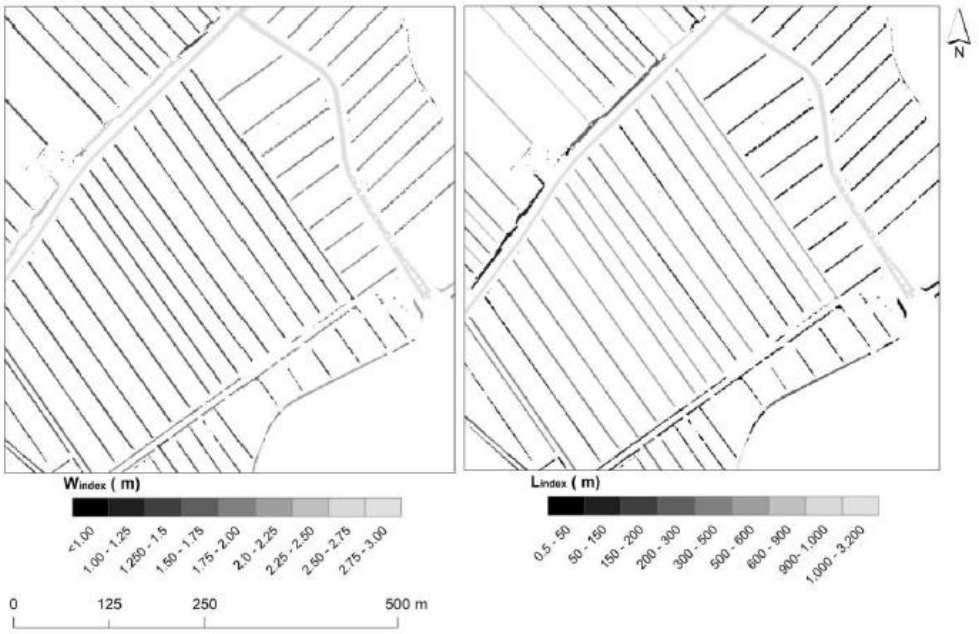

Fig. 4.7 Example of indexes derived for a drainage unit: width (W_{index}) and length (L_{index}) index for each cluster of pixel (Sofia, 2012).

From both indexes for each cluster, it is then possible to evaluate the areal drainage length (DL_u) and drainage density (DD_u). Drainage Length corresponds to the sum of Length indexes of the clusters belonging to the considered unit and, once the unit surface is known, the drainage density (DD_u) is evaluated as the ratio between drainage length and the actual surface of the unit of interest (Cazorzi *et al*., 2012).

The second part of this first-step approach aims to derive the network storage capacity by associating some characteristic cross-section areas to specific width ranges. Ditches in agrarian landscapes are usually fairly regularly-shaped due to the digging techniques adopted by the farmers to create them (Fig 4.8).

Fig. 4.8 Example of digging techniques to create a ditch (Maines Fernando, 2010).

For this reason, this approach considers a simplified representation of ditches cross-sections such as nested trapezoids, single trapezoids or rectangular and does not include detailed measurements of how depth varies with increasing widths. In addition, this averaging characterization also manages to take into account the differences in network geometry that might be anyway present over different plots due to the farmer choices. It is important to point out, anyway, that the relationship between width ranges and cross-sectional areas as it is formulated, cannot be applied for watersheds characterized by a more natural network, such as mountainous basins (Cazorzi et al. 2012).

Once the width index is automatically derived, it is possible to associate the user-defined cross-sectional areas (A_{index}) to the whole network, and the network storage capacity for drainage unit (SC_u) is defined as:

$$\boldsymbol{SC_u = \frac{\sum_{j=1}^{n}(L_{indexj} \cdot A_{index})}{S_u}} \qquad \textbf{15}$$

where L_{index} is the length index for each cluster (j), S_u is the surface of the considered drainage unit (Cazorzi *et al.*, 2012), and A is the associated cross sectional areas such as:

$$A_{index} = f(W_{index\ j}) \qquad \textbf{16}$$

where W_{index} derives from Eq. 13 (Cazorzi *et al*., 2012).

In this case, considering the characteristic of the network, the considered values for the area-width relationship are showed in Tab. 4.1, they derive from field surveys conducted in two different study sites (Cazorzi et al. 2012), and they are considered to be representative of the widths and cross section of our study site.

Table 4.1 Relation between the average widths and mean cross-sectional areas of the minor drainage network, obtained through the realization of 170 field surveys carried out in sample areas, chosen to be representative of the whole drainage network (Sofia *et al*., 2012).

Mean width (m)	Cross sectional area (m^2)
<= 2.0	0.4
>2.0 e <= 3.0	0.7
>3.0	1.5

For the present work, considering the large extent of the study area, comparisons between the automatically derived indexes and the actual network statistics have not been done, but the truthfulness of the procedure has already been tested by Cazorzi *et al*. (2012). They found out that, when the considered cluster is representative of a reach, the width index is also generally a correct local estimation, with a measured RMSE of about 0.2 m; the same consideration can be done about the length index: in this case, the RMSE is estimated to be about 2 m. According to the results obtained by Cazorzi *et al*. (2012), the procedure slightly underestimates the surveyed storage capacity (it accounts for the 98% of it) and the surveyed drainage length (97% of the real drainage length is accounted).

4.2 EFFECTS OF DRAINAGE NETWORK STORAGE CAPACITY ON DIRECT RUNOFF

The second step of the approach aims to:

1) compute the surface runoff produced by the October, 31st - November, 2nd 2010 rainfall event considering different land uses;
2) compare of the drainage network storage capacity on the direct surface runoff (Pe).

The surface runoff produced by the main rainfall event has been computed by applying the Soil Conservation Service Method to the area of interest. As the study area corresponds to the

agricultural floodplains, the mountainous watersheds have not been taken into consideration for such analysis. A complete evaluation would require to account also for the runoff coming from upstream, however this simplified approach is considered also with the idea to identify how much of the direct runoff can be effectively laminated by the minor network, requirement that is usually asked when planning land use changes (See Chapt. 1.1.1). Despite the fact that the contribution coming from the mountainous basins is not considered, the purpose of this part is to evaluate the presence of areas that may be already risky simply for the runoff directly produced by the input local rainfall.

The theoretical basis of the Soil Conservation Service Method has been developed in 1972 by the U.S. Soil Conservation Service, and it is based on a very simple conceptual model. It has been chosen because it can be applied by specifying a single parameter called Curve Number (CN), whose spatial distribution can be easily estimated from technical maps and field observations on the study area.

Through the SCS-CN method, it is possible to calculate the effective precipitation (Pe) (Eq. 17), thus that precipitation (mm) which is able to generate runoff (direct runoff):

$$\boldsymbol{P_e = \frac{(P-I_a)^2}{P-I_a+S}} \quad \textbf{17}$$

where:

- *P* is the total amount of water (mm) fallen during a rainfall precipitation event;
- *Ia* is the "initial abstraction" (Eq. 18), thus the amount of storage (mm) that must be satisfied before any flow can begin and it is equal to:

$$\boldsymbol{Ia = c\,S} \quad \textbf{18}$$

- *S* is a calibration parameter, called infiltration storativity. It corresponds to the maximum amount of precipitation (mm) that a watershed can hold and it is calculated according to the formula (Eq. 19):

$$\boldsymbol{S = S_0\left(\frac{100}{CN} - 1\right)} \quad \textbf{19}$$

where:

- *CN* is the Curve Number, an index of the propensity of a soil to produce runoff. It depends on four main features: soil type (according to SCS classification), hydrological conditions, land use and vegetation cover, antecedent soil moisture content.
- S_0 is a parameter that in the original SCS-CN equation is equal to 254 mm and that allows to use the spatial distribution of CN values and to simulate correctly, at the same time, the observed flood water balance.

The Curve Number may be considered as an index of "storm-runoff generation capacity" varying from 0 to 100. The higher is the value and the lower is the infiltration capacity of a soil and thus the greater is the runoff response. On the contrary, the lower is the parameter and the greater is the infiltration capacity of a soil and thus the runoff is much more weakened. Urbanization processes which make the soil sealing and cementation increase, cause a raise of CN values too (Tab. 4.2 and Fig. 4.9).

Table 4.2 Curve Numbers for urban/suburban land covers (U.S. Soil Conservation Service, 1975)

LAND USE		HYDROLOGIC SOIL GROUP A	B	C	D
Open spaces, lawns, parks, golf courses, cemeteries, etc.					
good condition: grass cover on 75% or more of the area		39	61	74	80
fair condition: grass cover on 50% to 75% of the area		49	69	79	84
Commercial and business area (85% impervious)		89	92	94	95
Industrial districts (72% impervious)		81	88	91	93
Residential*					
Average lot size	Average % Impervious†				
1/8 acre or less	65	77	85	90	92
1/4 acre	38	61	75	83	87
1/3 acre	30	57	72	81	86
1/2 acre	25	54	70	80	85
1 acre	20	51	68	79	84
Paved parking lots, roofs, driveways, etc.‡		98	98	98	98
Streets and roads					
Paved with curbs and storm sewers‡		98	98	98	98
Gravel		76	85	89	91
Dirt		72	82	87	89

From Table 4.2, it is evident as the Curve Number values sharply increase going from open spaces, lawns to paved parking lots.

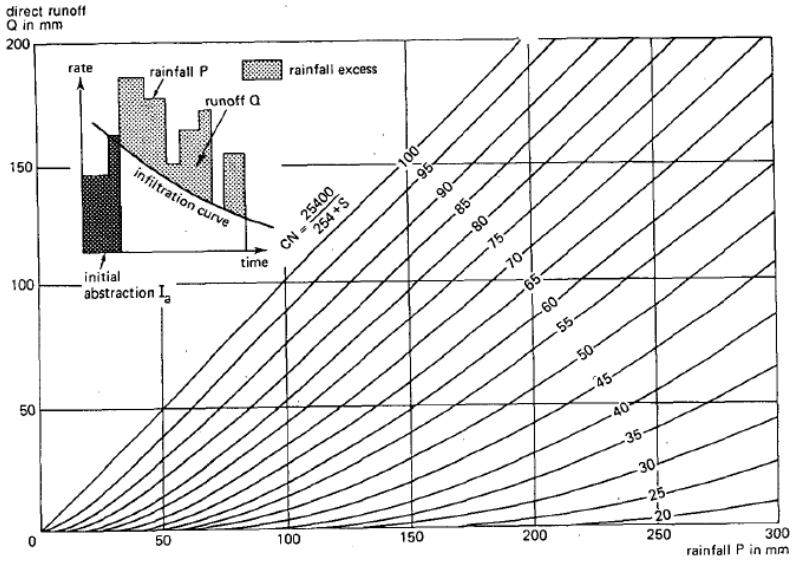

Fig. 4.9 Graphical solution of Eq. 17 showing runoff depth Q as a function of rainfall depth P and curve number CN. For paved areas, for example, S will be zero and CN will be 100; all rainfall become runoff. For highly permeable, flat-lying soils, S will go to infinity and CN will be zero; all rainfall infiltrate and there will be no runoff. In drainage basins, the reality is somewhere in between.

In this work, in order to obtain a curve number map spatially distributed over the study area (Fig. 4.12), the land-use data (Fig. 4.10) have been combined with the hydrological soil groups (Fig. 4.11).

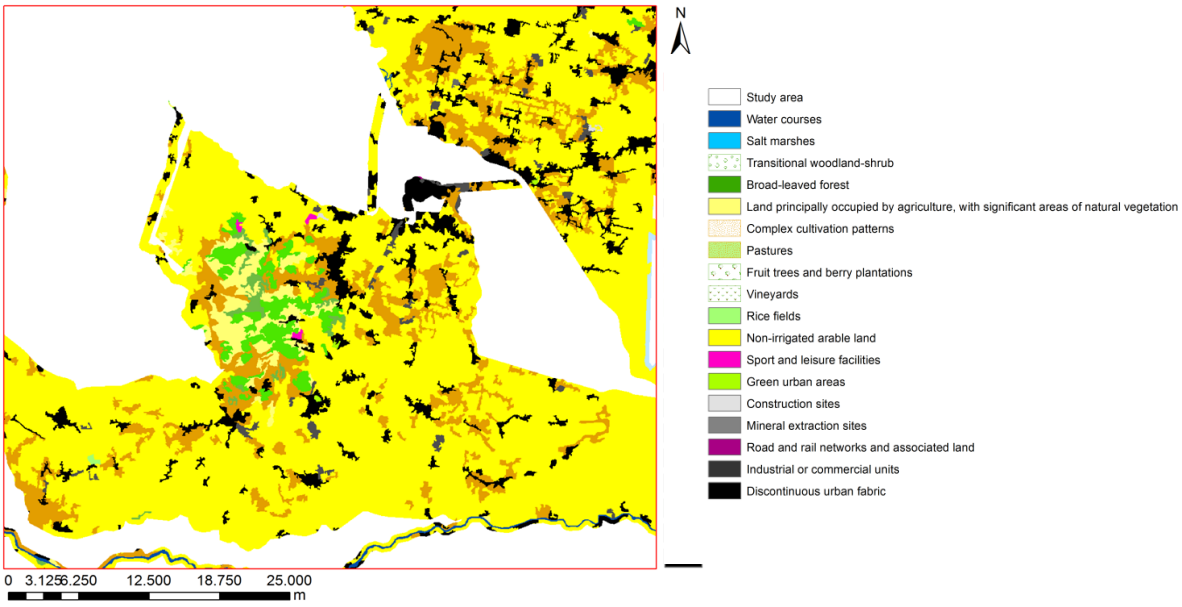

Fig. 4.10 Land use dated back to 1990 according to the CORINE land cover project. From the figure, it is clear how the most part of the area is covered by non-irrigated arable land, land principally occupied by agriculture (yellow) and discontinuous urban fabric (black).

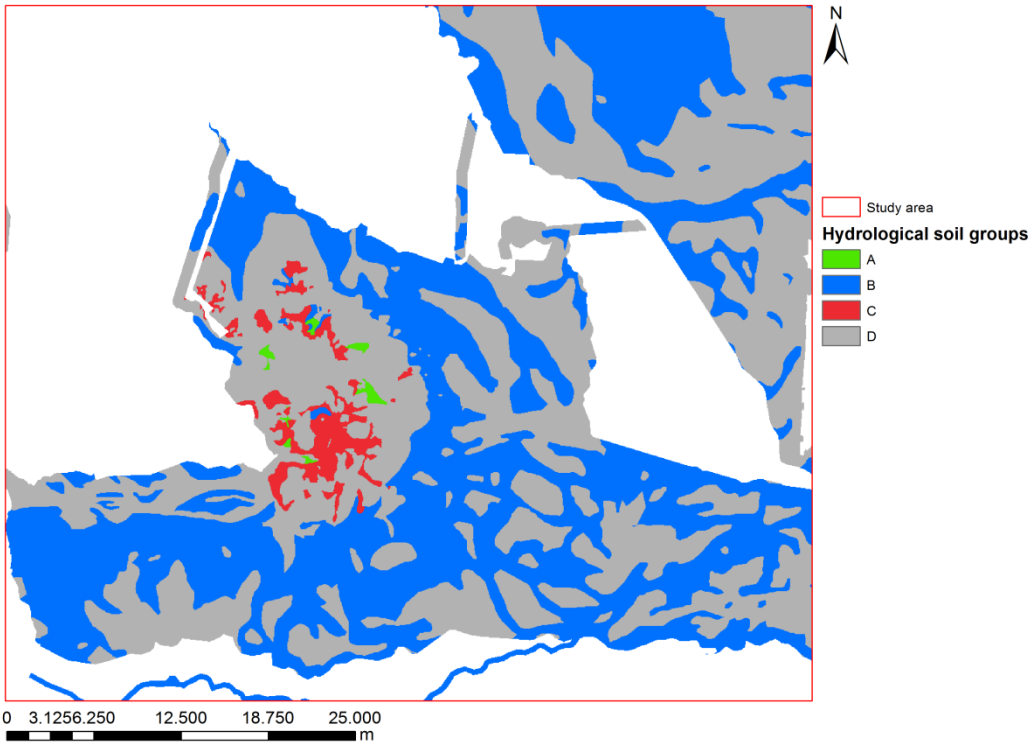

Fig. 4.11 Hydrological soil groups according to the Soil Conservation Service Method.

According to the SCS-CN method, as the soils go from group A to group D, the runoff potential increases (Tab. 4.3).

Table 4.3 Soil groups according to the SCS-CN methodology and repartition of the study area based on the soil categories. The results show that soil types B and D make up to 97.5% of the whole study area.

Soil type	Description	Area (Km^2)	Area %
A	Low runoff potential	5.37	0.30
B	Moderately low runoff potential	838.56	46.42
C	Moderately high runoff potential	39.27	2.17
D	High runoff potential	923.23	51.11
Tot		1806.43	100.00

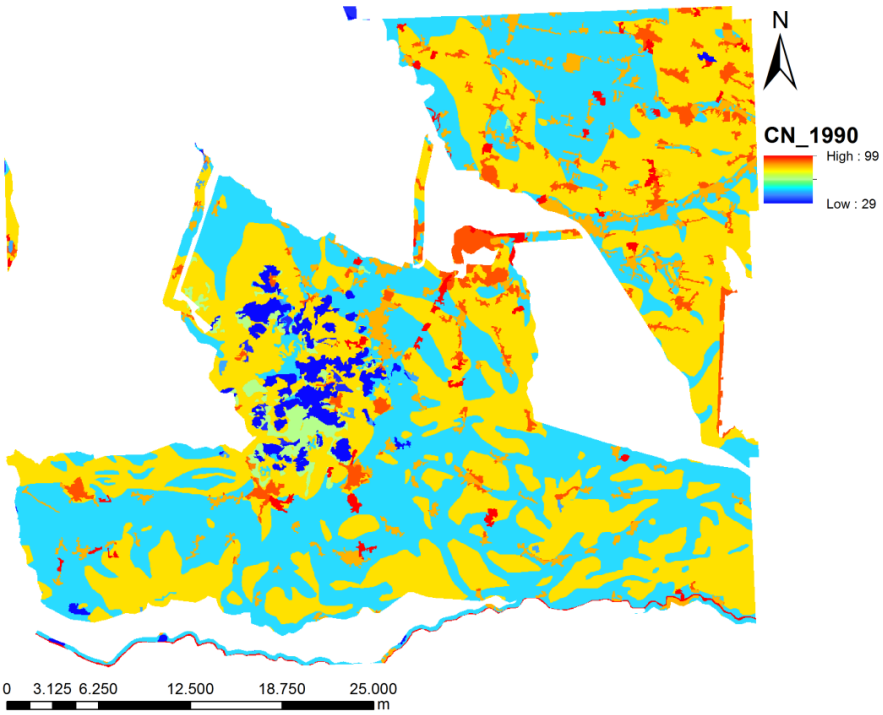

Fig. 4.12 Example of Curve Number map based on the land-use data of 1990.

Three land-uses, produced by the CORINE land cover project, respectively dated back to 1990, 2000 and 2006 years, have been used. The reason of that is to show how the land-use change affects the propension of a soil to produce runoff. In this way, three different curve number maps have been obtained according to the years of land-use data production. At his point, the surface runoff has been computed combining the three curve number maps with the rainfall map, obtained from the interpolation of sample rainfall data recorded by the monitoring network system during the October, 31st - November, 2nd 2010 rainfall event (Fig. 4.13). The so-obtained surface runoff corresponds to the effective precipitation as computed by the Soil Conservation Service Method (Eq. 17).

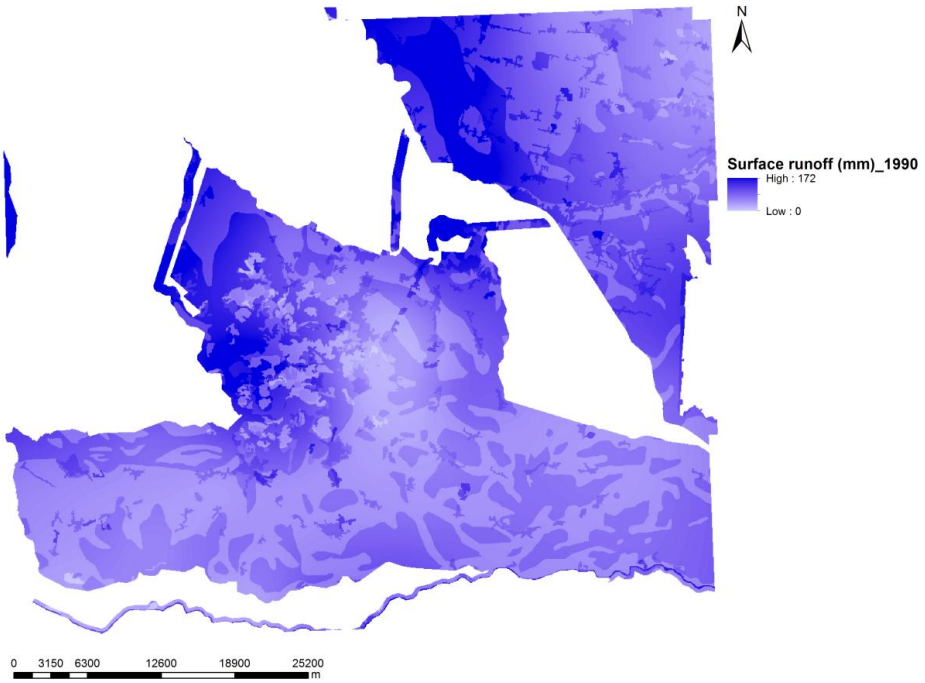

Fig. 4.13 Surface runoff computed through the SCS-CN method (1990).

The mean direct surface runoff has been computed taking into consideration the extension of each sub-area (250 000 m^2). From the so-found result, the storage capacity, obtained from the first step of the method, has then been subtracted. As it will be better describe in Chapt. 6, this difference has been considered a useful index to compute the lamination effect, and it has been named "residual runoff". All these operations have been done for the years 1990, 2000 and 2006 in order to show the differences occurred due to the land-use change. We then focused on the flooded areas in order to evaluate both if there is a correspondence between the drainage density and storage capacity values and to assess the possible presence of risky areas simply due to the rainfall. As already reported before, it is important to stress the fact that this analysis completely ignores the contributions of runoff coming from the mountainous watersheds. The results obtained will be given in Chapt. 6.

5 STUDY SITE

In this chapter, a general description of the study site, including location, extension, geology, hydrogeology, land use and climate, is at first, provided. Then, the attention shifts to the land-use change and to the flooding context for the study area.

The study site has been selected as representative of engineered landscapes, and in particular of floodplains of the North East of Italy. It is a 290000 ha site located in the lower Veneto plain, stretching between Adige and Marzenego Rivers, and mainly including the province of Padua (Fig. 5.1).

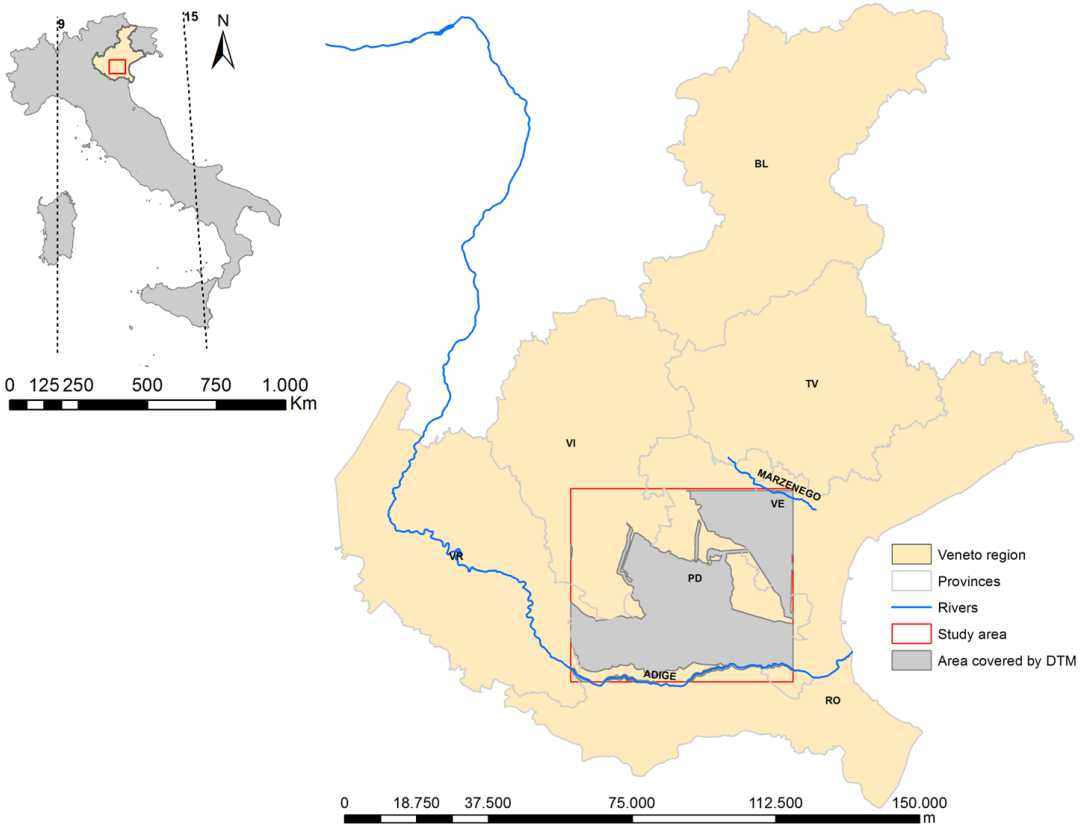

Fig. 5.1 Localization of the study area within the Veneto Region. The Adige and Marzenego rivers can be considered respectively as the southern and northern boundaries of the study area. Within the study site, delimited by the red rectangle, the effective area covered by DTM is shown in grey.

As it can be easily seen from the map above, the area covered by digital elevation data does not completely coincide with the borders of the study area: the DTM only covers those portions characterized by man-made ditches and highly modified channels. Since all the analysis, as they have been described in Chapt. 4.1, require the support of elevation data, the effective study area coincide with the one where DTMs are present. The actual study site has an extension of about 180 000 ha. The LiDAR DTM used has a resolution of 1 m (Fig. 5.2) and, as already stated in Chapt. 4, it has been realized within the "*Piano Straordinario di Telerivelamento Ambientale (PST-A)*" (Extraordinary Plan of Environmental Remote Sensing, EPRS-E) thanks to the cooperation of the Ministry of Environment and Territory of the Sea

(METS), Chairperson of the Council of Ministers – Department of Civil Protection (DCP), the Ministry of Defense (MD), the Regions and Autonomous Provinces.

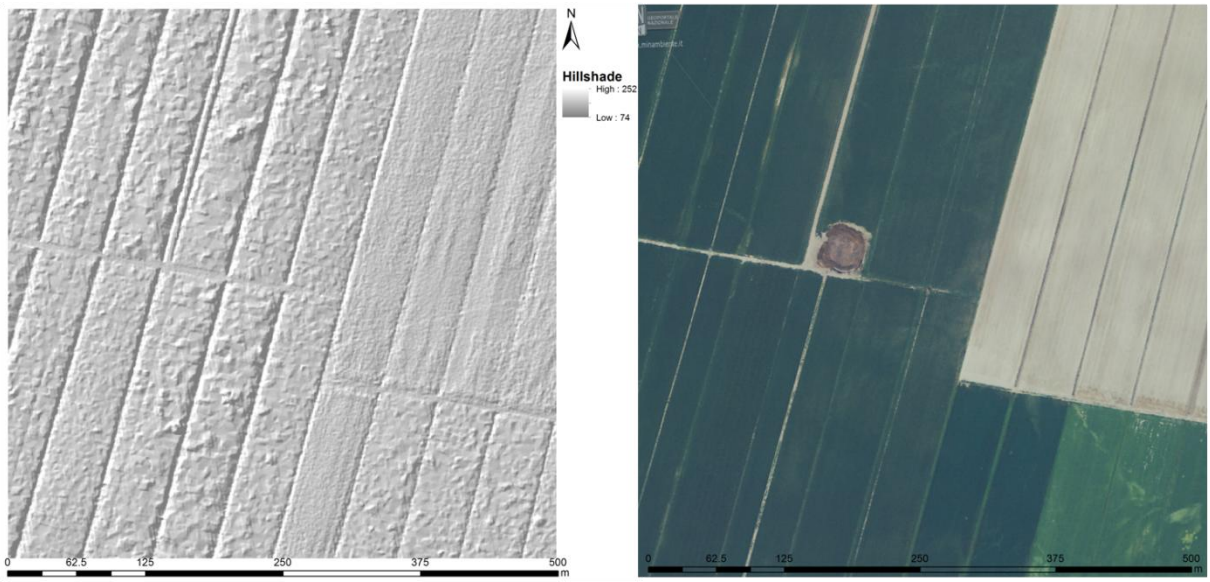

Fig. 5.2 The figure shows, on the left side, the hillshade computed for a portion of DTM. The high-resolution DTM (1 m) allows to detect the channels over the floodplain. On the right side, an ortophoto of the same portion is reported in order to show the elevated correspondence between what a DTM manages to identify and what exists in the reality.

The floodplains of the Veneto Region have been created by the deposition of alluvial materials especially carried by alpine rivers such as Po, Adige, Brenta, Piave and Tagliamento. In this context, three distinct environments can be distinguished: the high and low plains, separated each other by the line of groundwater springs, and the coastal zone (Servizio Osservatorio Suolo e Rifiuti, 2005). The study site mainly falls into the lower plain, where Brenta and Adige river basins and the Draining Basin of the Veneto lagoon are the principal responsible of the transportation of alluvial materials (Fig. 5.3).

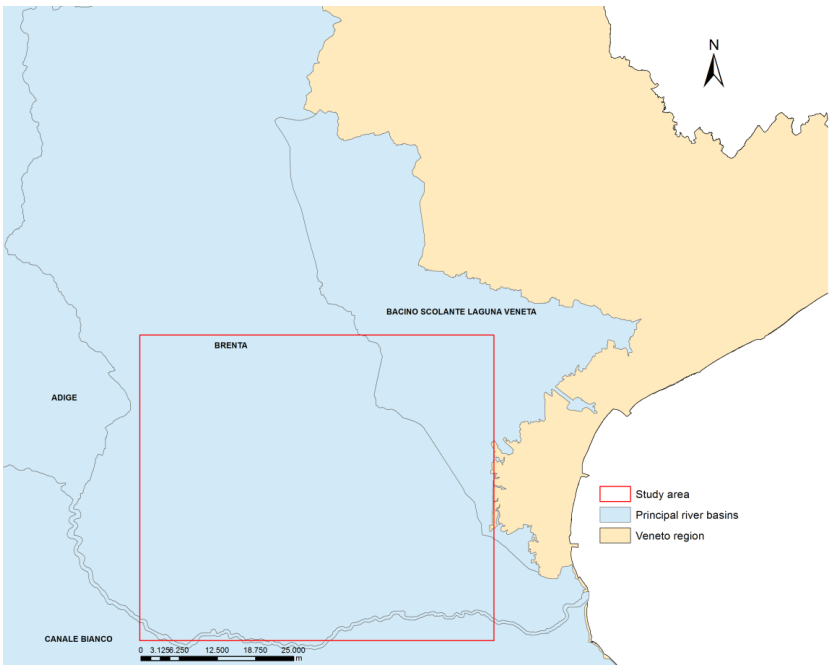

Fig. 5.3 Principal river basins of the study site. The Brenta watershed is without any doubts the most widespread.

The Brenta river basin, which is the widest in the study site, can be, in turn, subdivided into two minor river basins: the Gorzone and Bacchiglione basins (Fig. 5.4).

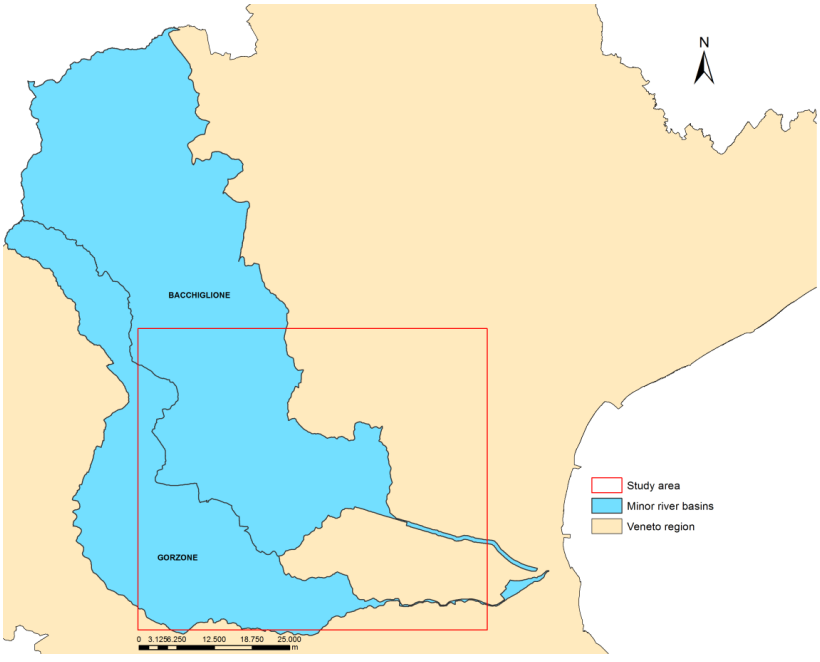

Fig. 5.4 Bacchiglione and Gorzone minor river basins that converge on the study site.

At this point, a brief explanation of the principal soils that are found in the study site is reported in succession, because the knowledge of the physical features of a soil allows to describe some important parameters that are useful for the water dynamics assessment in the soil itself: the composition and texture of a soil are, in fact, extremely important factors that influence hydrological processes such as infiltration, percolation, subsurface runoff etc…

The soils that can be found in the lower plain are made by an alternation of fine texture particles such as silts and clays and coarser texture materials such as sands, that may have variable contents of finer particles too (fine sand, loamy fine sand etc…). Generally, the types of soils on hillocks show a moderate profile differentiation, they are mainly made of coarse texture particles and they are well-drained soils characterized by a deep groundwater reservoir (Eutric or Calcaric Cambisols). On the contrary, in the lower areas, the silty and clay textures become predominant, the groundwater reservoir becomes shallower and the drainage gets slower (Cambisols and Calcisols). In addition, there also areas where the drainage results to be very critical, in which the soils may even show organic matter on the surface (Fluvisols) (Servizio Osservatorio Suolo e Rifiuti, 2005).

The soil map for the study site, derived from the one made by ARPAV (Agenzia Regionale per la Prevenzione e Protezione Ambientale del Veneto) 1:250 000, is shown in Fig. 5.5. The soils classification reported has been done according to the Soil Provinces.

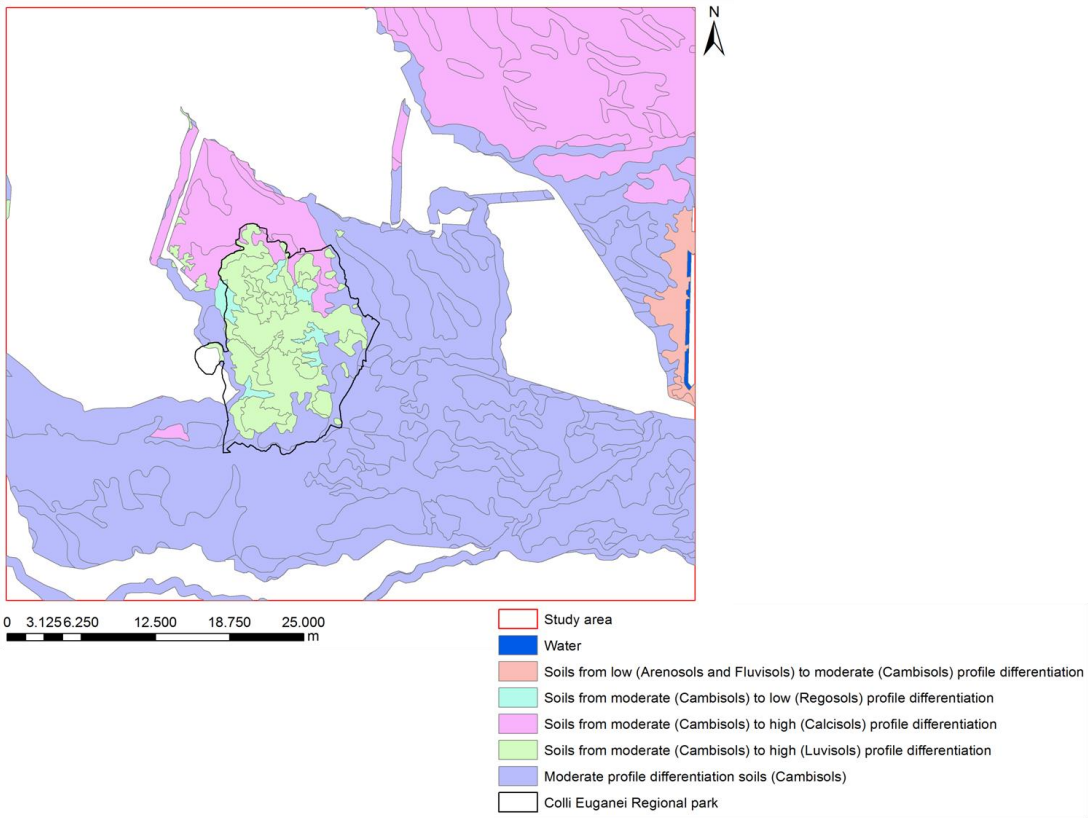

Fig. 5.5 Soil map derived for the study site, in particularly only for the portion covered by DTM. The map comes from the one made available by ARPAV for the regional level at 1:250000 scale and is dated to 2005. The soil classification shown is based on the Soil Provinces. In the map, the Colli Euganei Regional Park boundaries are reported as well, in order to show differences between the soils on hillocks and those ones on the lower areas.

An important soil characteristic that deserves attention, is the soil permeability, that is usually identified by the measure of the saturated hydraulic conductivity (*Ksat*, mm/hr), developed by Darcy in 1856 (Darcy, H. 1856). The soil permeability map of the Veneto Region is shown in Fig. 5.6.

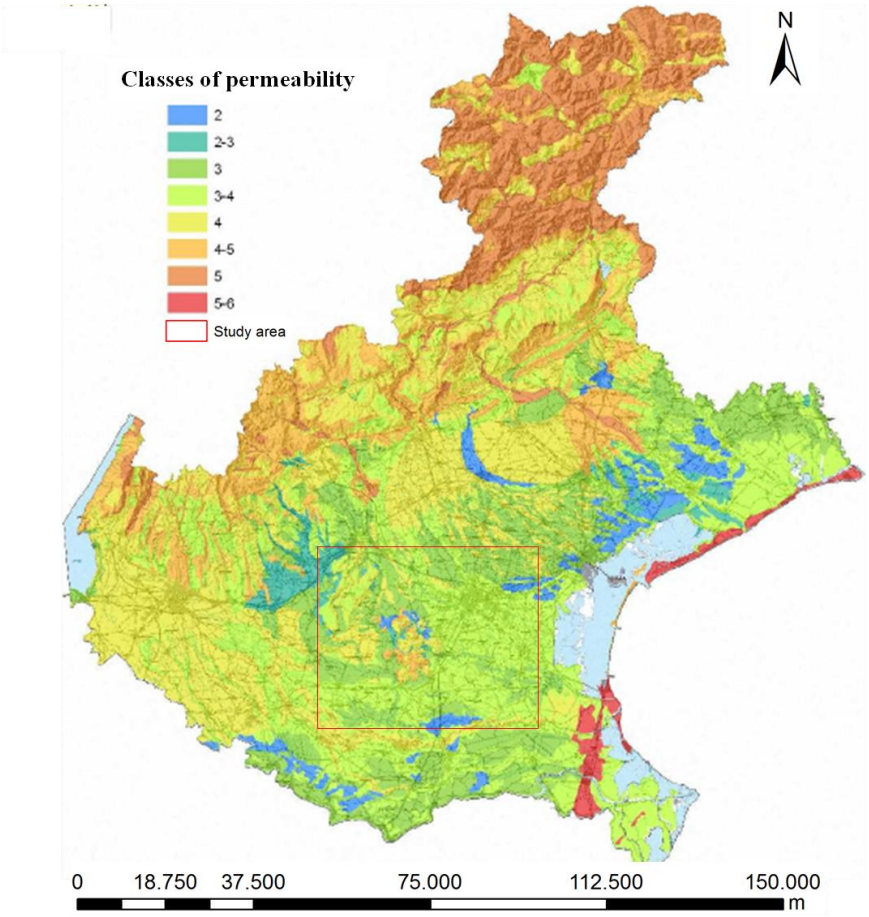

Fig. 5.6 Soil permeability map derived for the Veneto Region showing the localization of the study site (red rectangle). The map has been realized by ARPAV at 1:250000 scale (Servizio Regione Suoli, ARPAV, 2011).

Looking at the map above, the more permeable soils (classes 5-6) are located along the coastal areas, characterized by sandy textures. Classes of high permeability are especially found in the higher plain, where the soils are generally gravelly, in the lower plain in correspondence of hillocks and up in the mountains within the steep areas. Most of the floodplain falls into the intermediate classes of permeability (3-4), because of its silty texture composition. The less permeable areas are located in the lowest portions of the floodplain and they are characterized by a clay texture (classes of permeability from 1 to 3).

Still from Fig. 5.6, it is possible to notice that most of the study site is characterized by intermediate classes of permeability (3-4).

The permeability parameter allows also to group together soils that have similar hydrological characteristics. The method, developed in 1972 by the U.S. Soil Conservation Service, identifies four hydrological groups of soils: A, B, C and D. As already explained in Chapt. 4. 2, the potential runoff increases by shifting from group A to group D.

The map of hydrological soil groups derived for the study area is shown in Fig. 5.7. As it is evaluable at naked eyes too, the group D, that is the one showing the highest potential runoff, is the most widespread over the study site.

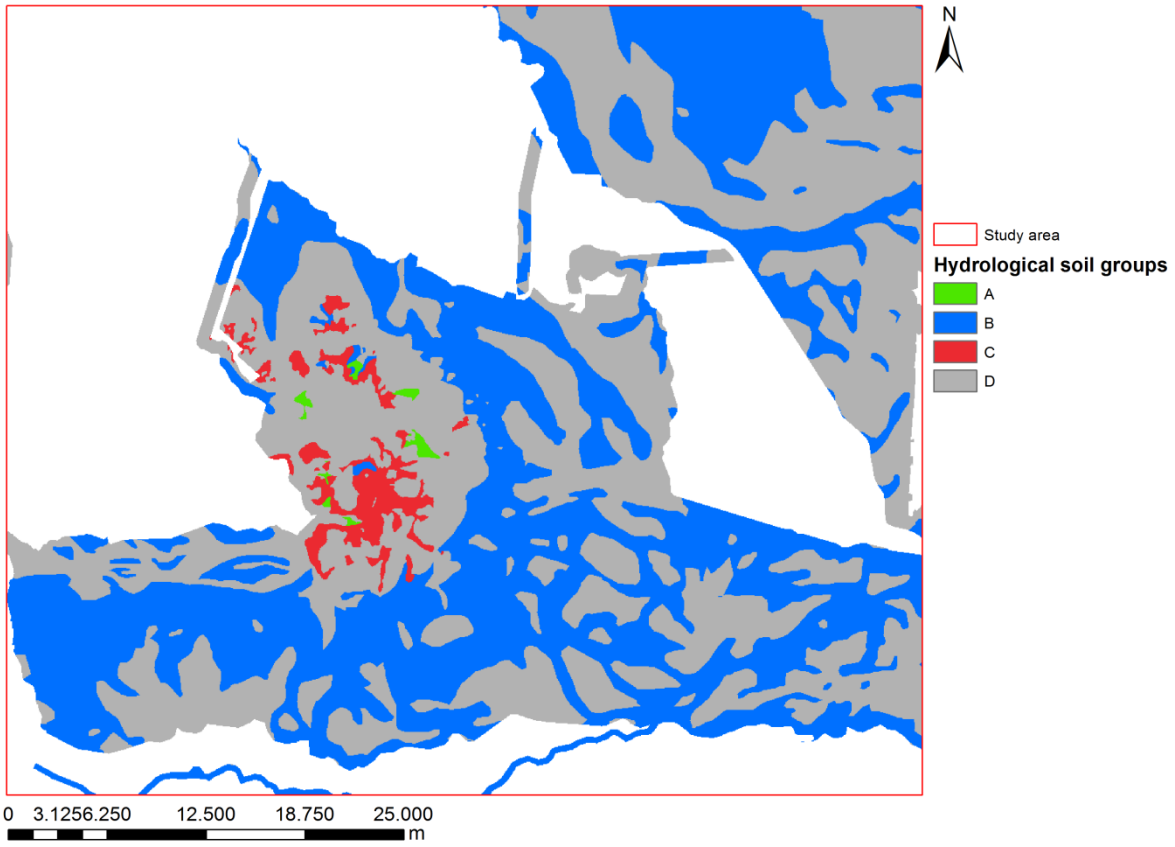

Fig. 5.7 Hydrological soil groups map derived for the study area, in particular only for the portion covered by DTM.

Thanks to the CORINE Land Cover project, it has also been possible to derive a land-use map for the study area (Fig. 5.8). The available data are dated to 2006.

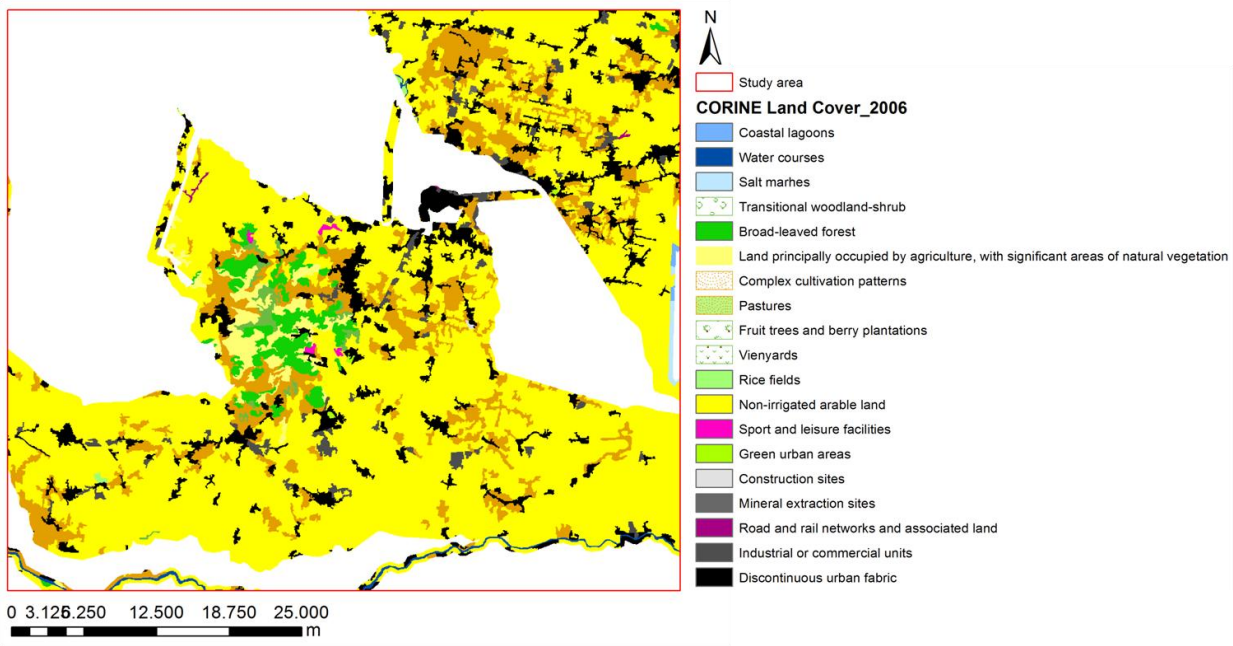

Fig. 5.8 Land-use map derived for the study site, in particular only for the portion covered by DTM, obtained thanks to the CORINE Land Cover data of 2006.

From the figure just reported, it is well visible how the most part of the study site is covered by non-irrigated arable land, land principally occupied by agriculture and discontinuous urban fabric. In Chapt 5.1, a comparison between three land-use data (1990, 2000 and 2006), is reported in order to show how the land-use has been changed over the years.

The general description of the study site ends with its collocation from a climatic point of view. According to Barbi *et al*., (2011) in the Veneto Region, three different mesoclimates can be distinguished: the plain, prealps and alpine mesoclimates. Therefore, the study site falls into the plain mesoclimate, which is characterized by a certain degree of continentality with relatively cold winters and warm summers. The precipitations are quite evenly distributed over the year with annual totals that are, on average, included in the range 800-1000 mm. The winter is usually the driest season while Atlantic and Mediterranean perturbations affect spring and autumn. In summer, rainstorms result to be frequent, often associated to hail events and, rarely, to whirlwinds (Barbi *et al*., 2011).

A climate map produced by Mario Pinna in 1978, derived for the Veneto region, is reported in Fig. 5.9.

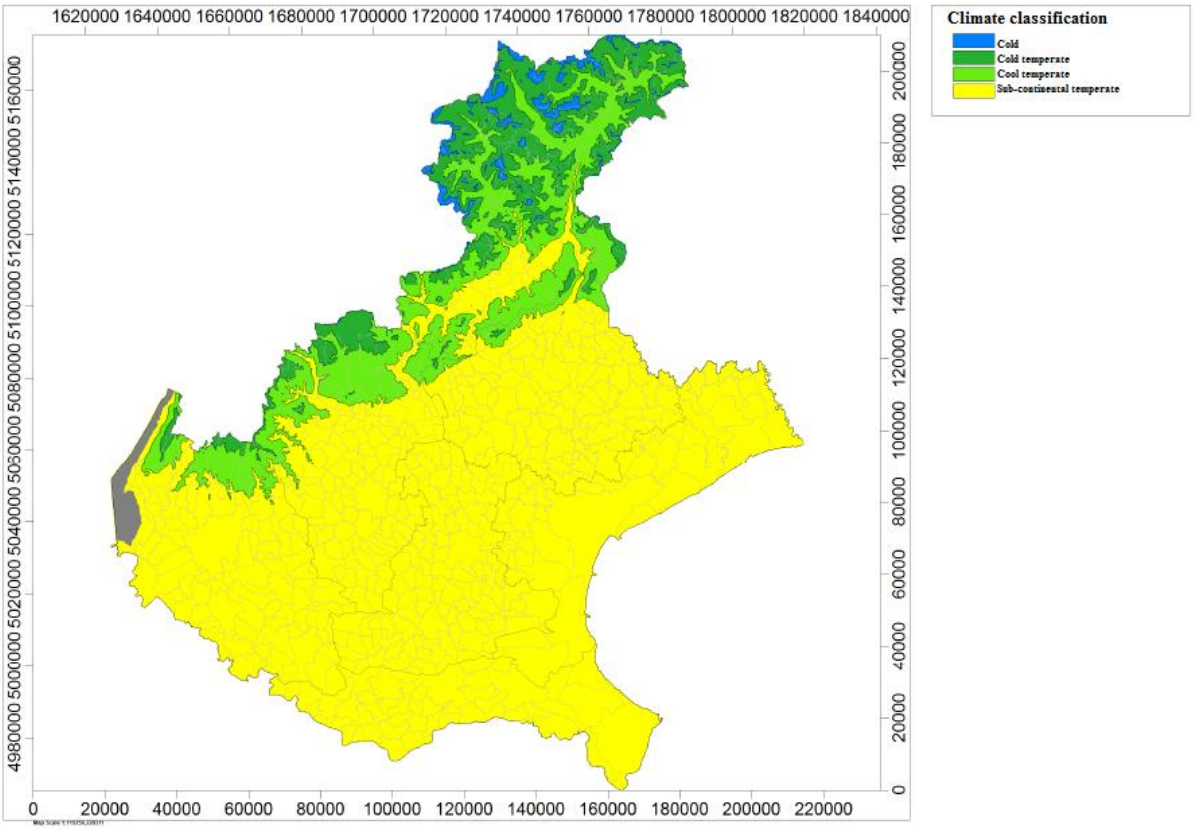

Fig. 5.9 Climate map of the Veneto Region realized by Mario Pinna in 1978 (modified from Barbi *et al.*, 2011).

The study area can be quite easily localized because it mainly includes the province of Padua. As it can be noticed from the map, the temperate sub-continental climate, corresponding to the yellow color, is the dominant one at both the regional e study area levels. The principal characteristics of such typology of climate are reported in Tab 5.1.

Table 5.1 Classification of the Italian climates in relation of the temperature, realized by Mario Pinna (Barbi *et al.*, 2011).

Climate	Mean annual temperature	Mean temperature of the coldest month	Annual temperature range
Temperate sub-continental	10 – 14.4 °C	0 – 3.9 °C	>19°C

5.1 OVERVIEW OF THE LAND-USE CHANGE FOR THE STUDY AREA

It is important to understand how much the territory has changed as time went by. At this purpose, the central part of the Veneto region has been taken into account as reference area for the investigation of urbanization processes which have affected the region of our interest. As it has already been explained in the introduction, such major change related to urbanization and anthropic activities, might have great influence on the hydrological behavior of an area, hence why we focus on such description.

Recently, this portion of land has undergone both significant territorial and socio-economic changes. This particular conformation arises due to the expansion of a metropolitan polycentric system, showing a strict functional connection between the medium-small size villages, and it is characterized by a dispersion of low-density residential functions and a homogeneous distribution of medium-small size productive activities (Fregolent 2005). These dispersion processes have been deeply studied since the 80s and a particular attention has been given to the phenomenon called "*urban sprawl*" (Indovina 1990; Secchi 1996; Indovina, Fregolent, Savino 2004; Tosi, Munarin 2004; Fregolent 2005; Indovina 2009). The geographical context under consideration spreads across the provinces of Venice, Padua, Vicenza and Treviso and shows important differences inside it: strongly fragmented areas characterized by sprawling urbanization, alternate with high-density areas. This happened in the last twenty-year period due to a thickening process around the principal junctions of the polycentric system and, in the last ten-year period, due to a filling process of the still free areas, that gradually turned this territory into a low-density sprawling area. The filling process has occurred with the expansion of new residential neighborhoods and productive/commercial areas to the detriment of agricultural fields, floodplains and other spaces dedicated to the attenuation of floods events. In order to show the magnitude of this process, two aerial photographs of the city of Padua and its suburbs, taken respectively in 1955 and 2010 by two flights operated by the Military Geographic Institution (IGM), are reported in figures 5.10 and 5.11. The two pictures well show the expansion of residential areas especially occurred on the left side of the ring road SR47; while fig. 5.12 focuses on the urbanization process happened in the Arcella neighborhood (province of Padua) during the period from 1945 to 2010. In this particular example, the picture with which to compare the situation of the 40s has been taken from Google Earth.

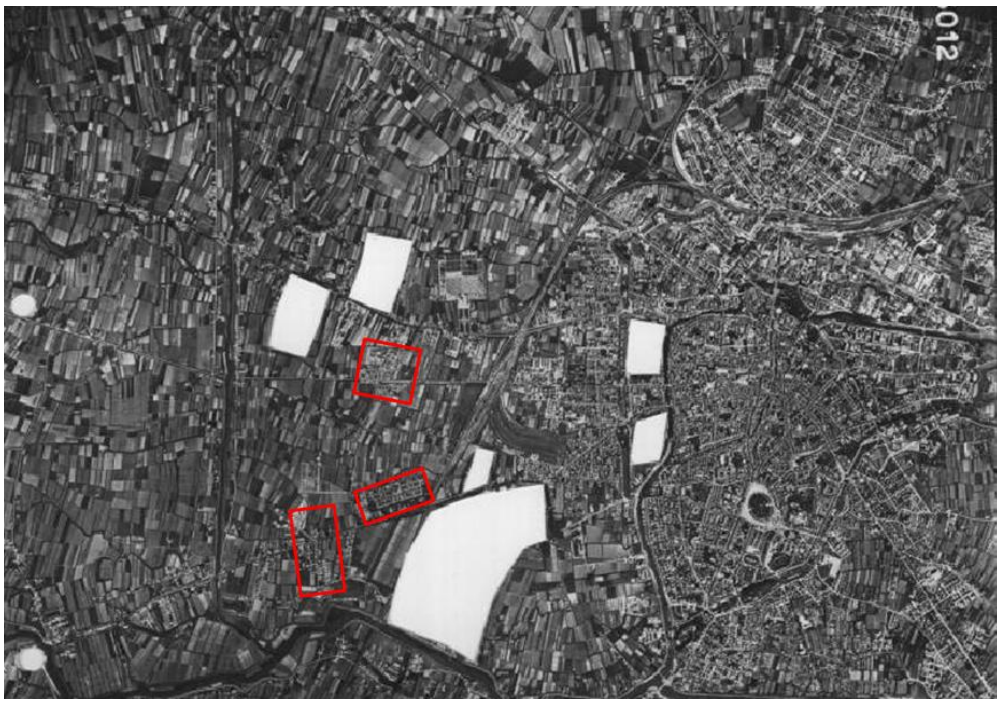

Fig. 5.10 City of Padua and its suburbs in 1955. On the left side of the ring road SR47, in red are highlighted the principal residential areas. They can be easily identified because they constitute an interruption of the regular spatial arrangement of the agricultural fields, which are represented by straight edge rectangular shapes (IGM flight 1955).

Fig. 5.11 City of Padua and its suburbs in 2010. If compared to the situation of 1955, the wide expansion of urban areas especially on the left side of the ring road SR47, is well visible (IGM flight 2010).

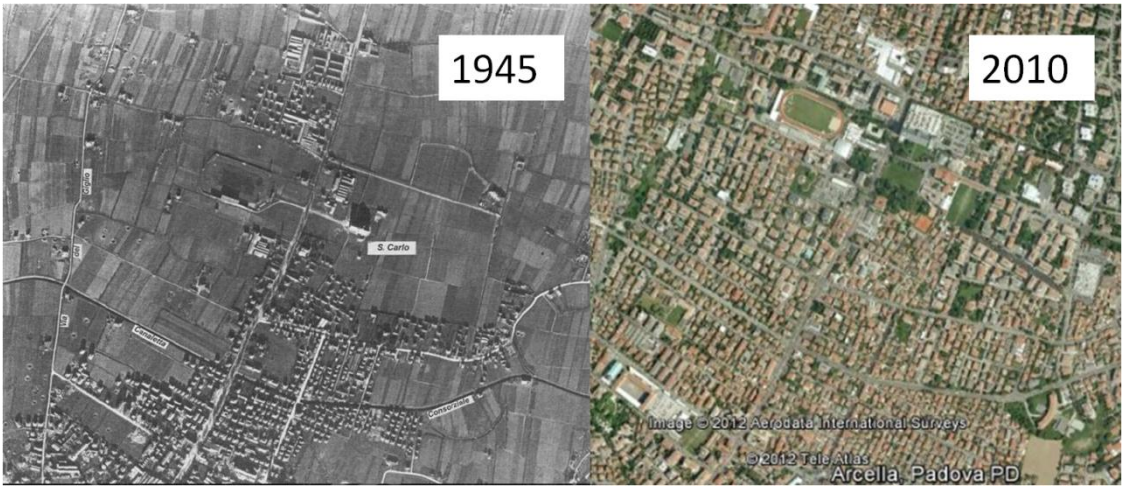

Fig. 5.12 The impact of urbanization in Arcella neighborhood (province of Padua) (IGM, 1945 and Google Earth, 2010).

In order to evaluate the land-use change occurred over time, it is also possible to look at the different land-use maps, obtained by the CORINE Land Cover project, derived for the study area (Figures 5.13, 5.14, and 5.15) and their relative histograms reported in Fig 5.16.

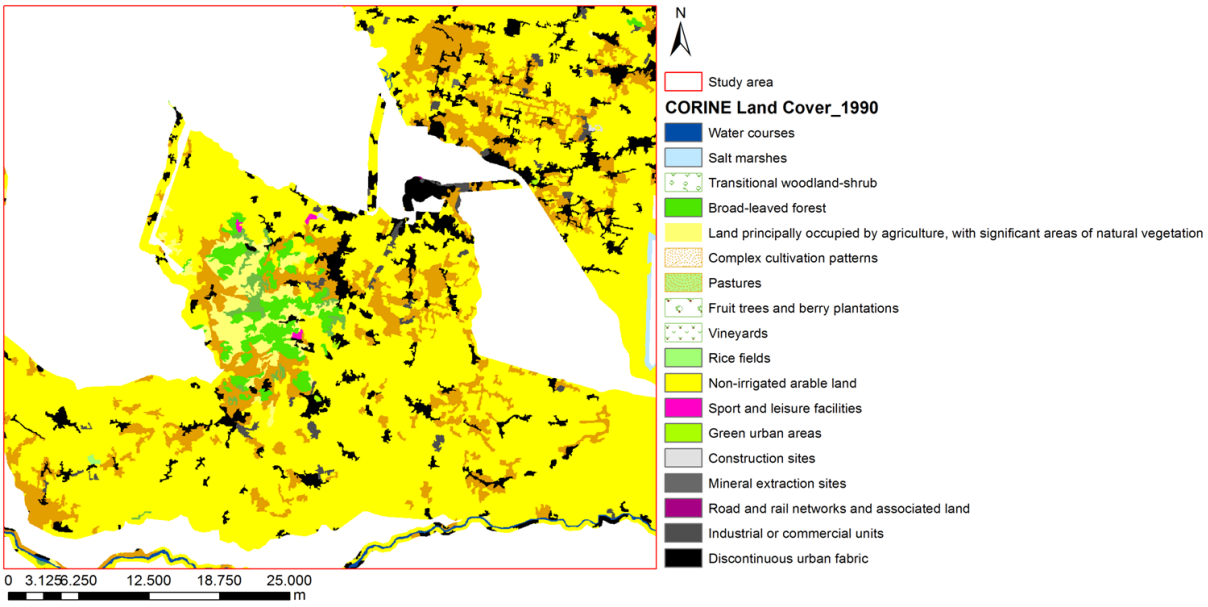

Fig. 5.13 Land-use map derived for the study site, in particular only for the portion covered by DTM, obtained thanks to the CORINE Land Cover data of 1990.

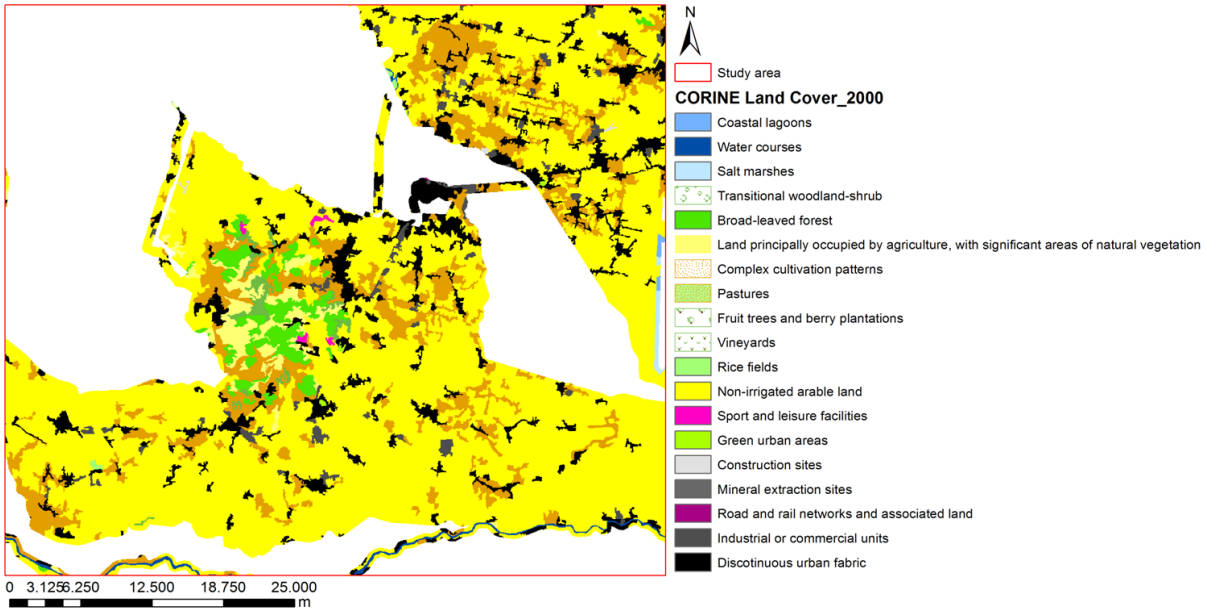

Fig. 5.14 Land-use map derived for the study site, in particular only for the portion covered by DTM, obtained thanks to the CORINE Land Cover data of 2000.

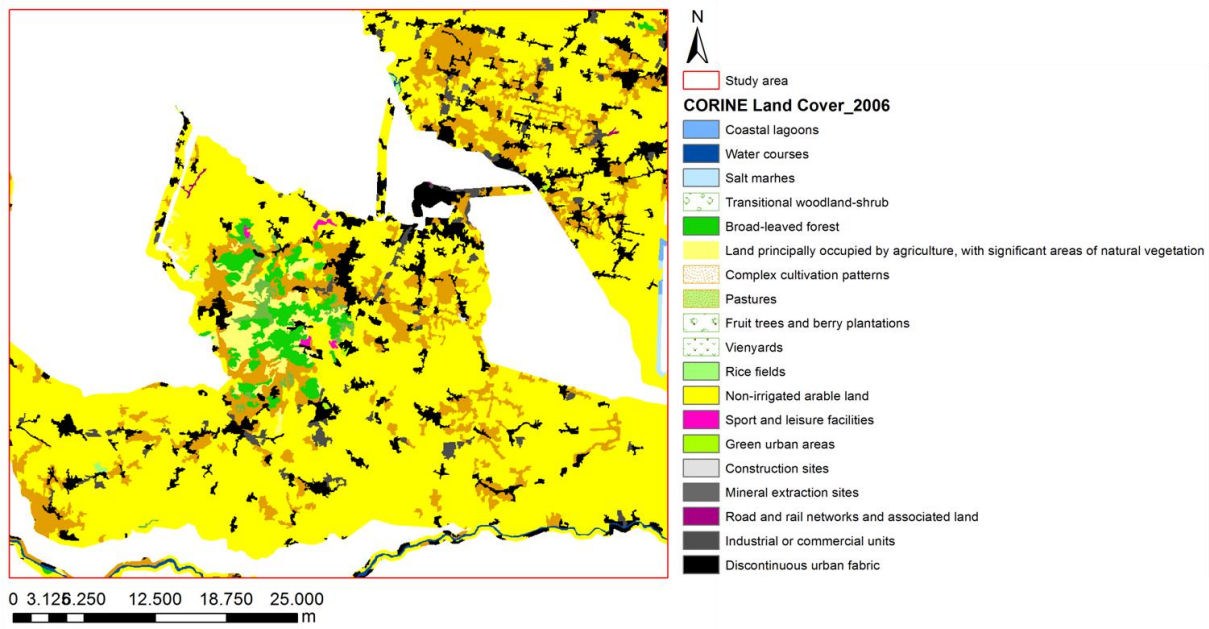

Fig. 5.15 Land-use map derived for the study site, in particular only for the portion covered by DTM, obtained thanks to the CORINE Land Cover data of 2006.

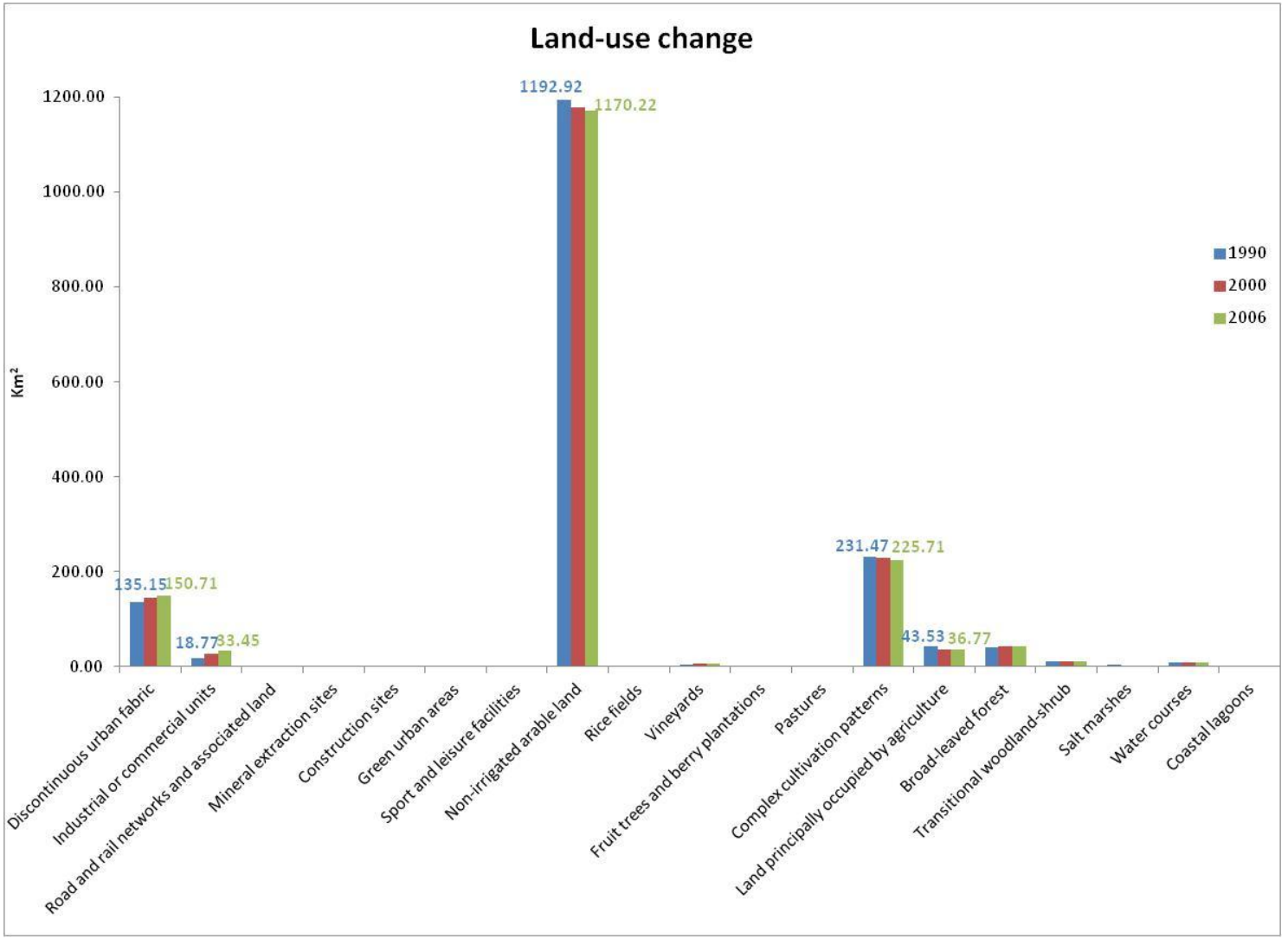

Fig. 5.16 Histogram showing the different typologies of land-use in relation to their areas, according to 1990, 2000 and 2006. Only the values, relative to 1990 and 2006 data, of the more distributed categories are reported.

Figure 5.16 well shows the categories of land-use that have undergone changes from 1990 to 2006. Discontinuous urban fabric and industrial or commercial units have both increased in surface over the years to the detriment of non non-irrigated arable land, complex cultivation patterns and land principally occupied by agriculture. As not all the categories can be seen from the histogram, all the land-use typologies whose differences have been registered over the years, are reported in Tab 5.2.

Table 5.2 Variation in extension (Km^2) of land-use categories over the years. What emerges is the decline of agricultural lands, that more than likely corresponded to an enlargement of urban areas.

Land-use typology	1990 (Km^2)	2000 (Km^2)	2006 (Km^2)
Discontinuous urban fabric	135.15	145.59	150.71
Industrial or commercial units	18.77	26.48	33.45
Road and rail networks and associated land	0.05	0.05	1.04
Construction sites	0.76	0.91	0.27
Sport and leisure facilities	1.46	2.13	2.13
Non-irrigated arable land	1192.92	1178.74	1170.22
Rice fields	0.63	1.11	1.11
Vineyards	4.70	7.33	7.30
Fruit trees and berry plantations	2.68	3.21	3.21
Complex cultivation patterns	231.47	229.51	225.71
Land principally occupied by agriculture	43.53	36.85	36.77
Broad-leaved forest	41.67	42.09	42.09
Transitional woodland-shrub	11.61	11.33	11.33
Salt marshes	4.55	3.27	3.27
Coastal lagoons	-	1.34	1.34

5.1.1 FLOODING CONTEXT

At this point, once analyzed the effects of urbanization on the land-use changes, the focus shifts to the Brenta-Bacchiglione river basin that has been taken into consideration because of its localization within the boundaries of the study area (Figures 5.3 and 5.4) and also due to the frequent flood events occurred. This watershed, being characterized by many artificial and highly-modified channels in a tight spot, is a really vulnerable and fragile area, whose the disastrous floods, occurred over the past years, are a direct consequence (Fig. 5.17).

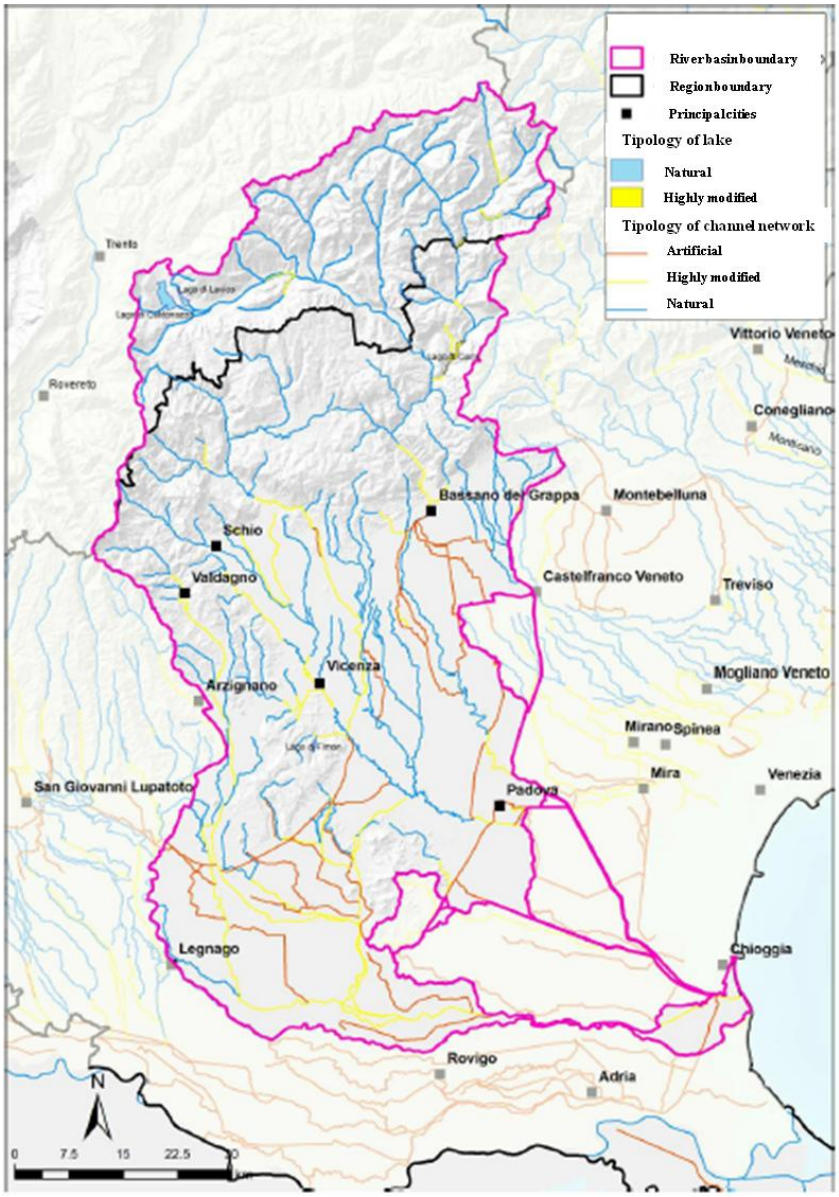

Fig. 5.17 Artificial, highly modified and natural channels within the Brenta-Bacchiglione river basin (modified from "Watershed plans of Eastern-Alps", 2010).

Among the reported flood events, which involved the Brenta-Bacchiglione river basin, those ones occurred in September 1882 and November 1966, have been the most critical because of the hydrometric level reached and duration of the event. In 1882, the inundation of Bacchiglione and its tributaries, affected Vicenza and its wide surrounding floodplains up to Thiene (province of Vicenza). In Padua, two embankments were destroyed near the areas of Limena and Bojon, the bridge located in Curtarolo collapsed and the weir of Strà was seriously damaged. In 1966, the flood was catastrophic because of the simultaneous occurrence of high-intensity rainfalls and a high tide of 1.95 m happened in the San Marco river basin (province of Venice) (Progetto di piano di stralcio per l'assetto idrogeologico dei bacini idrografici dei fiumi Isonzo, Tagliamento, Piave e Brenta-Bacchiglione). The sea-flood affected the nearby coastal territories and, in the convergent areas, it further obstructed the water flow carried by the rivers to the sea (Fig. 5.18). Floods occurred also due to the overflow stemming from the sewer system in the city of Padua. The Brenta river reached the hydrometric level of 5.6 m (above the zero hydrometric) recorded in Bassano del Grappa, while the Bacchiglione river achieved 8.6 m (above the zero hydrometric) in Montegaldella with a discharge value of 600 m^3/s.

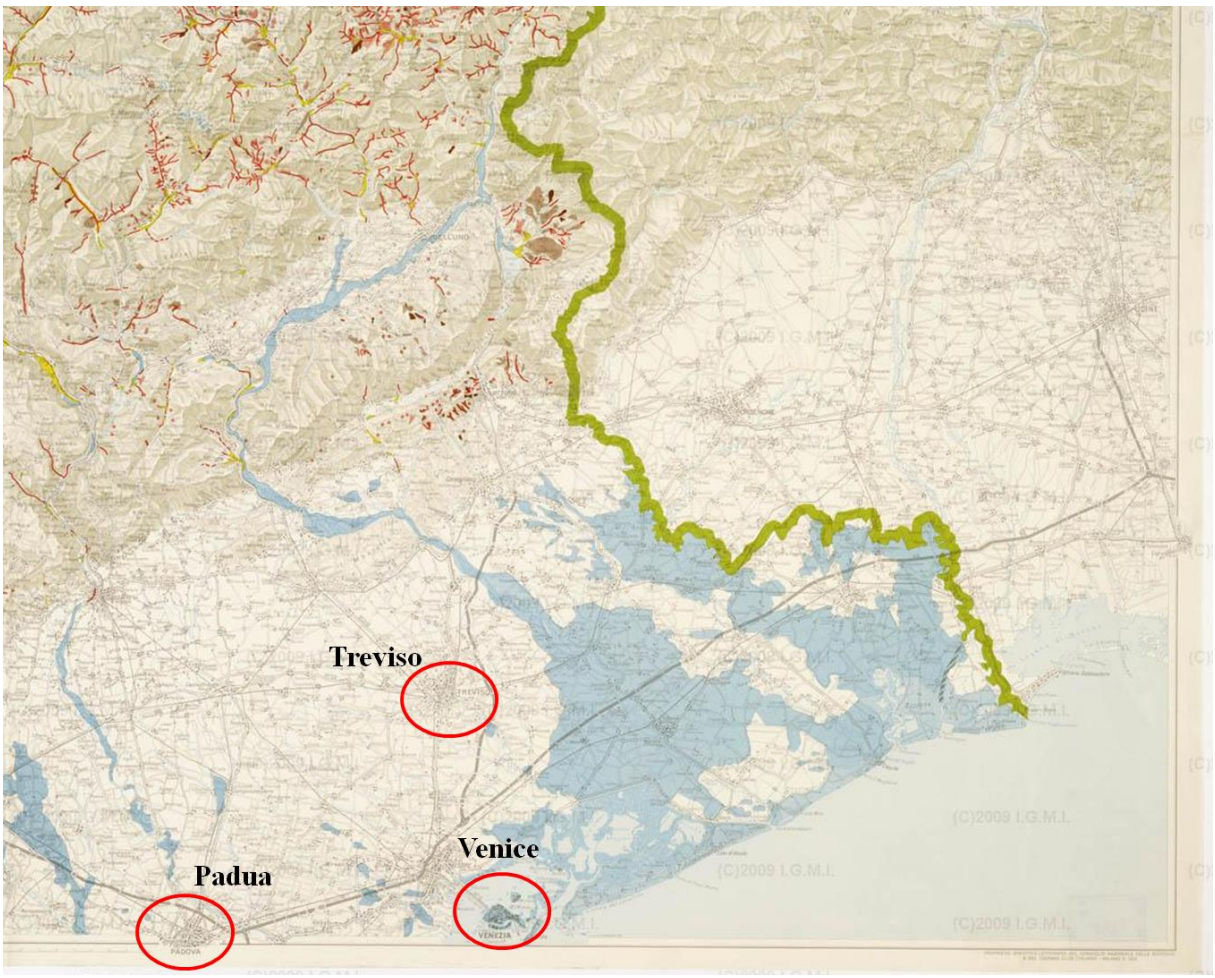

Fig. 5.18 The map of the 1966 flood in Veneto. Scale 1: 200000 (IGM, 1966).

Among the causes of these catastrophic events, it is extremely important to distinguish between those ones strictly related to the incapacity of the drainage network system (ditches and channels) to hold the discharges produced, from the problems which affect the big river basin systems. If, on one side, the issues related to the drainage network system mainly depend on fairly recent land-use changes, on the other one, the problems of the principal river systems, especially Brenta and Bacchiglione, date further back in the past. It is significant to highlight that, the discharges produced by the large rivers which affect the cities of the floodplains, are mainly produced in their respectively mountainous watersheds. The Brenta-Bacchiglione river basin system is extremely complex hydraulically speaking. Human beings caused evident transformations in order to solve the problems that occurred time by time over the years. One should bear in mind that the mouth of the Brenta river was moved from Fusina to Brondolo by the Venetians at the end of the fifteenth century in order to save the lagoon from the silting due to the materials carried by the water. On one side, this measure saved the

lagoon, but on the other one, made serious hydrological problems start in the city of Padua. Actually, Padua shows a really complex and fragile hydraulic configuration because of its location between the two rivers Brenta and Bacchiglione and the presence of various artificial and man-made channels which spread across the urban area. However, the actual hydraulic configuration is characterized by the presence of some significant elements for the flood risk prevention such as: the Scaricatore channel, the regulator support of Voltabarozzo located on the Scaricatore channel itself and the S. Gregorio channel (Fig. 5.19). These channels, with an intelligent management of their structures of regulation, have to prevent the city of Padua and its surroundings from the flood risk due to the Bacchiglione river. In fact, they should be able to route part of the discharge produced by the Bacchiglione river itself to the Brenta stream. In reality, the flood event of the November 1966 highlighted the vulnerability and precariousness of the state of hydraulic safety.

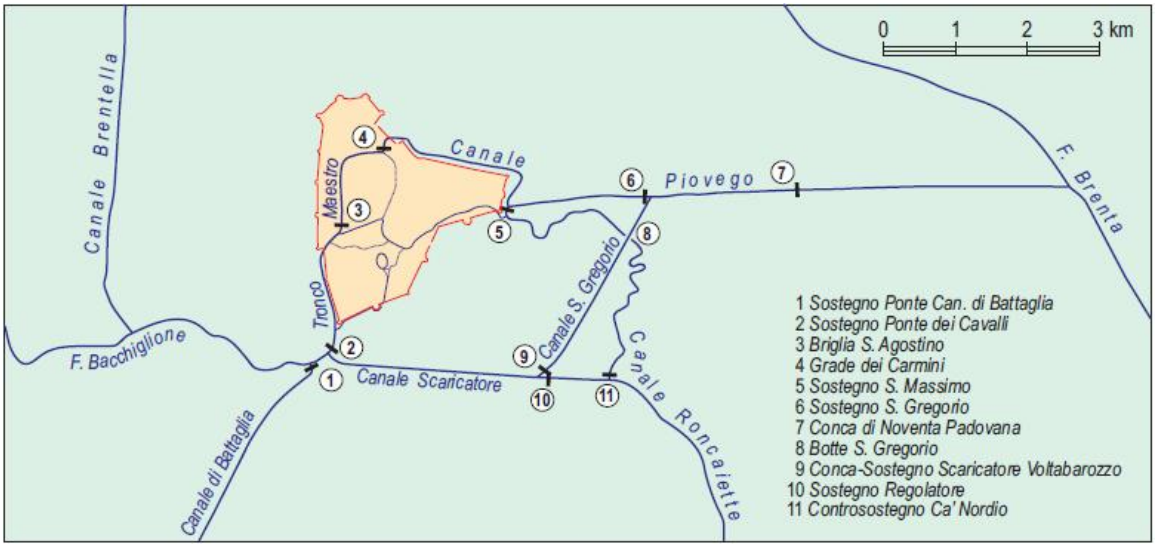

Fig. 5.19 Actual hydraulic configuration of Padua (d'Alpos, 2006).

At this point, the effects of the main flood event of 2010 that have been found in the study area, are reported. Five principal flooded areas have been identified within the boundaries of the study site and they have been obtained by grouping together the areas detected as flooded, according to warnings made by people (Fig. 5.20). The identification of these such flooded portions has been useful for the analysis successively made, reported in Chapt 6.

Fig. 5.20 Detection of the flooded areas according to the warnings made by common people. (http://www.downloadblog.it/post/13358/wiki-alluvione-veneto-2010).

This image (Fig. 5.20) has been georeferenced and the flooded areas copied and exported (Fig. 5.21).

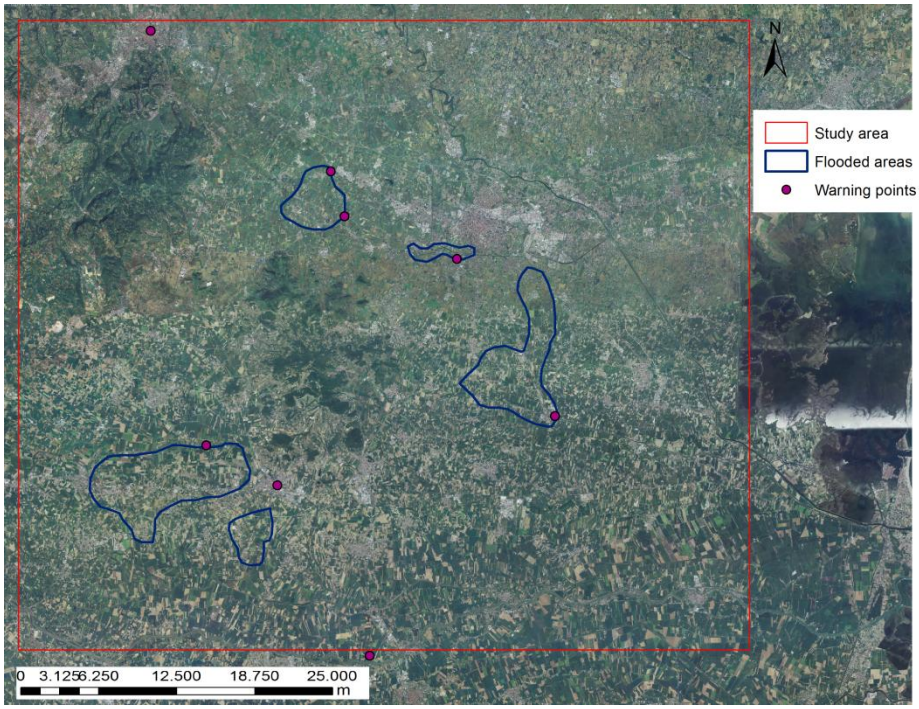

Fig. 5.21 Ortophoto of the study site showing the flooded areas in blue and the warning points georeferenced.

Other two georeferenced images relative to the floods occurred in the study site are reported in figures 5.22 and 5.23. Fig 5.22 shows the flooded areas detected using an image acquired by the Cosmo-SkyMed SAR sensor. Flooded areas are in cyan while permanent water bodies are in blue. The latter are identified on the basis of a Cosmo-SkyMed image under dry conditions and/or ancillary data such as a land cover map derived from optical images. On this map, the flooded areas identified thorough the warnings points, have been overlapped.

Figure 5.23, is a zoom in on the Bovolenta village, an area particularly damaged and affected by the flood event, that falls into the flooded area number 3. The flood of Bacchiglione river caused wide floods along the valley towards Casalserugo and Bovolenta. Some cities have been flooded, several roads, stretch of highways and railroads have been closed because impracticable due to water. Bovolenta was covered by several meters of water, as it can also be seen from the images 5.24 and 5.25. Many buildings and houses have been impracticable for days and schools have been closed by authorities.

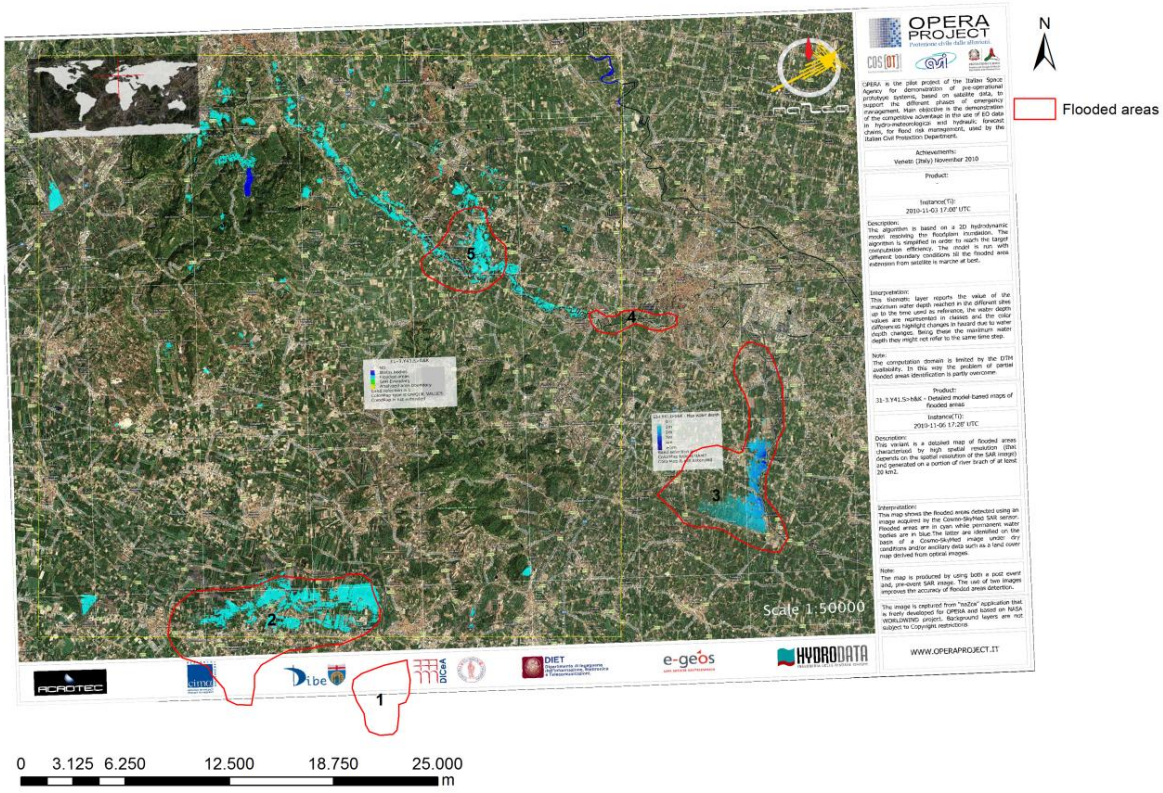

Fig. 5.22 Map showing the flooded areas detected using an image acquired by the Cosmo-SkyMed SAR sensor in 03/11/2010. This map is produced by using both a post event and, pre-event SAR image. The use of two images improves the accuracy of flooded areas detection.

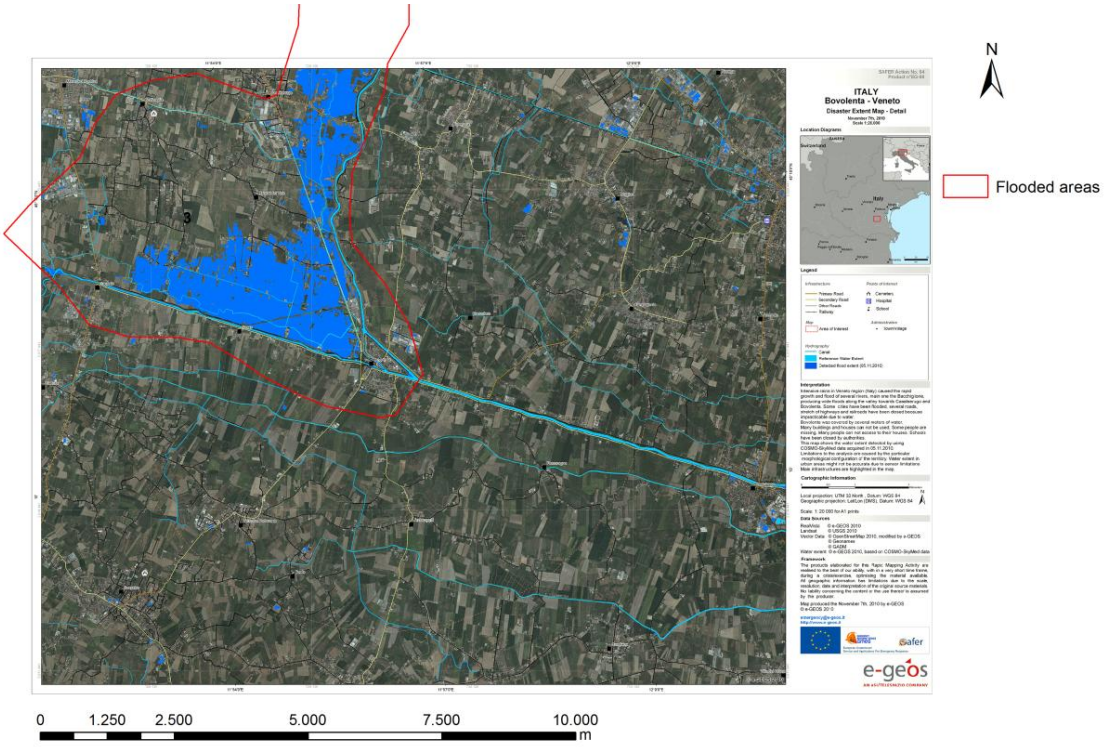

Fig. 5.23 Map showing the water extent detected by using COSMO-SkyMed data acquired in 05/11/2010. Limitations to the analysis are caused by the particular morphological configuration of the territory. Water extent in urban areas might not be accurate due to sensor limitations. Main infrastructures are highlighted in the map.

Fig. 5.24 Picture showing the critical situation in Bovolenta. The water level is higher than a truck (Alessandro Leorin, 2010).

Fig. 5.25 Other picture highlighting the catastrophic situation in Bovolenta. People are forced to roam by boats (Alessandro Leorin, 2010).

6 RESULTS AND DISCUSSION

The first step of the approach aimed to i) identify ditches and channels in a floodplain contexts, to ii) define some of the network statistics and to iii) analyze them in relation to the areas flooded during the flood event of October/ November 2010.

Even if, in some instances, the procedure detects localized pixels that do not correspond to the actual network location, and that can be classified as either noises or localized macro-depressions on the soil (Sofia, 2012), it proves to be reliable when the derived network is compared with the one in its real conformation. This correspondence is shown in Fig. 6.1, in which the derived network has been overlapped with an ortophoto of the agricultural floodplain.

Fig. 6.1 Example of the correspondence between the locations of the derived network and the real one.

In addition, in some cases, the procedure identifies the network better than the one represented by the official cartography (Regional Technical Maps), especially when this is not updated (Fig. 6.2).

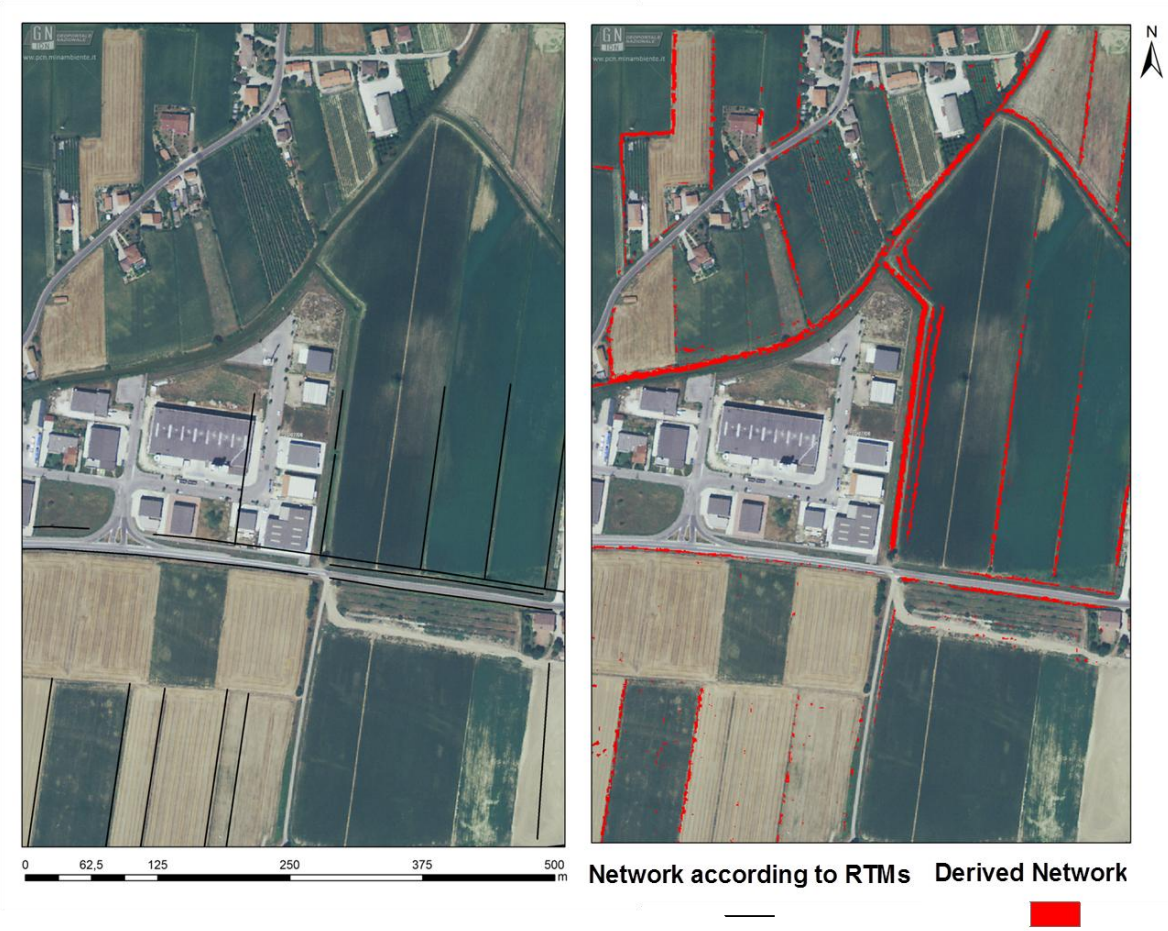

Fig. 6.2 Accuracy of evaluated network (red) and network as digitalized from official cartography (*Regional Technical Map – RTMs*-) (black) before updating. The underlying ortophoto shows how official cartography needs some update and adjustment.

Although some small inconsistencies between values exist due to the DTM grid cell constraint that determines a slight underestimation of the derived parameters (as it was registered by Cazorzi et al. 2011), the method allows the definition of some summary statistics generally available only through time-consuming and cost-prohibitive field surveys, such as network length, network width and storage capacity and drainage density indexes. As already reported in Chapt. 4.1, while the network length and drainage density have been computed directly, the storage capacity has been derived in a second step by associating some characteristic cross-section areas to width range.

Drainage density and storage capacity indexes are reported in figures 6.3 and 6.4. Areas flooded during the November event are also showed for further analysis. For both parameters, the respective distributions of values in relation to the surface of the study area have been reported in figures 6.5 and 6.6 respectively.

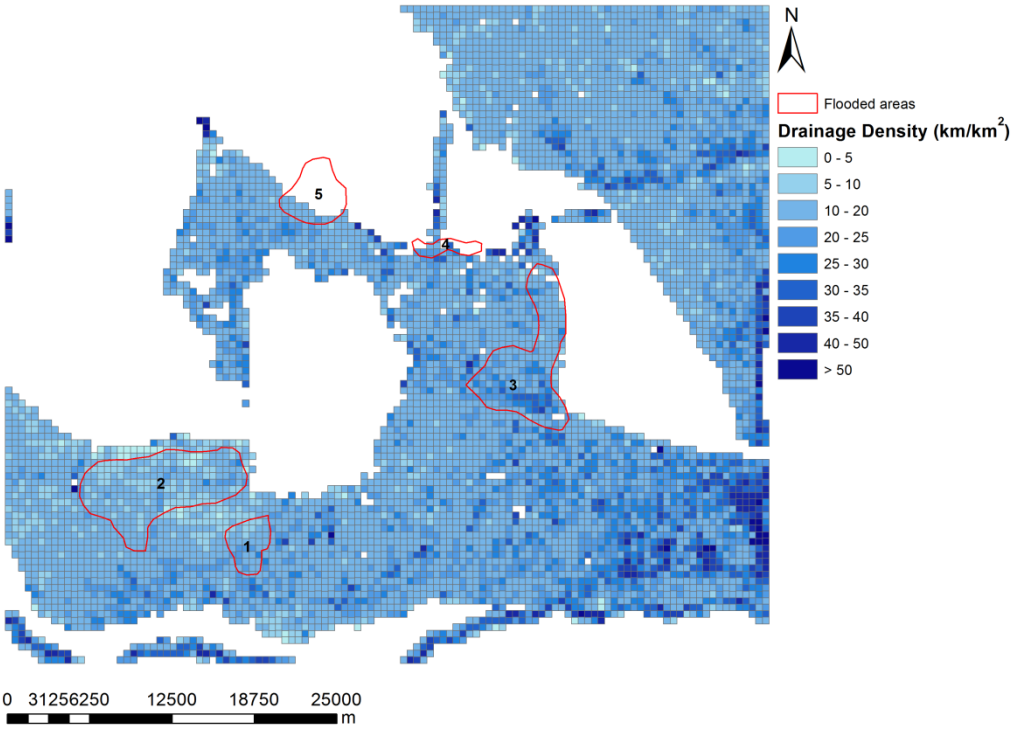

Fig. 6.3 Drainage density map derived for the study area. The areas that flooded during the flood event from October, 31st to November, 2nd 2010, are highlighted in red and numbered.

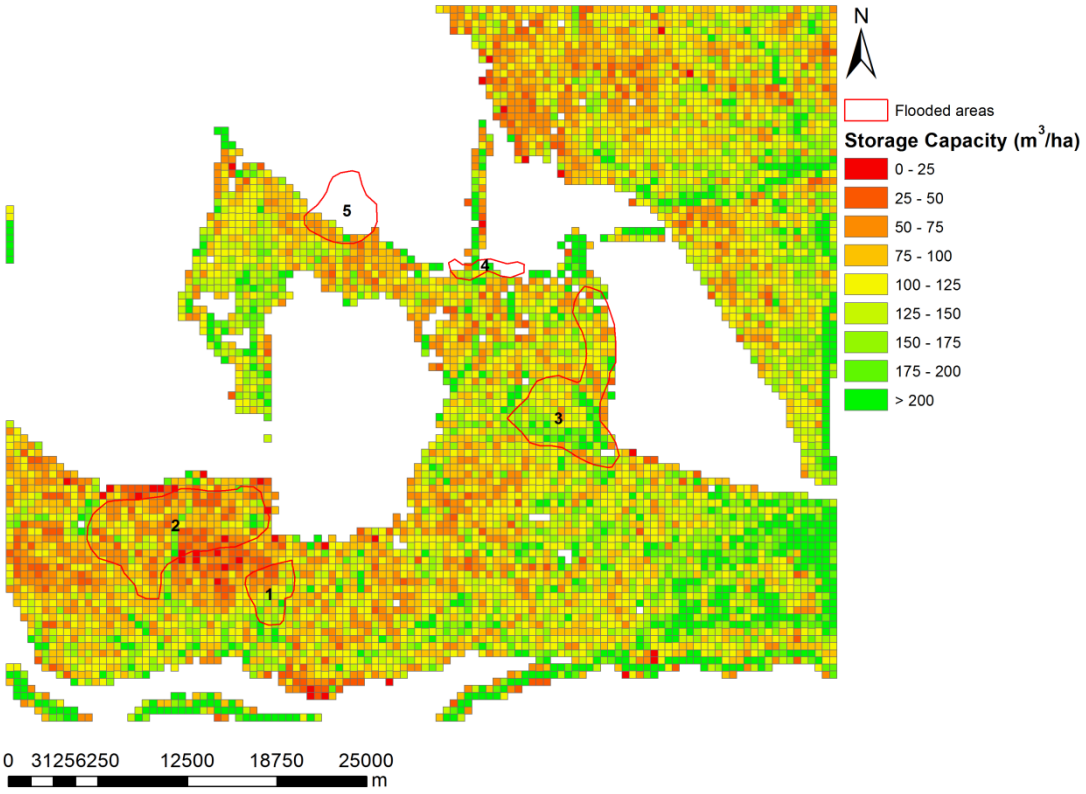

Fig. 6.4 Storage capacity map derived for the study area. The areas that flooded during the flood event from October, 31st to November, 2nd 2010, are highlighted in red and numbered.

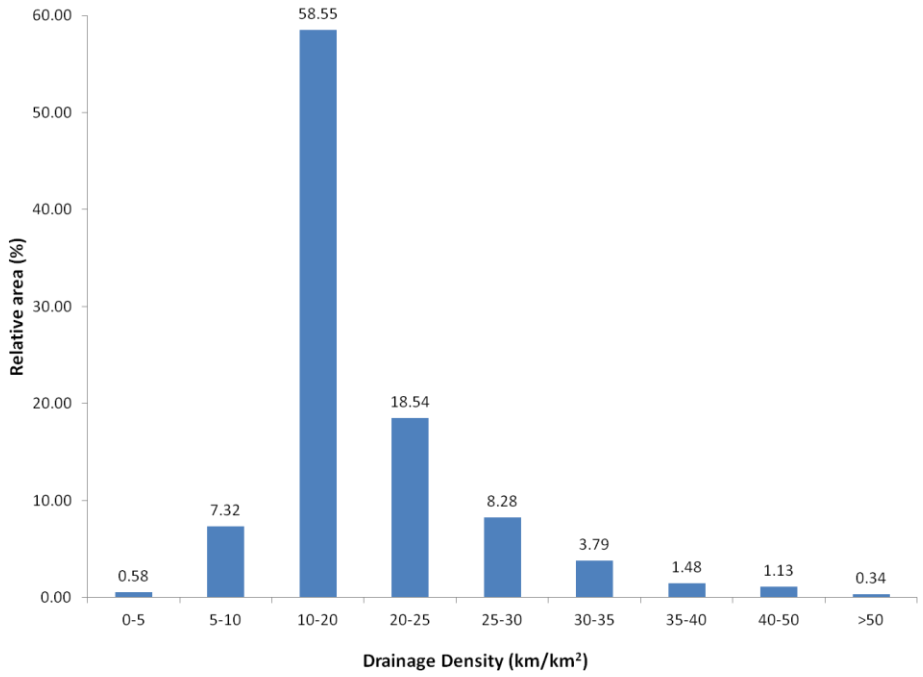

Fig. 6.5 Drainage density ranges in relation to the relative surface (%) of the study area. The most representative array of values is the one from 10 to 20 km/km^2.

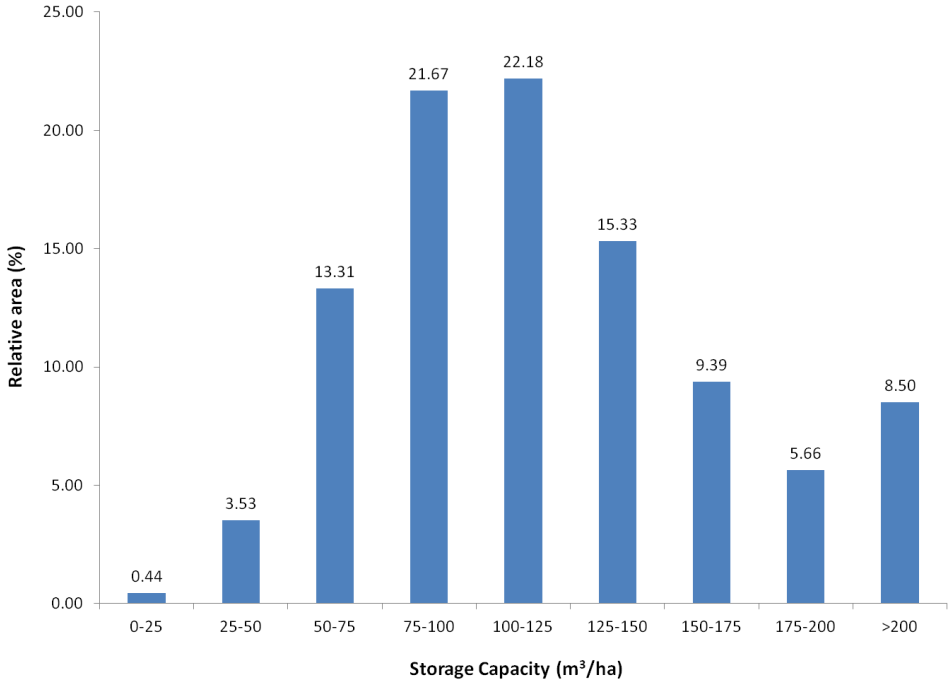

Fig. 6.6 Storage capacity ranges in relation to the relative surface (%) of the study area. The most representative arrays of values are the ones from 75 to 100 and from 100 to 125 m^3/ha.

Considering the drainage density, the area appears to be characterized mainly by a drainage density ranging from 10 to 20 km/km^2 (Fig. 6.5). High values of drainage density (>50

km/km^2) are registered in the south east part of the study area, where there is a higher fragmentation of fields, and in-field network varies greatly, depending on farmers choices. The same areas are indeed characterized also by high values of storage capacity (>200 m^3/ha). The lower values of storage capacity and drainage density are related instead to either expanding urban areas (majority of instances), or some small areas where surface irrigation has been progressively replaced by underground irrigation systems.

The evaluation of such indexes, in particular the evaluation of storage capacity, is extremely important in the perspective of flood management because low values of channel storage capacity can underline deficit in the network, and they can outline areas whose hydrological behavior is potentially critical during floods. In general, ditches should be able to drain about 40-50% of a 24hr rainfall with a return time of 5-10 years, and in average for Italy, such rainfall ranges between 50 and 70 mm. As a consequence, depending on the soil types, generally to have a good hydraulic efficiency it is suggested to maintain values of storage capacity of about 150 m^3/ha, or anyway values ranging between 100 and 200 m^3/ha. It is interesting to note that, according to the study results, about 40% of the whole area is characterized by values of storage capacity lower than 100 m^3/ha, and 18% of the area has values that are lower than 75 m^3/ha. These preliminary results underline how there might be some problems in the network, in the case of intense rainfall events.

To further investigate this aspect, a comparison between the drainage density, storage capacity maps and the areas that flooded during the flood event from October, 31st to November, 2nd 2010, has been carried out (Fig. 6.3 and 6.4). The flooded areas that have been identified are the same ones reported in Chapt 5.1.1, Fig. 5.21.

It is possible to assess if there might be a correspondence between low values of drainage density and channel storage capacity, and potentially critical areas. For example, the flooded area number 2, shows low values of both indexes and, as it will be later better discussed, a low capacity of attenuating the precipitation. Therefore, based only on this kind of evaluation, this specific area could be considered as potentially critical. A more detailed assessment should require to account also for the runoff coming from upstream: it is important to point out that the actual break of embankments, registered in the considered section, was not caused only by the local precipitation occurred in the floodplains, but was mainly due to the combination of upstream runoff and the incapacity of the minor drainage network to laminate the local surface runoff. In support of this, a spatially distributed rainfall map of the flood event is shown in Fig. 6.7, in order to stress how the local rainfall values were not so high to cause the flooding by themselves.

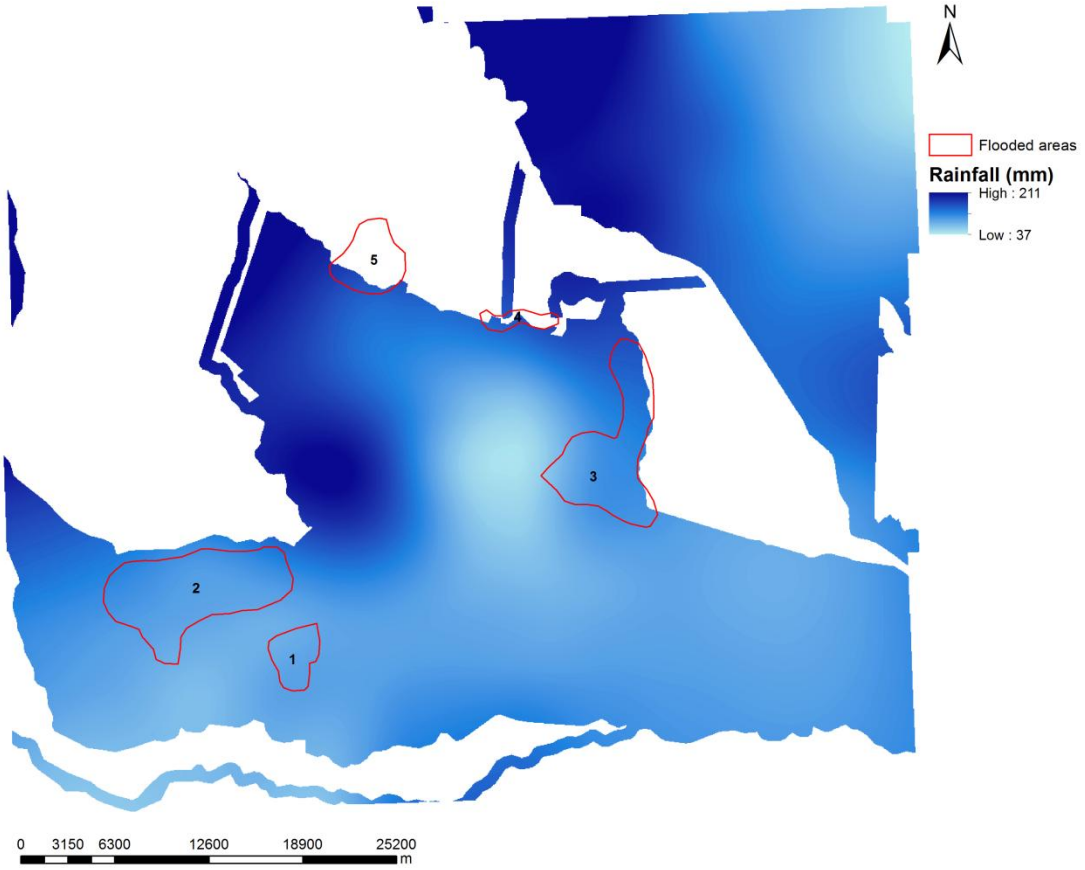

Fig. 6.7 Distributed rainfall map of the event occurred from October, 31st to November, 2nd 2010. Rainfall values in correspondence of the flooded areas are pretty low, especially in the southern ones. This fact confirms that the break of the embankments was mainly due to the runoff coming from upstream and, eventually, to the incapacity of the minor drainage network to laminate the local surface runoff.

To further investigate the relationship between network storage and critical aspect of the network, we computed the surface runoff produced during the flood event considering different land uses, and we compared the drainage network storage capacity with the direct surface runoff (Pe).

As already explained in Chapt. 4.2, three different land-use maps, dated back to 1990, 2000 and 2006, have been used in order to produce at first, the curve number and then, the direct runoff maps for the study area. It is important to remind that, differently from the CN maps that change according to the year of land-use data, the input rainfall map is always the same and it relies on the main rainfall event occurred between October and November 2010. This kind of analysis aims to assess how differently the land may respond to the same input of rainfall over the years. The curve number maps are shown in figures 6.8, 6.9 and 6.10. As it

can be seen from the legend, the more red are the areas and the higher are the CN values, and so the greater is the propension of a soil to produce runoff.

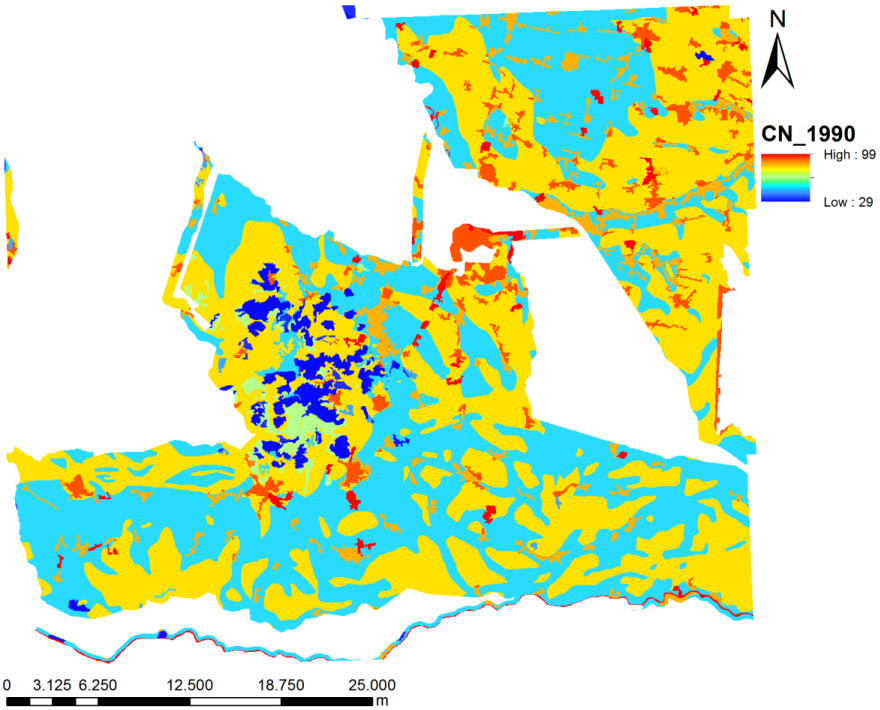

Fig. 6.8 Curve Number map based on the land-use data of 1990.

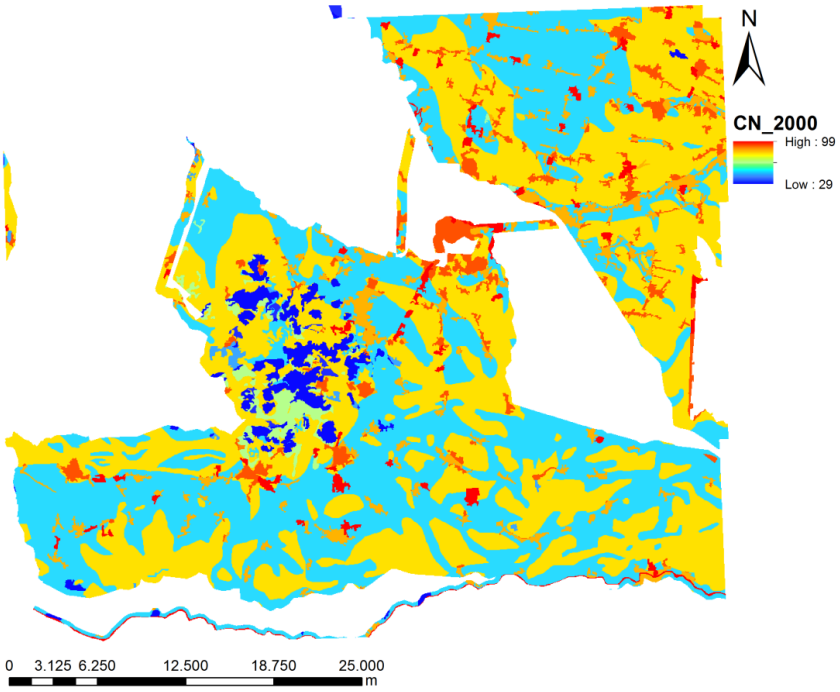

Fig. 6.9 Curve Number map based on the land-use data of 2000.

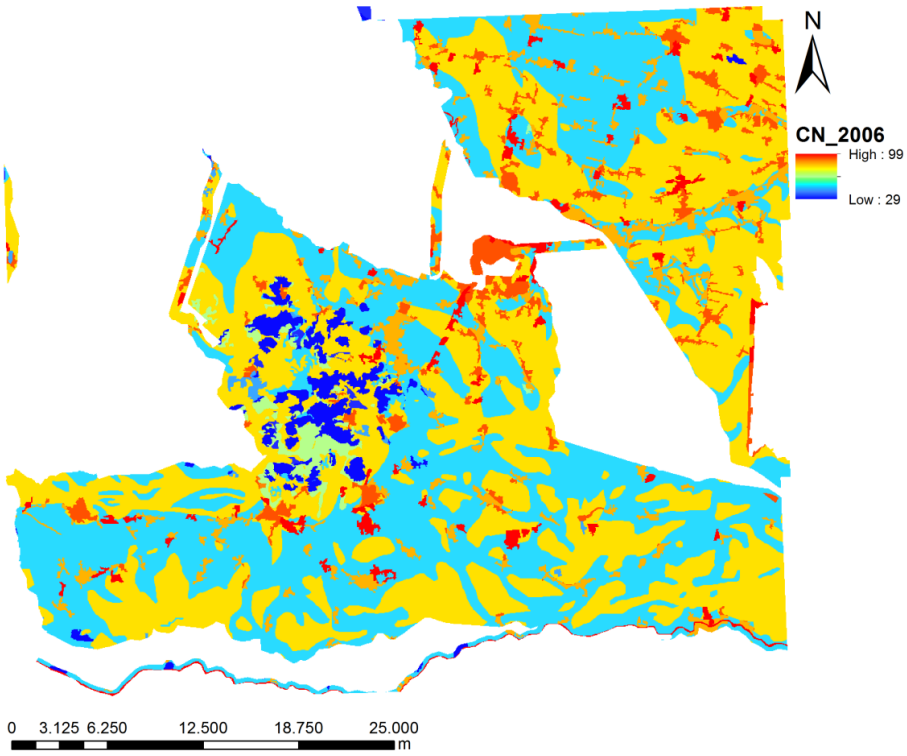

Fig. 6.10 Curve Number map based on the land-use data of 2006.

The direct runoff maps are shown in figures 6.11, 6.13 and 6.15 with the flooded areas highlighted in red. Histograms of the mean runoff computed for each of the 500m x 500m subareas are reported in figures 6.12, 6.14 and 6.16.

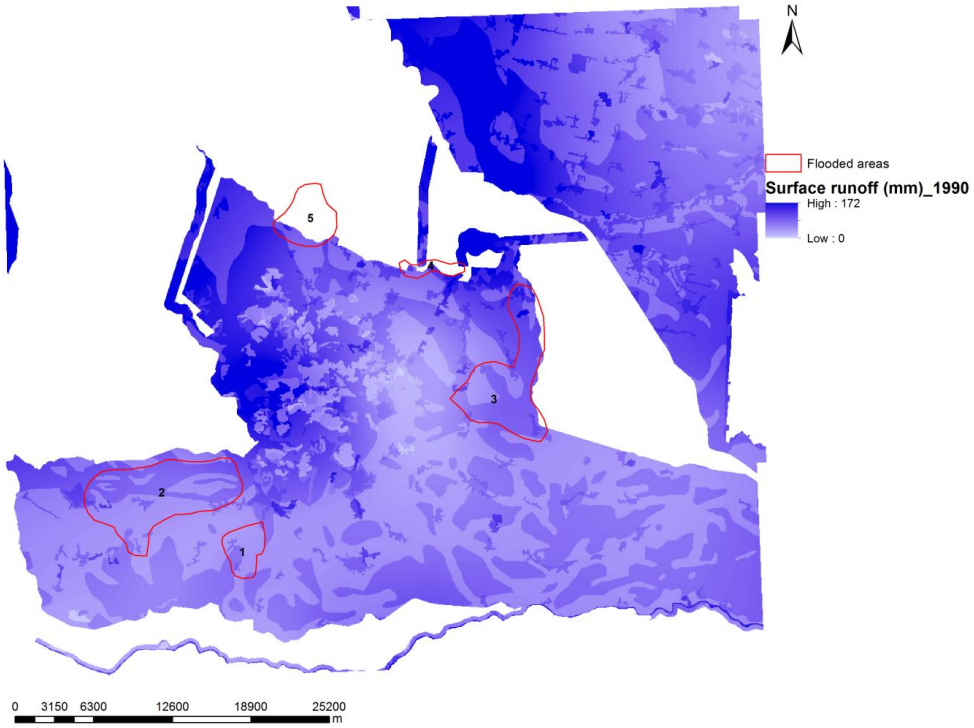

Fig. 6.11 Surface runoff map computed through the SCS-CN method (1990). The areas that flooded during the flood event from October, 31st to November, 2nd 2010, are highlighted in red and numbered.

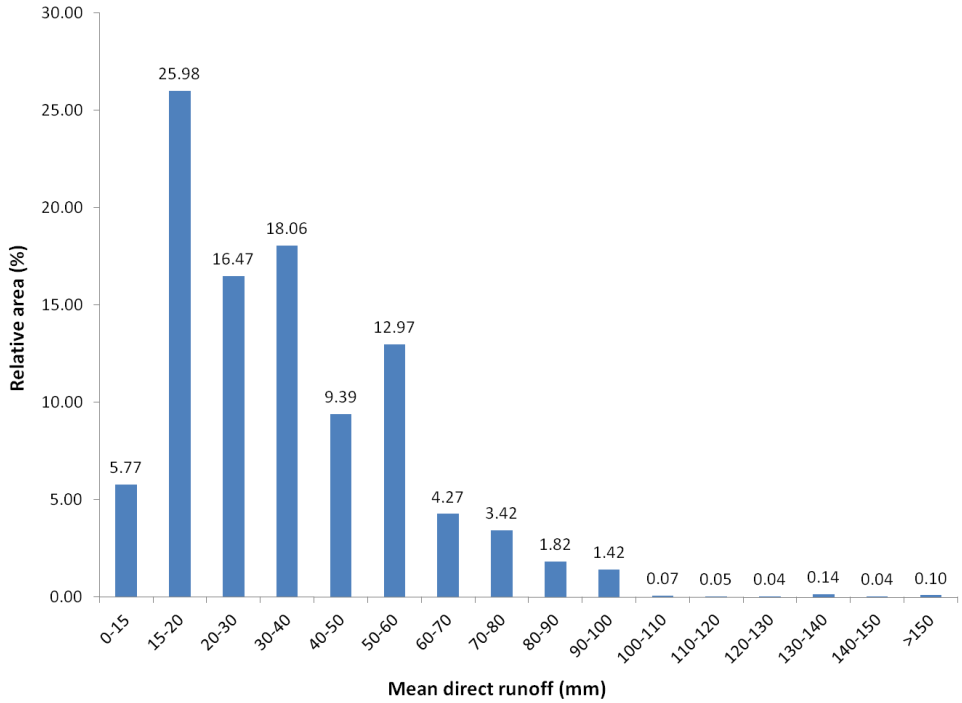

Fig. 6.12 Histogram showing the mean direct runoff in relation to the relative surface (%) of the study area, according to the land-use data of 1990. The ranges of values more distributed over the study area are the following ones: 15-20, 20-30 and 30-40 mm. In fact, they make together the 60.5 % of the whole area. From the class 90-100 mm on, the corresponding relative area (%) is almost nonexistent.

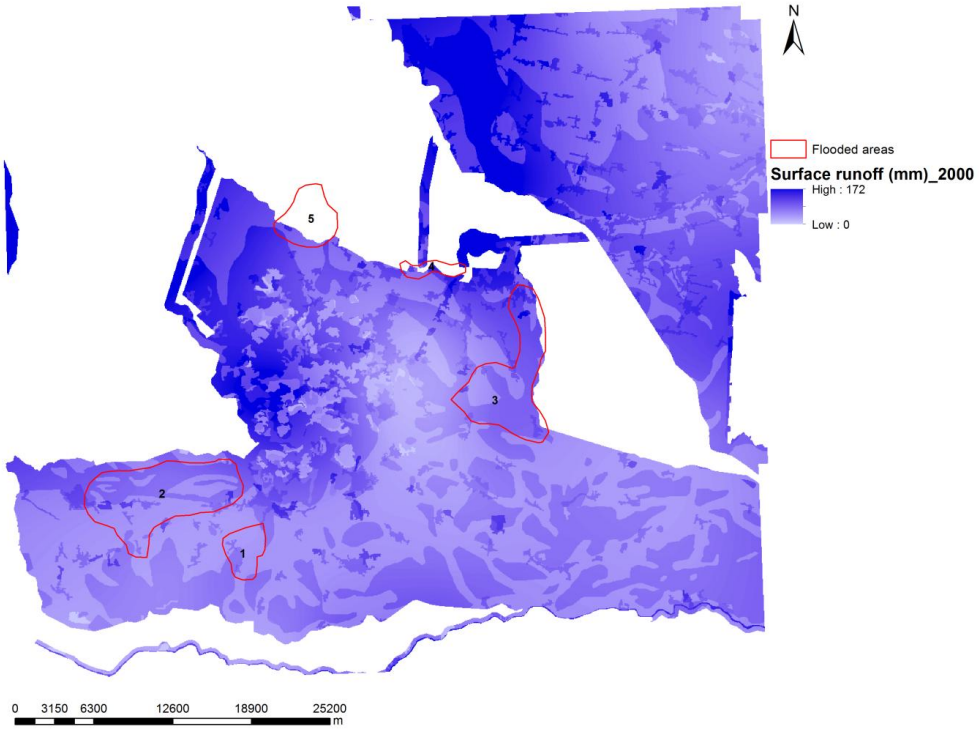

Fig. 6.13 Surface runoff map computed through the SCS-CN method (2000). The areas that flooded during the flood event from October, 31st to November, 2nd 2010, are highlighted in red and numbered.

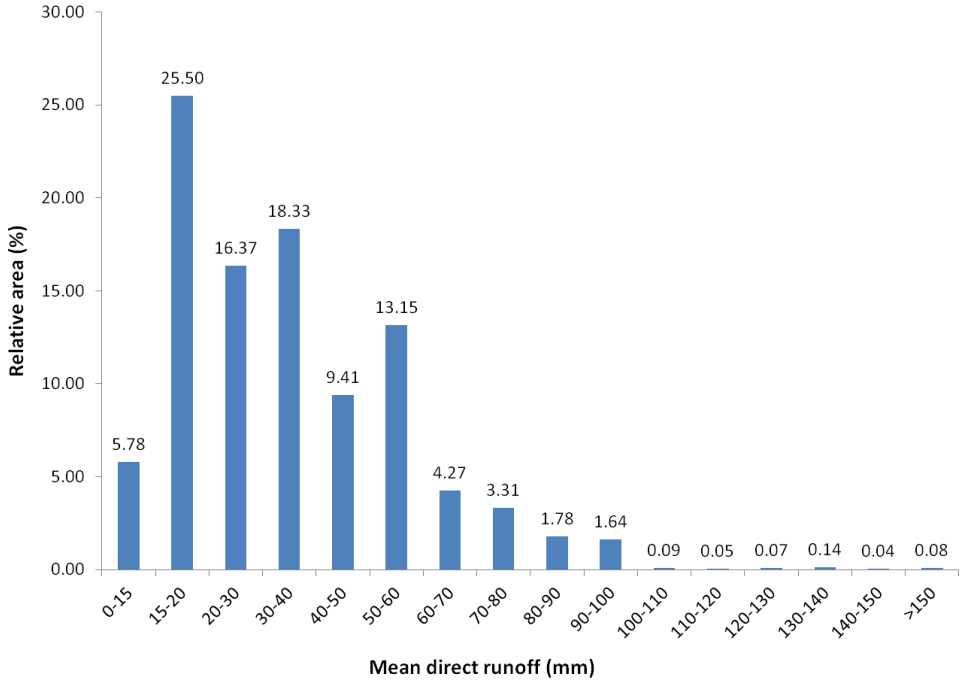

Fig. 6.14 Histogram showing the mean direct runoff in relation to the relative surface (%) of the study area, according to the land-use data of 2000. The situation shown is very similar to the one registered ten years before. The ranges of values more distributed over the study area are still the following ones: 15-20, 20-30 and 30-40 mm. From the class 90-100 mm on, the corresponding relative area (%) is almost nonexistent.

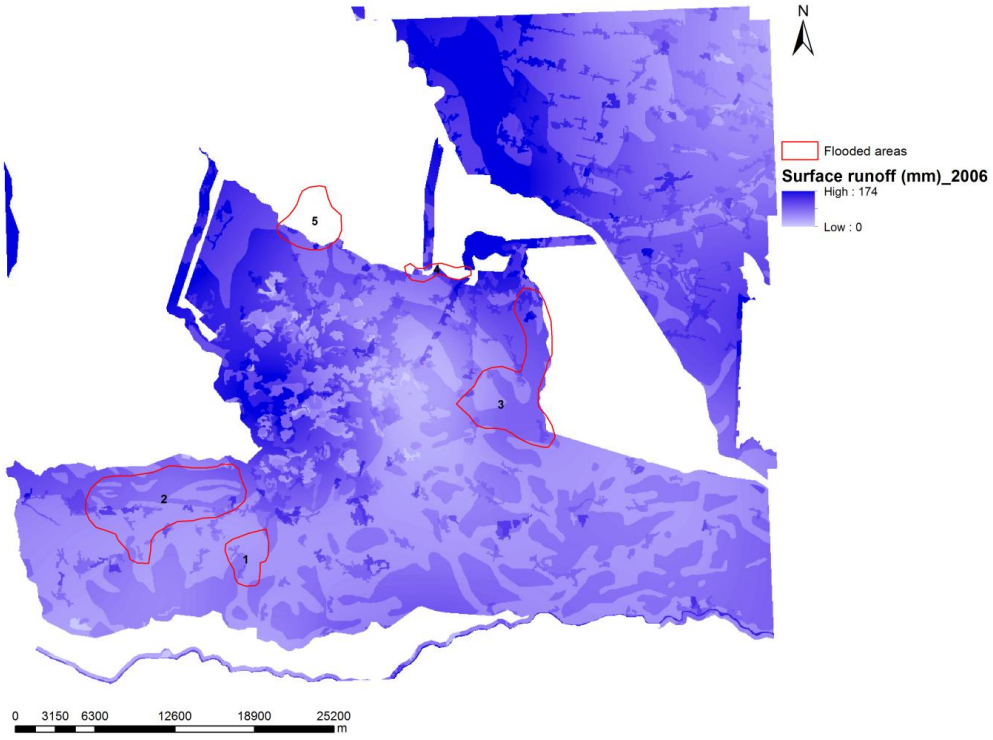

Fig. 6.15 Surface runoff map computed through the SCS-CN method (2006). The areas that flooded during the flood event from October, 31st to November, 2nd 2010, are highlighted in red and numbered.

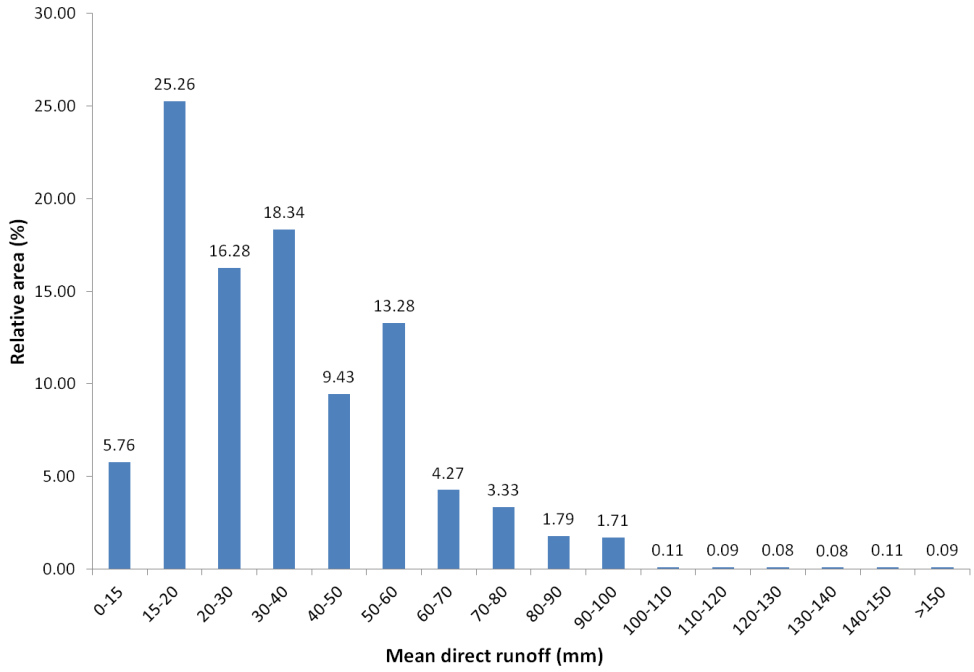

Fig. 6.16 Histogram showing the mean direct runoff in relation to the relative surface (%) of the study area, according to the land-use data of 2006. The situation shown is pretty similar to the ones previously analyzed. The ranges of values more distributed over the study area are still the following ones: 15-20, 20-30 and 30-40 mm and from the class 90-100 mm on, the corresponding relative area (%) is almost nonexistent.

To quantify runoff variations, the histograms have been compared in Fig. 6.17. In addition, differences between mean, maximum and minimum values of the direct runoffs computed for the three different years, are shown in Tab. 6.1.

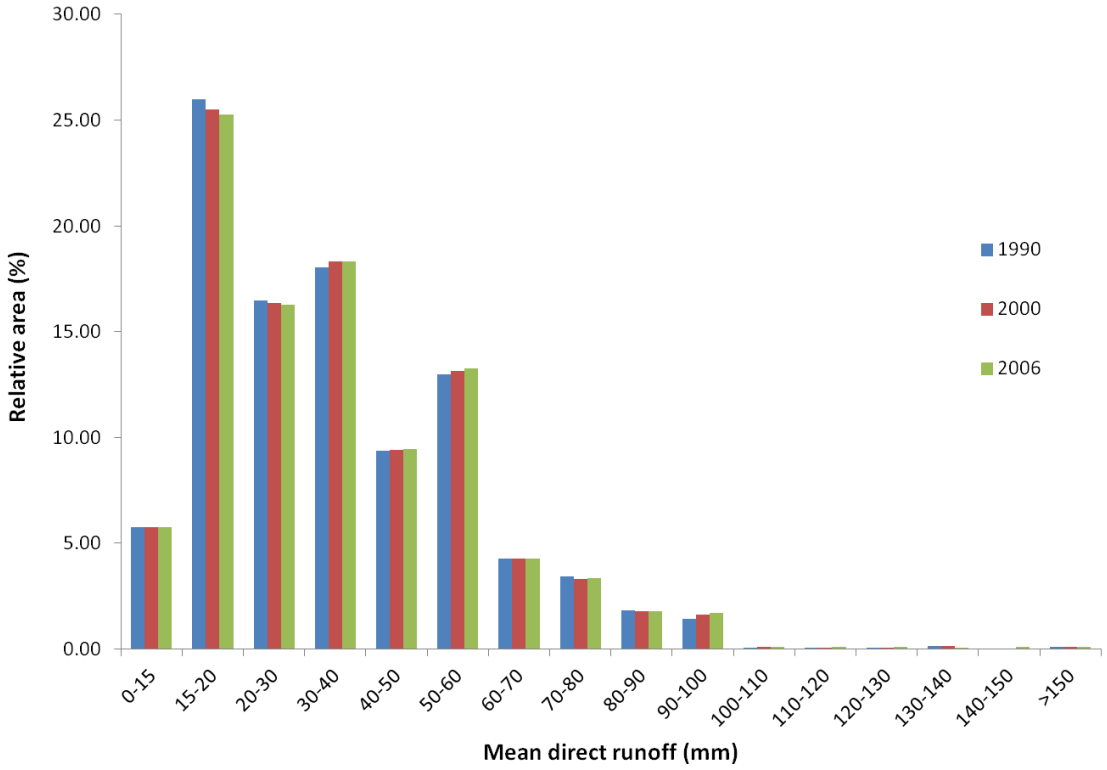

Fig. 6.17 Comparison between the three mean direct runoffs for the whole study area.

From Fig. 6.17, it emerges that, in 1990, more areas were affected by low values of runoff (lower than 30 mm). However, due to change in land use, higher values of mean direct runoffs are registered for larger areas in 2000 and 2006. This may be explained by considering a possible increase in impermeable surfaces.

Table 6.1 Mean, minimum and maximum values of the three direct runoffs for the whole study area.

	1990 (mm)	2000 (mm)	2006 (mm)
Mean	36.99	37.19	37.39
Minimum	0.06	0.06	0.06
Maximum	172.05	172.05	173.59

From Tab. 6.1, it emerges that the minimum value of direct runoff, equal to 0.06 mm, remains unchanged over the years, while both the mean and maximum ones, slightly increase from 1990 to 2006.

To sum up, based on the available land-use data and the elaborations obtained, it is possible to state that an alteration in direct runoff, computed through the SCS-CN method, has been registered over the years of analysis. This modification is due to the land-use change occurred from 1990 to 2006. This alteration manifests itself with an increase of the surface runoff probably due to the enlargement of impermeable areas caused by urbanization processes. Even though this increase in direct runoff is very small, it should be noticed that the values in consideration are in millimeters and that must be extended over an area which is about 1800 km^2. Therefore, also one additional millimeter multiplied per such an area, can produce significant outcomes.

At this point, the results of the effects of drainage network storage capacity on direct runoff, either for the entire study area and for the flooded parts, are reported. As already explained in Chapt. 4.2, the storage drainage capacities are analyzed in the perspective of laminating the direct runoff. The greater are the values of storage capacity and the higher is the capacity of the land to attenuate the surface runoff produced by a flood event. To compute the lamination effect, a simple index (residual runoff) has been computed, as the difference between the direct runoff and the effective storage capacity. Considering that the storage capacity relies on the computation based on the 2010 DTM, this value remains the same for the evaluation of residual runoff. As a consequence, a higher residual runoff correspond to an increase of direct runoff, as well as a lower residual runoff can only be explained through a reduction of direct runoff. The increase in direct runoff is related to the land-use change occurred over the years. This simple comparison is provided to verify the effectiveness of the actual network on laminating the direct runoff produced by the November flood event. It must be underlined that in such kind of analysis, for a more complete evaluation, the upstream contributions should be also accounted for, but this simplified assessment aims to identify the presence of areas that may be already risky simply for the runoff directly produced by the input local rainfall. This simplified analysis, however, is provided also to underline that change in land use (in this case considering the evolution during the years), should be also accounted in planning and managing procedures: the increase of the runoff due to land use change should always be accounted for, and it should be operationally compensated by a correspondent increasing of the storage capacity. Furthermore, it is likely thinkable that variations of the drainage network system are related to land use changes as well, and, although the quantification of the water

storage capacity for the past periods has not been possible, it could be very interesting and useful for future projects.

Figure 6.18 shows the mean residual runoff of the whole study area computed for the three available land-use data. Looking at the mentioned graph, the negative values of the residual runoff correspond to areas where the storage capacity is much higher than the direct runoff or, where the latter may is null. As the residual runoff increases, it means that the direct runoff increases as well. The graph assumes a bell-shaped form in which the central values are the most distributed ones over the study area. What emerges is that, as long as residual runoff is either negative or however fairly low (along the rising limb), the land-use change did not cause a worsening of the situation. On the contrary, along the recession limb, where the residual runoff is greater, the one of 2006, represented by the green color, is always higher than the other two; therefore, it means that to higher residual runoff correspond also higher relative areas.

The mean, minimum and maximum values of residual runoff computed for the three years are reported in Tab. 6.2.

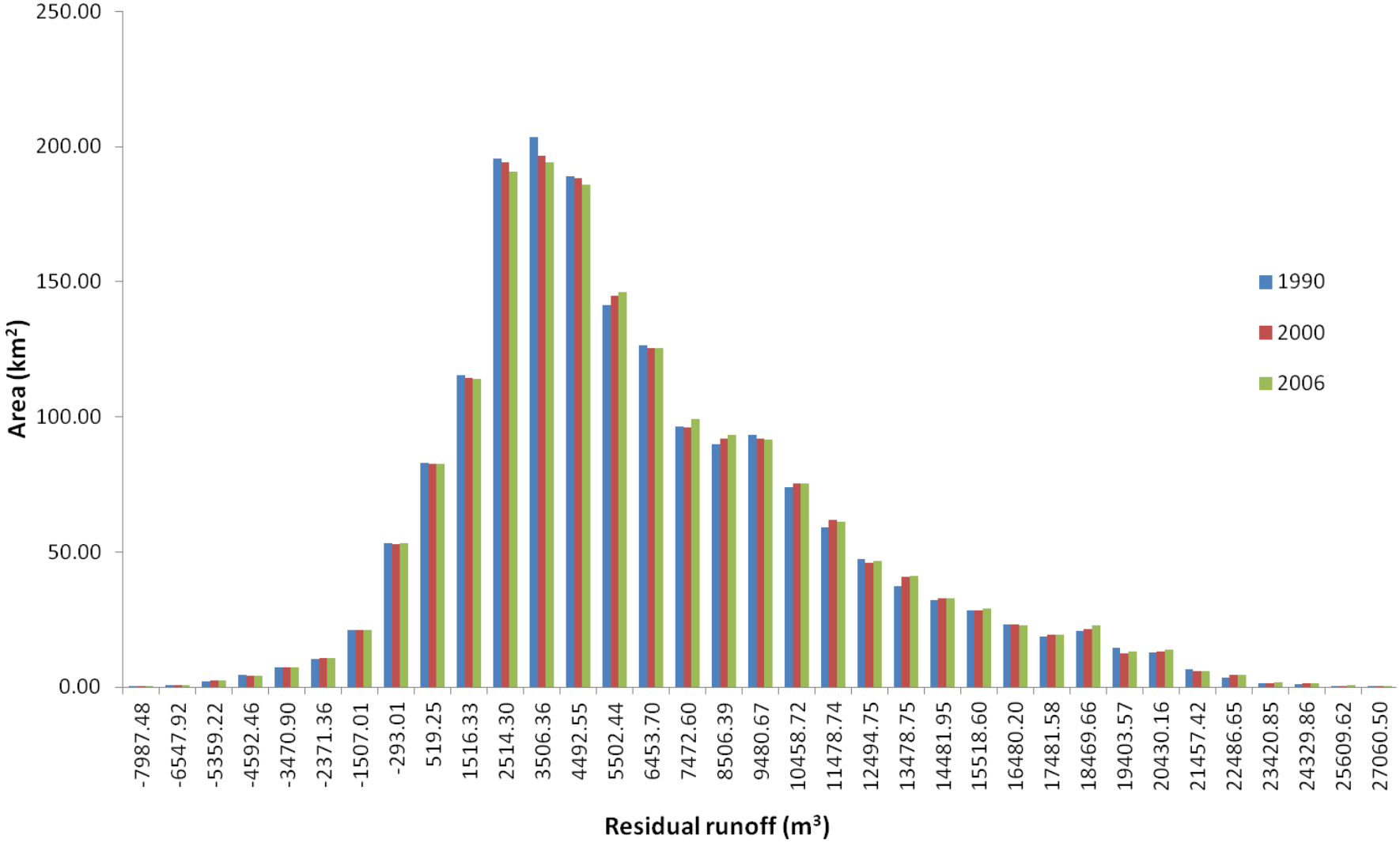

Fig. 6.18 Histogram showing the residual runoff of the whole study area computed for the three different land-uses.

Table 6.2 Mean, minimum and maximum values of residual runoff computed for the three different land uses over the whole study area. The increase of the mean value from 1990 to 2006 gives evidence of the increase of the direct runoff over the years.

	1990 (m^3)	2000 (m^3)	2006 (m^3)
Mean	6319.94	6365.15	6411.16
Minimum	-8000.00	-8000.00	-8000.00
Maximum	29000.00	28000.00	28000.00

At this point, we focused the analysis in each of the five flooded area (1 to 5 in figures 6.3 and 6.4), and the following results will be reported and assessed:

- drainage density and storage capacity maps and relative histograms;
- mean, minimum and maximum values of direct runoff according to 1990, 2000 and 2006 land uses;
- mean, minimum and maximum values of residual runoff for the three land-uses.

At the end, a summary table of the results will be shown and discussed (Tab. 6.13).

Flooded area number 1

The drainage density and storage capacity maps are respectively shown in Fig. 6.19, while their relative histograms are reported in Fig. 6.20.

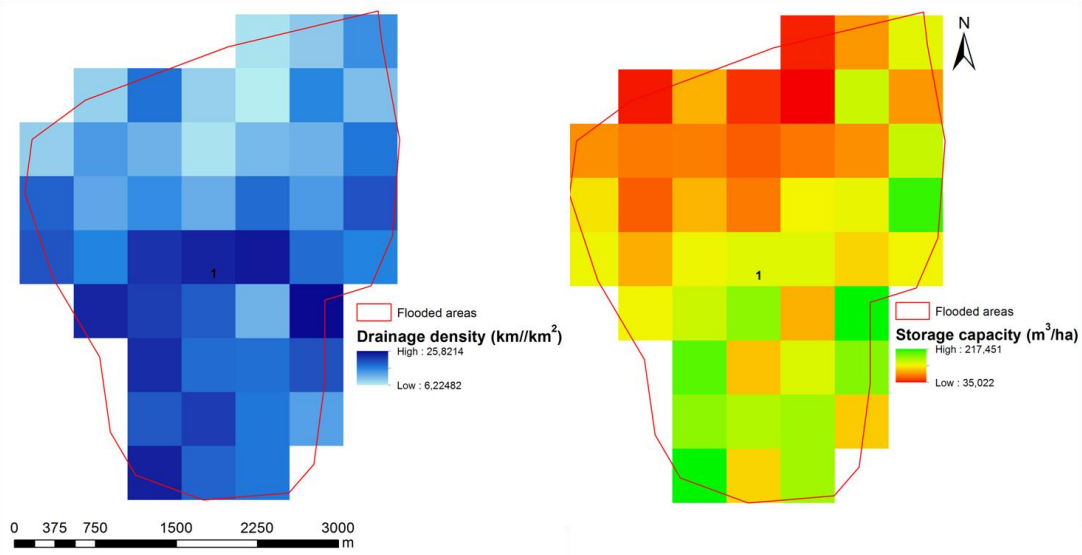

Fig. 6.19 Drainage density and storage capacity maps derived for the flooded area number 1. Low values of channel storage capacity can underline deficit in the network. See the correspondence between pixels that have high values of drainage density and high values of storage capacity too.

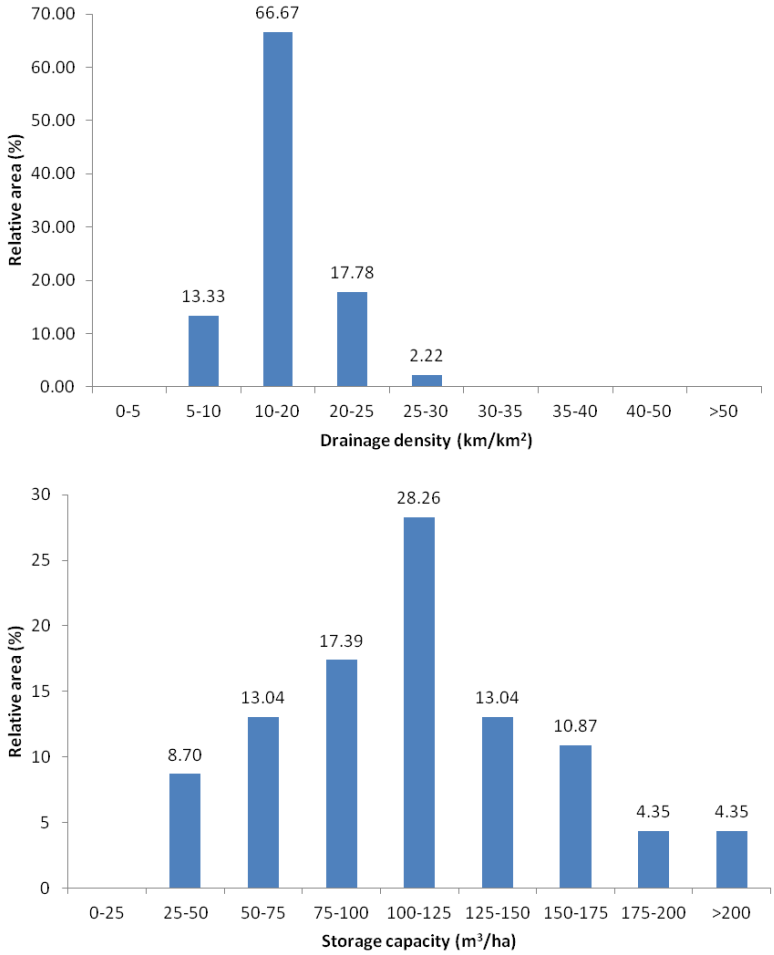

Fig. 6.20 Drainage density (a) and storage capacity (b) histograms for the flooded area number 1.

From Fig. 6.20, drainage density for the area is mainly characterized by values of 10-20 km/km^2 (66.67% of the area); in relation to the storage capacity, the central ranges 100-125 and 75-100 m^3/ha constitute the 45.65% of the area. In addition it is important to state that higher values of storage capacity are present, although represented by smaller portions of area.

In Tab. 6.3, the direct runoffs for the different land-uses, still computed through the SCS-CN method, are instead reported. From the table, emerges that, for this first flooded area, an increase of the mean value of direct runoff has been registered from 1990 to 2006.

Table 6.3 Mean, minimum and maximum values of direct runoffs (mm) computed for the three different land-uses in the flooded area number 1.

	1990 (mm)	2000 (mm)	2006 (mm)
Mean	21.68	21.72	21.80
Minimum	16.34	16.34	16.34
Maximum	41.89	41.89	41.89

Tab. 6.4 shows the mean, minimum and maximum values of residual runoff.

Table 6.4 Mean, minimum and maximum values of residual runoff computed for the three different land uses in the flooded area number 1.

	1990 (m^3)	2000 (m^3)	2006 (m^3)
Mean	3249.65	3259.22	3278.08
Minimum	800.00	800.00	800.00
Maximum	6400.00	6400.00	6400.00

Tab. 6.4 points out how the residual runoff has increased over the years. As, already explained before, this increase stands for an increase of direct runoff due to the enlargement of paved areas, and it underlines how the hydraulic efficiency of the area, without any network variation, is negatively influenced.

Flooded area number 2

The drainage density and storage capacity maps are respectively shown in Fig. 6.21, while their relative histograms are reported in Fig. 6.22.

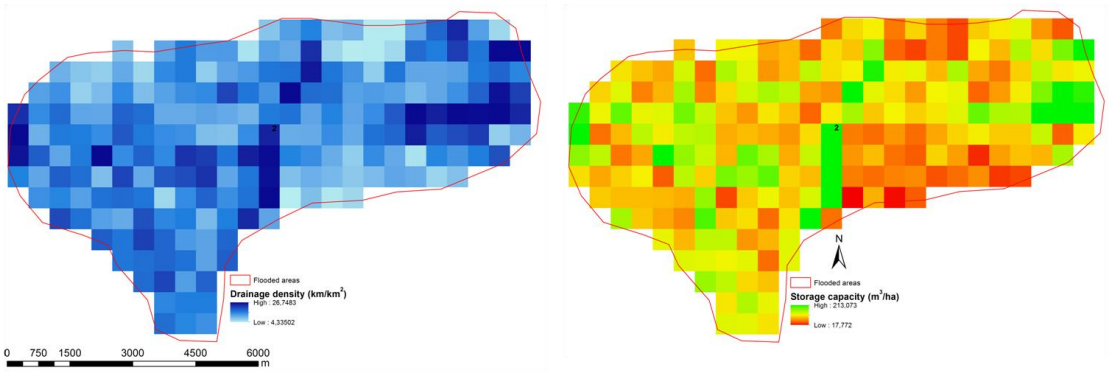

Fig. 6.21 Drainage density and storage capacity maps derived for the flooded area number 2. Low values of channel storage capacity can underline deficit in the network. See the correspondence between pixels that have high values of drainage density and high values of storage capacity too.

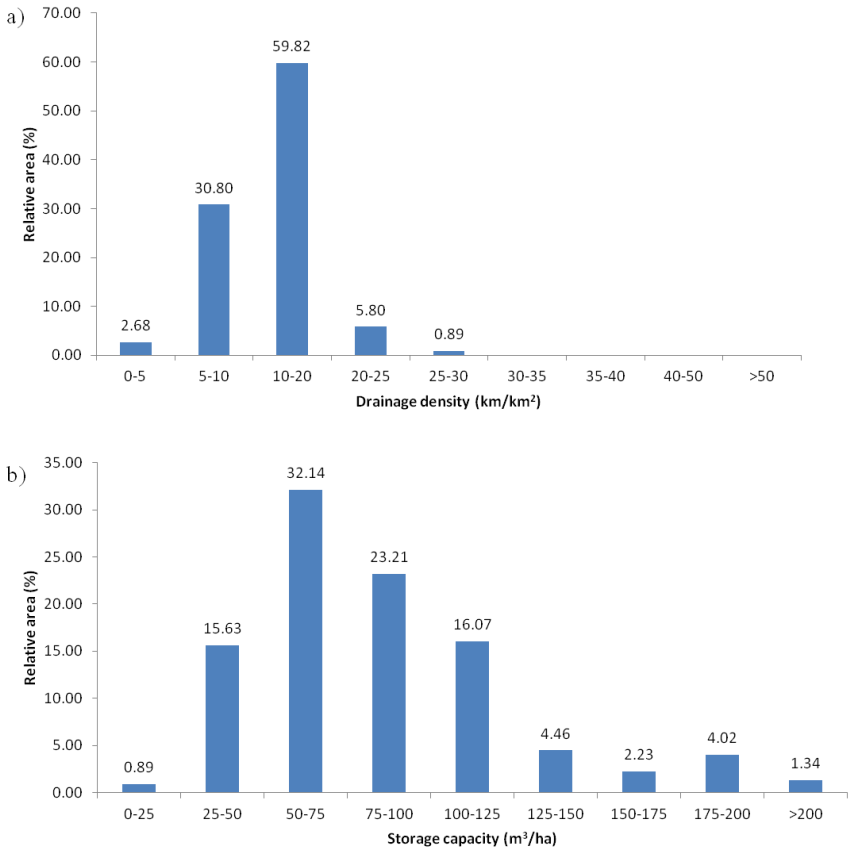

Fig. 6.22 Drainage density (a) and storage capacity (b) histograms for the flooded area number 2.

Fig. 6.22 points out the most representative classes of both drainage density and storage capacity indexes. Concerning the former one, the range 10-20 km/km^2 is greater than all the other ones, making the 59.82% of the area; while in relation to the storage capacity, the

ranges 50-75 and 75-100 m^3/ha constitute the 55.35% of the area. In addition, still talking about storage capacity, it is important to state that also the higher ranges of values are present, although they are less represented than they were in the flooded area number 1.

In Tab. 6.5, the direct runoffs computed through the SCS-CN method are reported for the three different land-uses. The table shows an increase in both the mean and maximum values of direct runoff from 1990 to 2006.

Table 6.5 Mean, minimum and maximum values of direct runoffs (mm) computed for the three different land-uses in the flooded area number 2. The mean value shifts from 28.50 mm in 1990 into 29.45 mm in 2006; while the maximum value shows an increase from 64.75 mm to 65.17 mm.

	1990 (mm)	2000 (mm)	2006(mm)
Mean	28.50	29.23	29.45
Minimum	6.64	6.64	6.64
Maximum	64.75	65.17	65.17

Tab. 6.6 shows the mean, minimum and maximum values of residual runoff.

Table 6.6 Mean, minimum and maximum values of residual runoff computed for the three different land uses in the flooded area number 2.

	1990 (m^3)	2000 (m^3)	2006 (m^3)
Mean	5116.44	5306.60	5363.54
Minimum	600.00	600.00	600.00
Maximum	10250.00	11750.00	11750.00

Tab. 6.6 shows how both the mean and the maximum residual runoff have increased over the years due to the land-use change.

It should be mentioned that even if the flooding of the area 1 and 2 during the November event was due to a bank outbreak, according to news report and local surveys, the same areas were flooded a second time during the event of December 2012, this because of the critical

condition of the minor network, whose hydraulic condition were deteriorated during the considered event.

Flooded area number 3

The drainage density and storage capacity maps are respectively shown in Fig. 6.23, while their relative histograms are reported in Fig. 6.24.

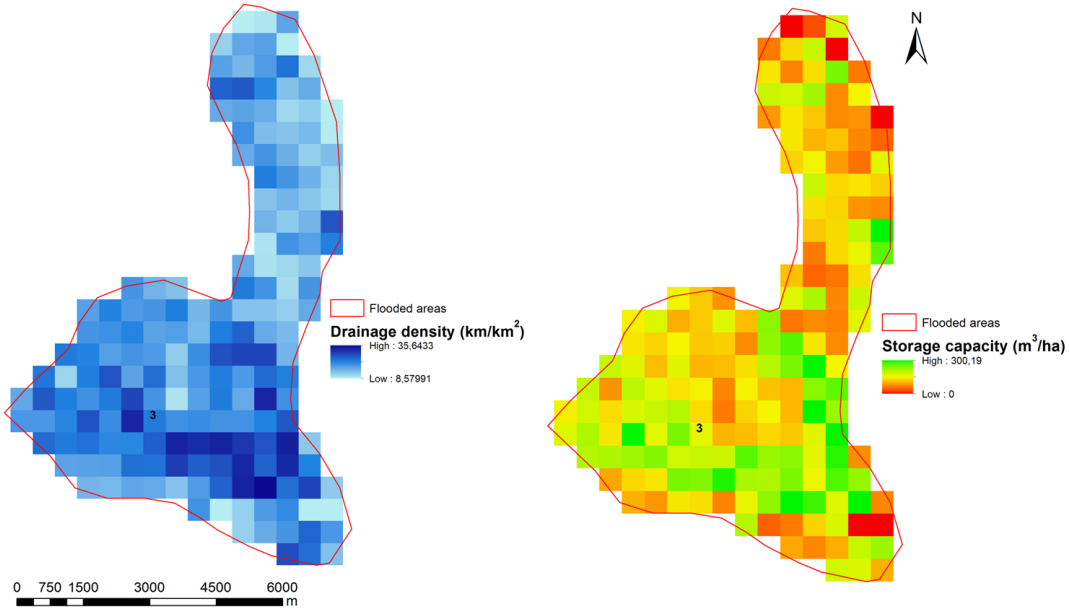

Fig. 6.23 Drainage density and storage capacity maps derived for the flooded area number 3. Low values of channel storage capacity can underline deficit in the network. See the correspondence between pixels that have high values of drainage density and high values of storage capacity too.

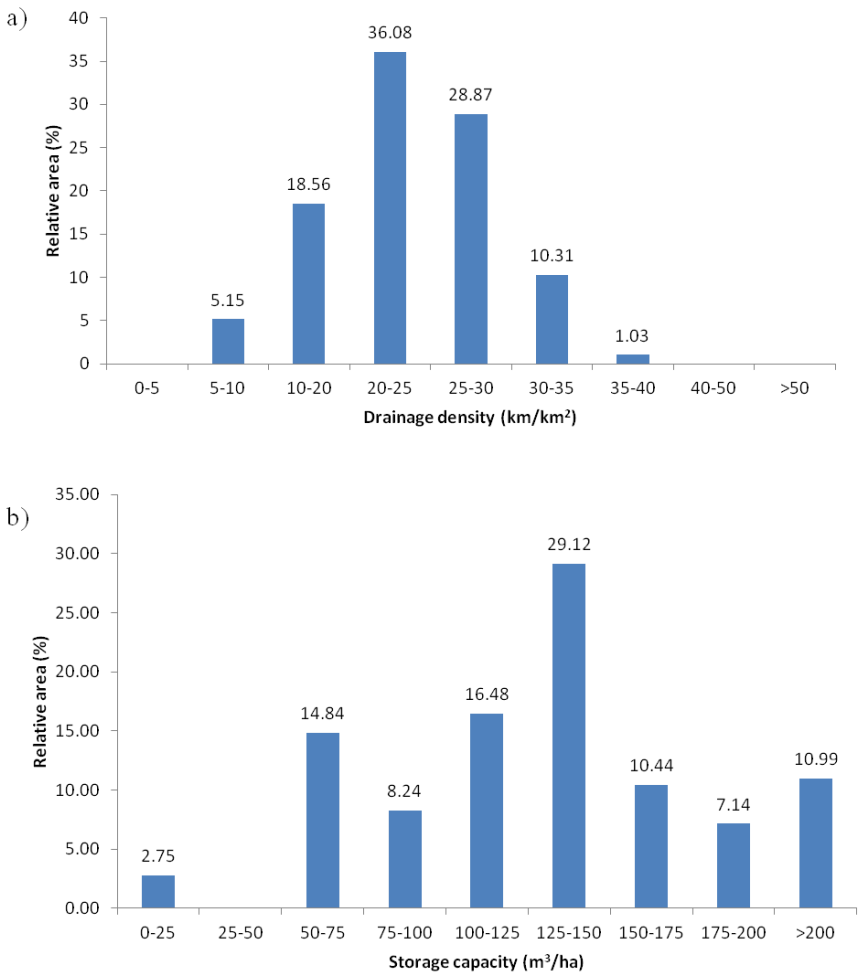

Fig. 6.24 Drainage density (a) and storage capacity (b) histograms for the flooded area number 3.

Fig. 6.24 points out the most representative classes of both drainage density and storage capacity indexes. Concerning the former one, the range 20-25 (km/km^2) is the highest one, making the 36.08% of the area; while in relation to the storage capacity, the range 125-150 m^3/ha is the most represented. In addition, still talking about storage capacity, it is significant to notice that higher ranges of values are not only present but also more represented than they were in the previous flooded areas seen. Here, the class >200m^3/ha constitute more than 10% of the area.

In Tab. 6.7, the direct runoffs computed through the SCS-CN method are reported for the three different land-uses. From the table, emerges that, a quite imperceptible increase in both the mean and maximum values have been registered from 1990 to 2006.

Table 6.7 Mean, minimum and maximum values of direct runoffs (mm) computed for the three different land-uses in the flooded area number 3.

	1990 (mm)	2000 (mm)	2006 (mm)
Mean	37.46	37.48	37.63
Minimum	14.41	14.41	14.41
Maximum	82.65	82.65	83.30

Tab. 6.8 shows the mean, minimum and maximum values of residual runoff.

Table 6.8 Mean, minimum and maximum values of residual runoff computed for the three different land uses in the flooded area number 3.

	1990 (m^3)	2000 (m^3)	2006 (m^3)
Mean	6435.08	6438.01	6466.25
Minimum	9.00	9.00	9.00
Maximum	16800.00	16800.00	16800.00

From Tab. 6.8, as already seen for the previous two flooded areas, it emerges that the residual runoff has increased from 1990 to 2006.
This area however, was entirely flooded because of the bank outbreak, more than because of the low capacity of the network to laminate the rainfall.

Flooded area number 4

The drainage density and storage capacity maps are respectively shown in Fig. 6.25, while their relative histograms are reported in Fig. 6.26.

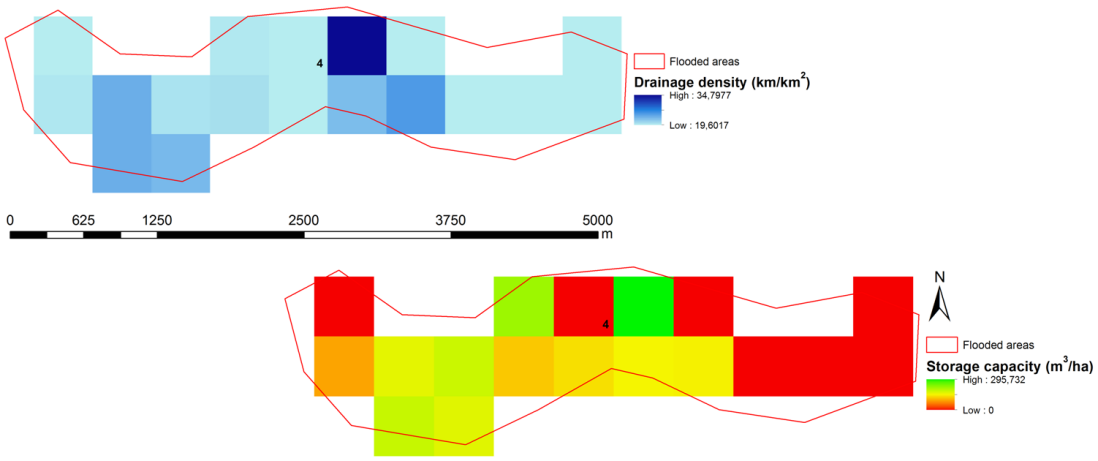

Fig. 6.25 Drainage density and storage capacity maps derived for the flooded area number 4. Low values of channel storage capacity can underline deficit in the network. See the correspondence between pixels that have high values of drainage density and high values of storage capacity too.

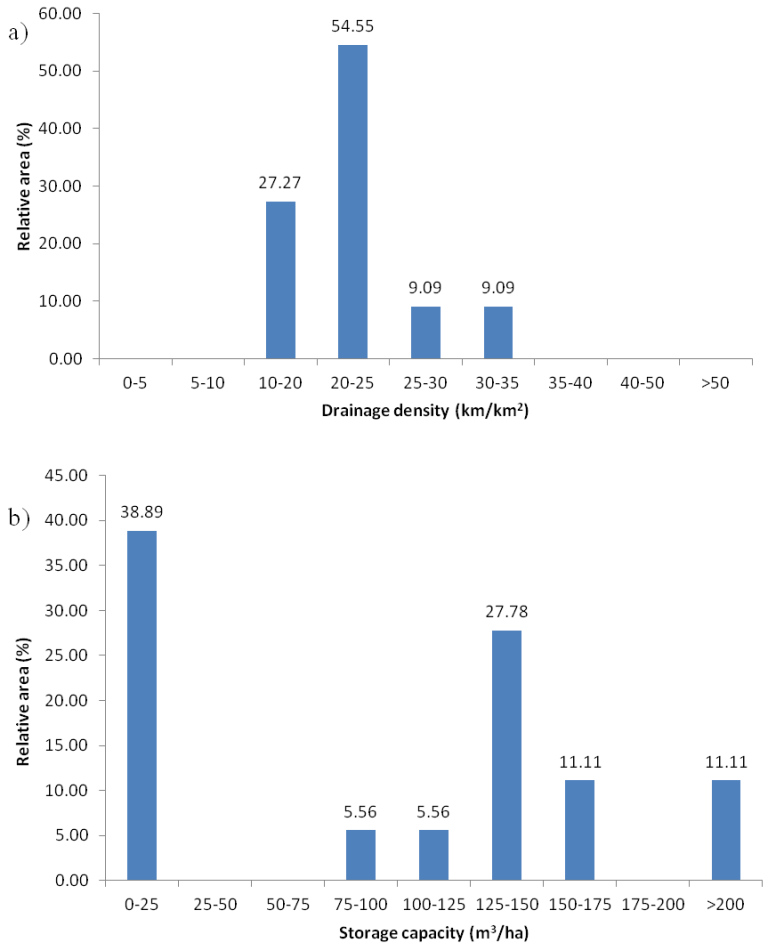

Fig. 6.26 Drainage density (a) and storage capacity (b) histograms for the flooded area number 4.

Fig. 6.26 shows the most representative classes of both drainage density and storage capacity indexes. Concerning the former one, the range 20-25 km/km^2 is the highest one, making the 54.55% of the area on its own; while in relation to the storage capacity, the range 0-25 m^3/ha is the most represented. Other than the just mentioned range of values, the class 125-150 m^3/ha is also pretty significant. If compared with the other flooded areas, this is the area where the lowest class of storage capacity values (0-25 m^3/ha) is better represented.
In Tab. 6.9, the direct runoffs computed through the SCS-CN method are reported for the three different land-uses. From the table, emerges that an increase in the mean values, greater than the ones previously noticed for the other flooded areas, has been registered over the years.

Table 6.9 Mean, minimum and maximum values of direct runoffs (mm) computed for the three different land-uses in the flooded area number 4.

	1990 (mm)	2000 (mm)	2006 (mm)
Mean	46.87	48.77	48.77
Minimum	31.71	31.71	31.71
Maximum	76.13	76.13	76.13

Tab. 6.10 shows the mean, minimum and maximum values of residual runoff.

Table 6.10 Mean, minimum and maximum values of residual runoff computed for the three different land uses in the flooded area number 4.

	1990 (m^3)	2000 (m^3)	2006 (m^3)
Mean	5176.40	5398.96	5398.96
Minimum	400.00	400.00	400.00
Maximum	10500.00	10500.00	10500.00

From Tab. 6.10, as already seen for the previous three flooded areas, it emerges that the mean storage capacity variation has increased from 1990 to 2006.

Flooded area number 5

The drainage density and storage capacity maps are respectively shown in Fig. 6.27, while their relative histograms are reported in Fig. 6.28. The reason that why only less than half of the flooded area is covered by the data is due to the availability of digital elevation data.

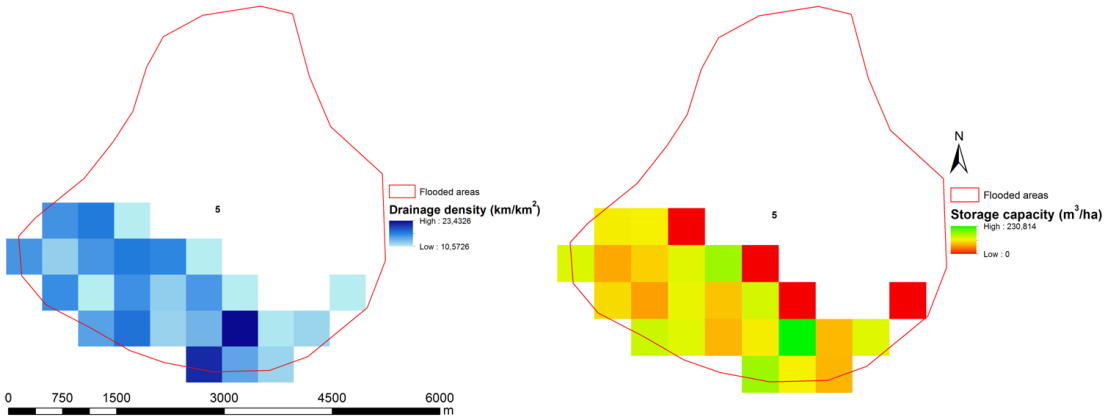

Fig. 6.27 Drainage density and storage capacity maps derived for the flooded area number 5. Low values of channel storage capacity can underline deficit in the network. See the correspondence between pixels that have high values of drainage density and high values of storage capacity too.

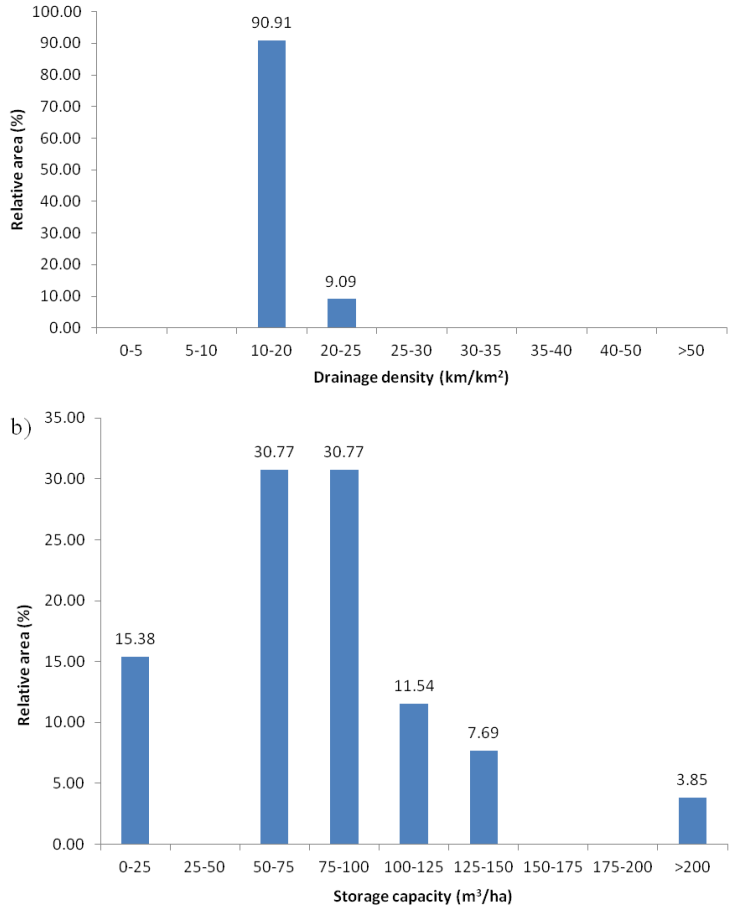

Fig. 6.28 Drainage density (a) and storage capacity (b) histograms for the flooded area number 5.

Fig. 6.28 shows the most representative classes of both drainage density and storage capacity indexes. Concerning the former one, the range 10-20 km/km^2 is the highest one, making the 90.91% of the area on its own; while in relation to the storage capacity, the ranges 50-75 and 75-100 m^3/ha result to be equally the most represented. As already noticed for the flooded area number 4, also in this case the lowest class of storage capacity values (0-25 m^3/ha) is pretty well represented (15.38%).

In Tab. 6.11, the direct runoffs computed through the SCS-CN method are reported for the three different land-uses. In this specific case, differences between the three years have been registered either for the mean and maximum values. The most significant increase is the one relative to the maximum value, from 68.80 mm to 74.92 mm.

Table 6.11 Mean, minimum and maximum values of direct runoffs (mm) computed for the three different land-uses in the flooded area number 5.

	1990 (mm)	2000 (mm)	2006 (mm)
Mean	43.32	43.39	45.58
Minimum	34.47	34.47	34.47
Maximum	68.60	68.60	74.92

Tab. 6.12 shows the mean, minimum and maximum values of residual runoff.

Table 6.12 Mean, minimum and maximum values of residual runoff computed for the three different land uses in the flooded area number 5.

	1990 (m^3)	2000 (m^3)	2006 (m^3)
Mean	6518.42	6527.94	6828.53
Minimum	0.00	0.00	0.00
Maximum	14100.00	14100.00	14100.00

From Tab. 6.12, as already seen for the previous four flooded areas, it emerges that the residual runoff has increased from 1990 to 2006.

In Tab 6.13, some summary statistics for each flooded area are reported in order to better notice possible differences. In “Drainage density” and “Storage capacity” columns, the two most represented classes of values are respectively reported, while in “Direct runoff” and “Residual runoff” columns, the presence or not of differences in mean, minimum and maximum values between the three years, are shown.

Table 6.13 Summary statistics table of the flooded areas.

	Drainage density (km/km^2)	Storage capacity (m^3/ha)	Direct runoff (mm) in relation to the three years 1990, 2000 and 2006	Residual runoff (m^3) in relation to the three years 1990, 2000 and 2006
Flooded area 1	66.67% → 10-20 17.78% → 20-25	28.26% → 100-125 17.39% → 75-100	Increase of mean value from 1990 to 2006	The mean value has increased from 1990 to 2006
Flooded area 2	59.82% → 10-20 30.80% → 5-10	32.14% → 50-75 23.21% → 75-100	Increase of mean and maximum values from 1990 to 2006	The mean value has increased from 1990 to 2006
Flooded area 3	36.08% → 20-25 28.87% → 25-30	29.12% → 125-150 16.48% → 100-125	Increase of mean and maximum value from 1990 to 2006	The mean value has increased from 1990 to 2006
Flooded area 4	54.55% → 20-25 24.27% → 10-20	38.39% → 0-25 27.78% → 125-150	Increase of mean value from 1990 to 2006	The mean value has increased from 1990 to 2006
Flooded area 5	90.91% → 10-20 9.09% → 20-25	30.77% → 50-75 30.77% → 75-100	Increase of mean and maximum values from 1990 to 2006	The mean value has increased from 1990 to 2006

From the table above some conclusions can be drawn. First of all, it is important to notice that in all the flooded areas, an increase of at least the mean value of direct runoff has always been registered from 1990 to 2006. To this alteration, a corresponding increase of residual runoff has also occurred, confirming in that way the strict relation between the two values. In fact, it should be reminded that an enhancement of residual runoff stands for a worsening of the hydraulic situation, even though the upstream contributions are not accounted for. Then, focusing on drainage density and storage capacity ranges of values, it is possible to assess that the flooded area number two has low values of both drainage density and storage capacity. In this specific area, as well as in the first one, the intense precipitations that occurred also in December 2010 caused the total break of embankments again. In addition, also the laminating effect offered by the channel storage capacity has been decreasing over the time due to the land-use changes. For all these reasons, even though the upstream contributions have not been accounted for, this area could be considered potentially critical from a hydrological point of view. Another area that shows very low values of storage capacity is the fourth one. Also in this case, the attenuating effect of the minor drainage network has been decreasing from 1990 to 2006. On the contrary, an area that shows pretty high values of both indexes is the flooded area number 3. This, can be explained by the fact that this area is mainly composed of agricultural fields where ditches and channels are distributed.

These preliminary results underline how there might be some problems in the network, in the case of intense rainfall events. This simplified analysis, also underlines how change in land use (in this case considering the evolution during the years), should be also accounted in planning and managing procedures: the increase of the runoff due to land use change should always be accounted for, and it should be operationally compensated by a correspondent increasing of the storage capacity. If this is not accomplished, an increasing of the residual runoff should be expected, with problems related to its control, especially when dealing with floods.

7 FINAL REMARKS

The availability of large scale information obtainable from high resolution topography, and in particular from airborne LiDAR data, has offered effective tools for the understanding of hydrological processes and for the recognition of morphological features at a level of detail previously unknown (Tarolli et al., 2009; Tarolli and Dalla Fontana, 2009; Sofia et al., 2011).

This thesis relies on the fundamental possibility to represent the surface morphology in a digital form, starting from the abundance at a regional scale of information embedded in these high resolution topographic data, applied to recognize the hydrogeomorphic features of interest trough the application of a semi-automatic approach. The work has been developed in the context of anthropogenic areas (agricultural floodplains). The method, proposed by Cazorzi et al. (2012), has allowed to detect the minor drainage network system, and to quantify the water storage capacity and other network statistics typical of agrarian landscapes. Considering the comparison between topographic parameters, the approach was based on the quantification of elevation residuals as the main parameter to detect the network. Despite the DTM grid cell constraint, that determines a slight underestimation of the derived parameters, the method allows to define some indexes generally available only through time-consuming and cost-prohibitive field surveys (Cazorzi et al., 2012). The network extracted in such way, furthermore, has been proven to be more reliable than the information provided by the cartography, when updates on the maps are not available. Since drainage networks in agrarian landscapes within floodplains are expected to affect hydrological response during floods, this assessment becomes a crucial tool for flood management. In fact, low values of channel storage capacity can i) underline deficit in the network, and they can outline areas whose hydrological behavior is potentially critical during floods, where change in land use might increase the level of risk, and ii) they allow to identify storage volumes already available on the surface that can effectively contribute to laminate flood peaks. This information is crucial in each project of land use transformation that causes a change of surface permeability and increases, as a consequence, the surface runoff. The only way to ensure the hydraulic invariance is to quantify and provide temporary runoff storage capacities that are able to compensate, through a laminating action, the increasing of discharge peaks caused by the increased runoff. Therefore, all the storage capacities, included both the ones provided by the principal collectors and those ones of the minor drainage system, behave as useful reservoirs.

This thesis also analyzed the effects of drainage network storage capacity on the direct surface runoff produced by the main rainfall event happened between October and November 2010 in Veneto, aiming in such way, to evaluate the presence of areas that may be already risky simply for the runoff directly produced by the input local rainfall. The purpose of the latter evaluation is also to notice if changes in land use have affected the direct runoff and therefore, the attenuating effect performed by the minor drainage system towards floods. In this perspective, to compute this such lamination effect, a simple index (residual runoff) has been computed, as the difference between the direct runoff and the effective storage capacity.

As main outcomes, the proposed work underlined that: 1) there might be some problems in the network, in the case of intense rainfall events, looking at the values of drainage density and storage capacity indexes; 2) change in land use (in this case considering the evolution during the years), should be accounted in planning and managing procedures: the increase of the runoff due to land use change, should always be accounted for, and it should be operationally compensated by a corresponding increasing of the storage capacity, in order to maintain the hydraulic invariance. If this is not accomplished, an increasing of the residual runoff should be expected, with problems related to its control, especially when dealing with floods.

Concluding, this thesis successfully tested a methodology for channel network identification and water storage in flood plain using high resolution topography over larger areas. As a matter of facts, for the first time, this kind of analysis has been done at a regional scale (180 000 ha). This preliminary analysis absolutely has to be enlarged with a wider historical dataset, in order to better understand the effects of land use change, especially urbanization, providing a useful tool for management purposes especially in flood prone areas.

8 REFERENCES

AA.VV. (2008a). Il rischio idrogeologico in Italia – Sintesi dei dati raccolti relative ai Piani straordinari approvati o ai Piani stralcio per l'Assetto Idrogeologico predisposti, adottati o approvati dalle Autorità di bacino, regioni e Province Autonome. Ministero dell'Ambiente e della Tutela del Territorio e del Mare – Direzione Generale per la Difesa del Suolo.

AA.VV. (2000). La caratterizzazione climatica della Regione Veneto. ARPAV, Quaderni per l'Ambiente Veneto, 22pp.

Albani, M.; Klinkenberg, B.; Andison, D.W.; Kimmins, J.P. (2004). The choice of window size in approximating topographic surfaces from digital elevation models. International Journal of Geographical Information Science, 18(6), 577-593.

Anderson, M.G.; Burt, T.P. (1978a). The role of topography in controlling through flow generation. Earth Surface Processes, 3:331-344.

Anderson, M.G.; Burt, T. P. (1978b). Toward more detailed field monitoring of variable source areas. Water Resources Research, 14:1123-1131.

ARPAV - Agenzia Regionale per la Prevenzione e Protezione Ambientale del Veneto.

ARPAV, Progetto SAMPAS. (2006). Le acque sotterranee della pianura veneta. Iniziativa cofinanziata dall'Unione Europea – FESR.

ARPAV, (2011). Valutazione della permeabilità e del gruppo idrologico dei suoli del veneto.

Ackermann, F. (1999). Airborne laser scanning – present status and future expectations. ISPRS Journal of Photogrammetry & Remote Sensing, 54, 64-67.

Ahlberg, S.; Soderman, U.; Elmqvist, M.; Persson, A. (2004). On modelling and visualisation of high resolution virtual environments using LiDAR data. Proceedings of 12th International Conference on Geoinformatics, Gavle, Sweden, 299-306.

Bailly, J.S.; Lagacherie, P.; Millier, C.; Puech, C.; Kosuth, P. (2008). Agrarian landscapes linear features detection from LiDAR: application to artificial drainage networks. International Journal of Remote Sensing, 29(12), 3489.

Band, L.E. (1986).Topographic partition of watersheds with digital elevation models. Water Resources Research, 22(1), 15-24.

Barbi, A.; Cola, G.; Mariani, L. (2012). Inquadramento climatico del Veneto. Atlante Agroclimatico del Veneto.

Beven K.J.; Kirkby, M.J. (1979). A physically based, variable contributing area model of basin hydrology. Hydrol. Sci. Bull.; 24, 43–69.

Bielders, C.L.; Ramelot, C. and Persoons, E. (2003). Farm perception of runoff and erosion and extent of flooding in the silt-loam belt of Belgian Walloon Region. Environmental Sciences Policy, 6, 643-658.

Bloschl, G.; Sivapalan, M. (1995). Scale Issues in Hydrological Modelling: A Review. Hydrological Processes, 9, no 3-4 (243 p.) (7 p.3/4), pp. 251-290.

Boardman, J.; Evans, R. and Ford, J. (2003). Muddy flows on the South Downs southern England: problem and responses. Environmental Sciences Policy, 6, 69-83.

Boserup, E. (1965). The conditions of agricultural growth: the economics of agrarian change under population pressure. London, UK: Allen and Unwin.

Brath, A.; Montanari, A.; Moretti, G. (2006). Assessing the effect on flood frequency of land use change via hydrological simulation (with uncertainty). Journal of Hydrology, 324, 141-153.

Briese, C. (2010). Extraction of digital terrain models. In Vosselman, G.; Maas, H.G. (eds.) Airborne and terrestrial laser scanning. First ed. Whittles Publishing, UK, pp. 135-168.

Bronstert, A. (1996). River flooding in Germany: influenced by climatic change? Physics and Chemistry of the Earth 20(5-6): 445-450.

Bronstert, A. (1999). Capabilities and limitations of detailed hillslope hydrological modeling. Hydrological Processes, 13: 21-48.

Bronstert, A.; Burger, G.; Heidenreich, M.; Katzenmaier, D.; Kohler, B. (1999). Effects of climate change influencing storm runoff generation: basic considerations a pilot study in Germany. In The Impact of Climate Change on Flooding and Sustainable River Management. Balabanis, P.; Bronstert, A.; Casale, R.; Samuels, P. (eds). Proceedings of the final RIBAMOD Workshop, Wallingford, February, 26-27, 1998. Office for Official Publications of the European Communities: Luxembourg; 325-340.

Bronstert, A.; Niehoff, D.; Burger, G. (2001). Effects of climate and land-use change on storm runoff generation: present knowledge and modeling capabilities. Hydrological Processes, 16, 509-529.

Burel, F.; Baudry, J. (2005). Habitat quality and connectivity in agricultural landscapes: the role of land use systems at various scales in space and time. Ecological Indicators, 5, 305-313.

Burrough, P.A.; McDonnell, R.A. (1998). Principles of Geographic Information Systems. Oxford University Press, Oxford (GB).

Carluer, N.; De Marsily, G. (2004). Assessment and modelling of the influence of man-made networks n the hydrology of a small watershed: implications for fast flow components, water quality and landscape management. Journal of Hydrology, 285, 76-95.

Carraro, M.; Domeneghetti, F. (2012). Come affrontare il rischio idraulico nella pianificazione urbanistica. L'ACQUA E LE SMART CITIES-STADIUM. Politecnico di Milano.

Carturan, L.; Cazorzi, F.; Dalla Fontana, G. (2009). Enhanced estimation of glacier mass balance in unsampled areas by means of topographic data. Annals of Glaciology, 50, 37– 56

Casella V, 2003. Introduzione al laser scanning aereo. In: La tecnica del laserscanning – Teoria ed applicazioni, Crosilla, F. e Galletto, R. , CISM, Udine, 1-37.

Cavalli, M.; Tarolli, P.; Marchi, L.; Dalla Fontana, G. (2008). The effectiveness of airborne LiDAR data in the recognition of channel-bed morphology. Catena, 73(3), 249-260.

Cavalli, M.; Marchi, L. (2008). Characterisation of the surface morphology of an alpine alluvial fan using airborne LiDAR, Nat. Hazards Earth Syst. Sci.; 8, 323-333, doi:10.5194/nhess-8-323-2008.

Cavalli, M.; Trevisani S.; Goldin, B.; Mion E.; Marchi, L. (2011). Derivation of channel network of an alpine region from high-resolution DTM: the example of the Autonomous Province of Trento (Italy), Geophysical Research Abstracts, 13, EGU2011-8188, eISSN: 1607-7962.

Cazorzi, F.; Dalla Fontana, G.; De Luca, A.; Sofia, G.; Tarolli, P. (2012). Drainage network detection and assessment of network storage capacity in agrarian landscape. Hydrological Processes.

Challis, K.; Howard, A.J. (2006). A review of trends within archaeological remote sensing in alluvial environments. Archaeological Prospection, 13(4), 231–240. DOI: 10.1002/arp.296.

Charaniya, A.P.; Manduchi, R.; Lodha, S. K. (2004). Supervised parametric classification of aerial LiDAR data. Proceedings of 2004 Conference on Computer Vision and Pattern Recognition Workshop (CVPRW'04), Washington D.C, USA.

C.N.G., 2010. Rapporto sullo stato del territorio italiano. Consiglio Nazionale dei Geologi.

Cobby, D.M.; Mason, D.C.; Davenport, I.J. (2001). Image processing of airborne scanning laser altimetry data for improved river flood modeling. ISPRS Journal of Photogrammetry and Remote Sensing 56(2), 121–138.

Cohen, J. (1960). A coefficient of agreement for nominal scales. Educational and Psychological Measurement, 20, 37–46.

Crutzen, P.J. (2002) Geology of mankind. Nature 415, 23, doi: 10.1038/415023a.

D'Alpos, L. (2006). I rischi di inondazione nella provincia di Padova. Padova e il suo territorio. Anno XX, Rivista di storia arte cultura.

Dal Cin, C.; Moens, L.; Dierickx, P.; Bastin, G.; Zech, Y. (2005). An integrated approach for realtime floodmap forecasting on the Belgian Meuse river'. Natural Hazards, 36(1–2), 237–256.

Dalla Fontana, G.; Marchi, L. (2003). Slope-area relationships and sediment dynamics in two alpine streams. Hydrological Processes 17(1): 73-87.

Darcy, H. (1856). Les Fontaines Publiques de la Ville de Dijon. Dalmont, Paris. 647 p. & atlas.

Davies, D.B.; Finney, J.B.; Richardson, S.J. (1973) Relative effects of weight and wheel slip in causing soil compaction. J. Soil Sci., 24, 339-409.

Dodds, P. S. , Rothman, D.H. (2000). Scaling, universality, and geomorphology. Annu. Rev. Earth Planet. Sci. 28, 571-610.

Doneus, M.; Briese, C. (2006). Full-waveform airborne laser scanning as a tool for archaeological reconnaissance. In: From Space to Place. 2nd International Conference on Remote Sensing in Archaeology, Campana S, Forte M (eds). BAR International Series 1568, 99–105. Archaeopress: Oxford.

Dunn, S.M.; Mackay, R. (1996). Modelling the hydrological impacts of open ditch drainage. Journal of Hydrology 179: 37-66.

Duke, G.; Kienzle, S.; Johnson, D.; Byrne, J. (2006). Incorporating ancillary data to refine anthropogenically modified overland flow paths. Hydrological Processes 20, 1827-1843.

Earle, T. & Doyle, D. (2008). The engineered landscapes of irrigation. In Cliggett, L. & Pool, C.A. (ed.) (2008) Economies and transformation of landscape. Lanham, Md.: Altamira Press, 19-46.

Ellis, E. C.; Rammankutty, N. (2008). Putting people in the map: anthropogenic biomes of the world. Front Ecol Environ; 6(8): 439-447, doi: 10.1890/070062.

Ellis, E.C. (2011) Anthropogenic transformation of the terrestrial biosphere. Phil. Trans. R. Soc. A 369, 1010-1035, doi: 10.1098/rsta.2010.0331.

El-Sheimy, N.; Valeo, C. and Habib, A. (2005) Digital terrain modeling: acquisition, manipulation, and application. Boston and London: Artech House.

Erikson, C.L. (2006a). The domesticated Landscapes of the Bolivian Amazon. Time and complexity in historical ecology: studies in the neotropical lowlands. New York: Columbia University Press, 235-278.

Eshani, A.H.; Quiel, F. (2008). Geomorphometric feature analysis using morphometric parameterization and artificial neural networks. Geomorphology, 99, 1–12.

Eurostat, Demography – Regional data, 2010.

Eurostat, LUCAS (Land-use/Cover Area frame statistical Survey) analysis, 2009.

Evans, I.S. (1972). General geomorphology, derivatives of altitude and descriptive statistics. In: Chorley, R.J. (Ed.), Spatial Analysis in Geomorphology. Methuen & Co. Ltd, London, pp. 17-90.

Evans, I.S. (1979). An integrated system of terrain analysis and slope mapping. Final report on grant DA-ERO-591-73-G0040, University of Durham, England.

Farr, T.G., Rosen, P.A., Caro, E., Crippen, R., Duren, R., Hensley, S., Kobrick, M., Paller, M., Rodriguez, E., Roth, L., Seal, D., Shaffer, S., Shimada, J., Umland, J.,Werner, M., Oskin, M., Burbank, D., Alsdorf, D. (2007). The Shuttle Radar Topography Mission. Reviews of Geophysics 45, RG2004.

Florinsky, I.V. (2002). Errors of signal processing in digital terrain modelling, International Journal of Geographical Information Science, 15 (5), 475–501.

Florinsky I.V. (1998). Accuracy of local topographic variables derived from digital elevation models. International Journal of Geographical Information Science 12(1): 47-61.

Foley, J.A.; DeFries, R.; Asner, G.P. (2005) Global consequences of land use. Science 309: 570-74.

Fregolent, L. (2005). Governare la dispersione. FrancoAngeli, Milano.

Fregolent, L. (2012). Low-Density City: Problems and Management. TeMa, Journal of Land Use, Mobility and Environment.

French, J.R. (2003). Airborne LiDAR in support of geomorphological and hydraulic modeling. Earth Surface Processes and Landforms, 28(3), 321–335. DOI: 10.1002/esp.484.

Fujisada, H., Bailey, G.B., Kelly, G.G., Hara, S., Abrams, M.J. (2005). ASTER DEM performance. IEEE Transactions on Geoscience and Remote Sensing 43 (12), 2707–2713.

Gallant, J.C.; Wilson, J.P. (2000). Primary Topographic Attributes. In: Terrain Analysis: Principles and Applications, J. P. Wilson and J. Gallant (eds.). New York: John Wiley & Sons Inc.; 51-85.

Garcia, M.; Camarasa, A. (1999). Use of geomorphological units to improve drainage network extraction from a dem : Comparison between automated extraction and photointerpretation methods in the carraixet catchment (valencia, spain). International Journal of Applied Earth Observation and Geoinformation, 1 (3-4), 187-195.

Gascuel-Odoux, C.; Aurousseau, P.; Doray, T.; Squividant, H.; Macary, F.; Uny, D.; Grimaldi, C. (2011). Incorporating landscape features to obtain an object-oriented landscape drainage network representing the connectivity of surface flow pathways over rural catchments. Hydrological Processes 25: 3625-3636.

Grayson, R.; Bloschl G (2001). Spatial Patterns in Catchment Hydrology : Observations and Modelling, Cambridge University Press, Cambridge, U.K. ; New York.

Guzzetti, F.; Stark, C.P.; Salvati, P. (2005). Evaluation of Flood and Landslide Risk to the Population of Italy. Environmental Management Vol. 36, No. 1, pp. 15-36.

Gallart, F.; Llorens, P.; Latron, J. (1994). Studying the role of old agricultural terraces on runoff generation in a small Mediterranean mountainous basin. Journal of Hydrology, 159, 291–303.

Guha-Sapir, D.; Vos, F.; Below, R.; Ponserre, S. (2011). Annual Disaster Statistical Review 2011 – The number and trends. WHO (World Health Organization) collaborating Centre for Research on the Epidemiology of Disasters –CRED.

Guzzetti, F.; Stark,C.P.; Salvati, P. (2005). Evaluation of Flood and Landslide Risk to the Population of Italy. Environmental Management, 36 (1); 15-36.

Habib, A.; Ghanma, M.; Morgan, M.; Al-Ruzouq, R. (2005). Photogrammetric and LiDAR data registration using linear features. Photogrammetric Engineering and Remote Sensing 71(6), 699- 707.

Harvey, D. (1982). The limits to capital. Oxford: Blackwell.

Heathwaite, A.L.; Burt, T.P.; Trudgill, S.T. (1989). Runoff, sediment, and solute delivery in agricultural drainage basins: a scale-dependent approach. IAHS Publication no. 182, 175-190.

Heathwaite, A.L.; Burt, T.P.; Trudgill, S.T. (1990). Land-use controls on sediment production in a lowland catchment, south-west England. In: Soil Erosion on Agricultural Land, J. Boardman, I.D.L. Foster and J.A. Dearing (Eds.), Wiley, Chichester, UK: 69-86.

Heipke, C.; Mayer, H.; Wiedemann, C.; Jamet, O. (1997). Automated reconstruction of topographic objects from aerial images using vectorized map information. International Archives of Photogrammetry and Remote Sensing 23: 47-56

Hiller, J.K.; Smith, M. (2008). Residual relief separation: digital elevation model enhancement for geomorphological mapping. Earth Surface Processes and Landforms, 33, 2266–2276. DOI: 10.1002/esp.1659.

Hirano, A., Welch, R., Lang, H. (2003). Mapping from ASTER stereo image data: DEM validation and accuracy assessment. ISPRS Journal of Photogrammetry and Remote Sensing 57, 356–370.

Hodgson, M.E.; Jensen, J.R.; Raber, G.; Tullis, J.; Davis, B.; Thompson, G.; Schuckman, K. (2005). An Evaluation of LIDAR-Derived Elevation and Terrain Slope in Leaf-off Conditions. Photogrammetric Engineering & Remote Sensing,71(7):817–823.

Hollis, J.M.; Dresser, M.; Thompson, T.R.E.; Newland, R. (2003). Comparison of agricultural soil conditions in the Uck and Bourne catchments during the winter periods of 2000/2001 and 2002/2003. Draft Report, Contract No. 12622, Environmental Agency, Bristol, UK. 98pp.

Horn, B.K.P. (1981). Hill shading and the reflectance map. Proceedings of the IEEE, 69(1), 14-47.

Humme, A.; Lindenbergh, R.; Sueur, C. (2006). Revealing Celtic fields from LiDAR data using kriging based filtering. Proceedings of the ISPRS Commission V Symposium, Dresden, 25–27 September, Vol. XXXVI, part 5.

Hutchinson, M.F. (1988). Calculation of hydrologically sound digital elevation models. Proceedings, 3rd International Symposium on Spatial Data Handling, International Geographical Union, Sydney, Australia, 117-133.

Indovina, F. (1990). La città diffusa, Daest-IUAV, Venezia.

Indovina, F. (2009). Dalla città diffusa all'arcipelago metropolitano, FrancoAngeli, Milano.

Istat - Istituto Nazionale di Statistica – Italian National Statistics Institute.

Istat, Consumo del suolo, Gennaio 2012.

Jakubicka, T.; Vos, F.; Phalkey, R.; Marx, M.; Guha-Sapir, D. (2010). Health impacts of floods in Europe – Data gaps and information needs from a spatial perspective. MICRODIS report. Centre for Research on the Epidemiology of Disasters – CRED.

James, L.A.; Watson, D.G.; Hansen, W.F. (2007). Using LIDAR data to map gullies and headwater streams under forest canopy: south carolina, USA. Catena 71(1),132-144.

Jones, A.F.; Brewer, P.A.; Johnstone, E.; Macklin, M.G. (2007). High resolution interpretative geomorphological mappign of river valley environments using airborne LiDAR data. Earth surface processes and landform, 21, 1574-1592.

Karel W.; Kraus K. (2006). Quality parameters of digital terrain models. In Semina on Autmated Quality Control of Digital Terrain Models, EuroSDR Seminar, 18-19 August 2005, Aalborg, Denmark; available online at 180 http://www.ipf.tuwien.ac.at/publications/2006/Karel_Kraus_QualityPar4DTM.pdf.

Kothe, R.; Bock, M. (2009). Preprocessing of Digital Elevation Models – derived from Laser Scanning and Radar Interferometry – for Terrain Analysis in Geosciences. Proceedings of Geomorphometry, Zurich, Switzerland, 31 August - 2 September.

Kraus K.; Pfeifer, N. (1998). Determination of terrain models in wooded areas with airborne laser scanner data, ISPRS Journal of Photogrammetry and Remote Sensing, 53/4, 193–203.

Kruger, T.; Meinel, G. (2008). Using Raster DTM for Dike Modelling. In: Advances in 3D Geoinformation Systems, 2008, Part II, Theme I:,101-113, DOI: 10.1007/978-3-540-72135-2_6.

Kundzewicz, Z.W.; Takeuchi, K. (1999). Flood protection and management: quo vadimus? Hydrological Sciences Journal, 44(3): 417-432.

Kundzewicz, Z.W.; Kaczmarek, Z. (2000). Coping with hydrological extremes. Water International, 25(1): 66-75.

Lagacherie, P.; Diot, O.; Domange, N.; Gouy, V.; Floure, C.; Kao, C.; Moussa, R.; Robbez-Masson, J.; Szleper V. (2004). An indicator approach for describing the spatial variability of human-made stream network in regard with herbicide pollution in cultivated watersheds. Ecological indicators, 6, 265-279.

Lansing, J.S. (1991). Priests and programmers: technologies of power in the engineered landscape of Bali. Princeton University Press, Princeton, New Jersey, USA.

Lashermes, B.; Foufoula-Georgiou, E.; Dietrich, W.E. (2007). Channel network extraction from high resolution topography using wavelets. Geophysical Research Letters 34, L23S04. doi:10.1029/2007GL031140.

Lee, S.; Shan, J.; Bethel, J.S. (2003). Class-guided building extraction from Ikonos imagery. Photogrammetric Engineering and Remote Sensing 69(2): 143-150.

Levavasseur, F.; Bailly, J.S.; Lagacherie P.; Colin, F.; Rabotin, M. (2011). Simulating the effects of spatial configurations of agricultural ditch drainage networks on surface runoff from agricultural catchments. Hydrological processes, 'Accepted Article', doi: 10.1002/hyp.8422.

Leopold, B.L. (1968). Hydrology for Urban Land Planning – A Guidebook on the Hydrologic Effects of Urban Land Use. Geological Survey Circular 554. Washington.

Lohr, U. (1998). Digital elevation models by laser scanning. Photogrammetric Record 16, 105-109.

Liu, X.; Zhang, Z.; Peterson, J.; Chandra, S. (2007). LiDAR-derived high quality ground control information and DEM for image orthorectification. GeoInformatica 11(1), 37-53.

Liu, X. (2008). Airborne LiDAR for DEM generation: some critical issues. Progress in Physical Geography: an international review of geographical work in the natural and environmental sciences, 32 (1). pp. 31-49. ISSN 0309-1333.

Lohani, B.; Mason, D.C. (2001). Application of airborne scanning laser altimetry to the study of tidal channel geomorphology. ISPRS Journal of Photogrammetry and Remote Sensing, 56(2): 100–120. DOI: 10.1016/S0924-2716(01)00041-7.

Longfield S.A.; Mackin, M.G. (1999). The influence of recent environmental change on flooding and sediment fluxes in the Yorkshire Ouse basin. Hydrological Processes, 13(7): 1051-1066.

Malano, H.; Hofwegen, P.V. (1999). Management of Irrigationand Drainage Systems: A Service Approach. Monography IHE 3.A.A.Balkema,Rotterdam,Netherlands.ISBN 90 5410 482 1.

Mark, D.M. (1988). Network models in geomorphology. In Modeling Geomorphological Systems, M.G. Anderson (eds.), 73–97, John Wiley, New York.

Marofi, S. (1999). Role des echanges nappes-fosses dans le fonctionnement hydrologique d'un bassin versant en milieu mediterraneen cultive. PhD thesis, Ecole Nationale Superieure Agronomique de Montpellier, France, 240 pp.

Matson, A.P.; Vitousek, M.P.; Aber, D.J.; Howarth, W.R.; Likens, E.G.; Schindler, W.D.; Schlesinger, H.W.; Tilman, G.D. (1997). Human alteration of the global nitrogen cycle: sources and consequences. Ecological Applications, 7:737-750.

Matthews, E. (1983). Global vegetation and land use: new high-resolution databases for climate studies. J Clim Appl Meteorol 22: 474-87.

Mazzeo, G. (2012). Scenario Analysis: toward a change in the use of the soil consumption paradigm. TeMa, Journal of Land Use, Mobility and Environment.

McGlynn, B.L.; McDonnell, J.J. (2003). Quantifying the relative contributions of riparian and hillslope zones to catchment runoff, Water Resour. Res.; 39(11), 1310.

Min, S.-K., Zhang, X.; Zwiers, F.W.; Hegerl, C.G. (2011). Human contribution to more-intense precipitation extremes. Nature 470, 378-381.

Mitasova, H.; Hofierka, J. (1993). Interpolation by Regularized Spline with Tension: II. Application to Terrain Modeling and Surface Geometry Analysis. Math. Geol. 25, 641-655.

Molloy I.; Stepinski, T.F. (2007). Automatic mapping of valley networks on Mars. Computers and Geosciences 33,728–738.

Montgomery, D.R.; Dietrich, W.E. (1994). A physically based model for the topographic control on shallow landsliding. Water Resources Research 30: 1153-1171.

Moore, I.D.; Grayson, R.B.; Ladson, A.R. (1991). Digital terrain modelling: A review of hydrological, geomorphological, and biological applications. Hydrological Processes 5:3-30.

Moore, I.D.; Gessler, P.E.; Nielsen, G.A.; Peterson, G.A. (1993). Soil attribute prediction using digital terrain analysis. Soil Science Society of America Journal, 57:443-452.

Moussa, R.; Voltz, M.; Andrieux, P. (2002). Effects of the spatial organization of agricultural management on the hydrological behavior of a farmed catchment during flood events. Hydrological Processes, 16(2), 393–412.

Mukai, T.; Nakamura, A.M.; Sakai, T. (2006). Asteroidal surface studies by laboratory light scattering and LIDAR on HAYABUSA. Advances in Space Research 37(1), 138-141.

Nelson, P.A.; Smith, J.A.; Miller, A.J. (2006). Evolution of channel morphology and hydrologic response in an urbanizing drainage basin. Earth Surface Processes and Landforms, 31(9), 1063– 1079. DOI: 10.1002/esp.1308

Netting, R.M. (1993). Smallholders, householders: farm families and the ecology of intensive sustainable agriculture. Stanford, CA: Stanford University Press.

O' Callaghan, J.F.; Mark, D.M. (1984). The extraction of drainage networks from digital elevation data. Computer Vision, Graphics and Image Processing, 28, 323–344.

O' Connell, E.; Ewen, J.; O' Donnell, G.; Quinn P, P. (2007). Is there a link between agricultural land-use management and flooding? Hydrol. Earth Syst. Sci.; 11(1), 96-107.

Olson, D.M.; Dinerstein, E.; Wikramanayake, E.D. et al. (2001). Terrestrial ecoregions of the world: a new map of life on Earth. BioScience 51: 933-38.

Orlandini, S.; Moretti, G. , Franchini, M.; Aldighieri, B.; Testa, B. (2003). Path-based methods for the determination of nondispersive drainage directions in grid-based digital elevation models, Water Resour. Res.; 39(6), 1144, doi: 10.1029/2002WR001639.

Orlandini, S.; Tarolli, P.; Moretti, G.; Dalla Fontana, G. (2011). On the prediction of channel heads in a complex alpine terrain using gridded elevation data, Water Resour. Res.; 47, W02538, doi:10.1029/2010WR009648.

Pall, P.; Aina, T.; Stone, A.D.; Scott, A.P.; Nozawa, T. Hilberts, G.J.A.; Lohmann, D. & Allen, R.M. (2011). Anthropogenic greenhouse gas contribution to flood risk in England and Wales in autumn 2000. Nature, 470, 382-385.

Palmer, R.C. (2002). Soil conditions in the Tone and Parrett, catchments during February and March 2002. NSRI research report No. SR 9046V for Environmental Agency, Cranfield University, Silsoe, UK.

Palmer, R.C. (2003a). Soil conditions in the Tone and Parrett, catchments during February and March 2003. NSRI research report No. SR 9093V for Environmental Agency, Cranfield University, Silsoe, UK.

Papa, R. (2012). Landscape of urban sprawl. TeMA, Journal of Land Use, Mobility and Environment.

Passalacqua, P.; Do Trung, T.; Foufoula-Georgiou, E.; Sapiro, G.; Dietrich, W.E. (2010a). A geometric framework for channel network extraction from LiDAR: Nonlinear diffusion and geodesic paths. Journal of Geophysical Research 115: F01002. doi:10.1029/2009JF001254.

Passalacqua, P.; Tarolli, P.; Foufoula-Georgiou, E. (2010b). Testing space-scale methodologies for automatic geomorphic feature extraction from LiDAR in a complex mountainous landscape. Water resources research, 46, W11535. doi:10.1029/2009WR008812.

Peuker, T.; Douglas, D.H. (1975). Detection of surface-specific points by local parallel processing of discrete terrain-elevation data. Computer Graphics and Image Processing 4 (1975), 375–387.

Pfeifer, N.; Briese, C. (2007). Geometrical aspects of airborne laser scanning and terrestrial laser scanning. International Archives of Photogrammetry, Remote Sensing and Spatial Information Sciences 36(part 3/W52), 311-319.

Pinna, M. (1978). L'atmosfera e il clima, Utet, Collana il nostro universo, 478 pp.

Pirotti, F.; Tarolli, P. (2010). Suitability of LiDAR point density and derived landform curvature maps for channel network extraction. Hydrological Processes 24: 1187-1197. doi: 10.1002/hyp.758.

Pistocchi, A. (2001). La valutazione idrological dei piani urbanistici – un metodo semplificato per l'invarianza idraulica nei piani regolatori generali. Ingegneria Ambientale, vol. XXX, no. 7/8, luglio/agosto2001.

Pfister, L.; Kwadijk, J.; Musy, A.; Bronstert, A.; Hoffmann, L. (2004). Climate change, land use change and runoff prediction in the Rhine-Meuse basins. River Research and Applications 20: 229-241. doi: 10.1002/rra.775.

Prentice, C.J.; Cramer, W.; Harrison, P.S.; Leemans, R.; Monserud, A.R.; Solomon, M.A. (1992). A global biome model based on plant physiology and dominance, soil properties and climate. Journal of Biogeography, 19, 117-134.

Prima, O.D.A.; Echigo, A.; Yokoyama, R.; Yoshida, T. (2006). Supervised landform classification of Northeast Honshu from DEM-derived thematic maps. Geomorphology, 78, 373–386.

Prosser I.P.; Abernethy, B. (1996). Predicting the topographic limits of gully network using a digital terrain model and process thresholds. Water resources research, 32: 2289-2298.

Quinn, P.; Beven, K.; Chevallier, P.; Planchon, O. (1991). The prediction of hillslope flow paths for distributed hydrological modeling using digital terrain models, Hydrol. Processes, 5, 59-79.

Raber, G.T.; Jensen, J.R.; Hodgson, M.E.; Tullis, J.A.; Davis, B.A.; Berglend, J. (2007). Impact of LiDAR nominal post-spacing on DEM accuracy and flood zone delineation. Photogrammetric Engineering and Remote Sensing 73(7), 793-804.

Rabus, B., Eineder, M., Roth, A., Bamler, R. (2003). The shuttle radar topography mission — a new class of digital elevation models acquired by spaceborne radar. ISPRS Journal of Photogrammetry and Remote Sensing 57, 241–262.

Ramankutty, N.; Foley, J.A. (1999). Estimating historical changes in global land cover: croplands from 1700 to 1992. Global Biogeochemical Cycles, 13, 997-1027.

Ramirez, J.R. (2006). A new approach to relief representation. Surveying and Land Information Science 66(1), 19-25.

Reutebuch, S.E.; Andersen, H.E.; McGaughey, R. J. (2005). Light detection and ranging (LIDAR): an emerging tool for multiple resource inventory. Journal of Forestry 103(6), 286-292.

Robinson, M.; Boardman, J.; Evans, R.; Heppell, K.; Packman, J.; Leeks, G. (2000). Land use change. In The Hydrology of the UK – A study of Change, Acreman, M. (ed.). Routledge: London.

Scott, P.A.; Stone, D.A.; Allen, M.R. (2004). Human contribution to the European heatwave of 2003. Nature, 432, 610-614.

Secchi, B. (2005) La città del ventesimo secolo, Laterza, Roma.

Servizio Osservatorio Suolo e Rifiuti. (2005). Documento interno predisposto per la pubblicazione “Il Veneto e il suo ambiente nel XXI secolo”.

Shary, P.A.; Sharaya, L.S.; Mitusov, A.V. (2002). Fundamental quantitative methods of land surface analysis, Geoderma, 107, 1-32.

Shary, P.A.; Sharaya, L.S.; Mitusov, A.V. (2005). The problem of scale-specific and scale-free approaches in geomorphometry. Geografia Fisica e Dinamica Quatrenaria, 28 (1), 81-101.

Sheng, Y.; Gong, P. and Biging, G. S. (2003). Orthoimage production for forested areas from large-scale aerial photographs. Photogrammetric Engineering and Remote Sensing 69(3), 259-266.

Shepard, D. (1968). "A two-dimensional interpolation function for irregularly-spaced data". *Proceedings of the 1968 ACM National Conference*. pp. 517–524. doi:10.1145/800186.810616.

Sibson, R. (1981). A brief description of natural neighbor interpolation (Chapter 2). in V. Barnett: Interpreting Multivariate Data. Chichester: John Wiley, pp. 21-36.

Sithole, G.; Vosselman, G. (2003). Report: ISPRS Comparison of Filters. The Netherlands: department of geodesy, Faculty of Civil Engineering and Geosciences, Delft University of Technology.

Sivakumar, B. (2008). Dominant Processes Concept, Model Simplification and Classification Framework in Catchment Hydrology. Stochastic Environmental Research and Risk Assessment, 22(6), 737-748.

Sivapalan, M. (2005). Pattern, process and function: elements of a unified theory of hydrology at the catchment scale. In: Anderson, M.G. (Ed.), Encyclopaedia of Hydrological Sciences, chp. 13. pp. 193–219.

Sofia, G.; Tarolli, P.; Cazorzi, F.; Dalla Fontana, G. (2011). An objective approach for feature extraction: distribution analysis and statistical descriptors for scale choice and channel network identification. Hydrol. Earth Syst. Sci.; 15, 1387–1402. ISSN: 1027-5606, doi:10.5194/hess-15-
1387-2011.

Sofia, G. (2012). Digital terrain analysis for hydrogeomorphic feature recognition. PhD Thesis.

Souchère, V.; King, D.; Daroussin, J.; Papy, F.; Capillon, A. (1998). Effects of tillage on runoff directions: consequences on runoff contributing area within agricultural catchments. Journal of Hydrology, 206: 256-267.

Smil, V. (1991). General energetic: energy in the biosphere and civilization, 1st edn. New York, NY: John Wiley & Sons.

Speirs, R.B.; Frost, C.A. (1985). The increasing incidence of accelerated soil water erosion on arable land in the east of Scotland. Res. Develop. Agric.,2, 161-168.

Tarboton D.G.; Ames, D. P. (2001). Advances in the mapping of flow networks from digital elevation data. In: Proceedings of World Water and Environmental Resources Congress, Orlando, Florida.

Tarboton D.G.(1997). A new method for the determination of flow directions and contributing areas in grid digital elevation models. Water Resources Research, 33, pp. 309–319.

Tarboton D.G. (2003). Terrain Analysis Using Digital Elevation Models in Hydrology, ESRI Users Conference, San Deigo, 7-11 July, 2003.

Tarboton D.G.; Bras R.L.; Rodriguez-Iturbe I. (1991). On the extraction of channel network from digital elevation data. Hydrological processes 5, 81-100.

Tarolli, P., 2008c. High resolution topography: new opportunities, issues, future trends. Invited Seminar presented at St. Anthony Falls Laboratory, University of Minnesota, Minneapolis, July 30, 2008.

Tarolli, P.; Borga, M.; Dalla Fontana, G. (2008). Analyzing the influence of upslope bedrock outcrops on shallow landsliding. Geomorphology 93: 186-200.

Tarolli, P.; Dalla Fontana, G. (2008). High resolution LiDAR-derived DTMs: some applications for the analysis of the headwater basins' morphology. International Archives of Photogrammetry, Remote Sensing and Spatial Information Sciences 36 (5/C55): 297-306.

Tarolli, P.; Dalla Fontana, G. (2009). Hillslope to valley transition morphology: new opportunities from high resolution DTMs. Geomorphology 113: 47-56. doi:10.1016/j.geomorph.2009.02.006.

Tarolli, P.; Dalla Fontana, G.; Moretti, G.; Orlandini, S. (2009). Cell Size Dependence of Threshold Conditions for the Delineation of Drainage Networks from Gridded Elevation Data. Geomorphometry 2009, University of Zurich.

Tarolli, P.; Arrowsmith, J.R.; Vivoni, E.R. (2009). Understanding earth surface processes from remotely sensed digital terrain models. Geomorphology 113: 1-3. doi:10.1016/j.geomorph .2009.07.005.

Tarolli, P.; Sofia, G.; Dalla Fontana, G. (2010). Geomorphic features extraction from high resolution topography: landslide crowns and bank erosion, Natural Hazards, ISSN: 0921-030X, doi:10.1007/s11069-010-9695-2.

Thommeret, N.; Bailly, J.S.; Puech, C. (2010). Robust extraction of thalwegs network from DTM: application on badlands. Hydrol. Earth Syst. Sci.; 14, 1527-1536, doi:10.5194/hess-14-1527- 2010.

Udvardy, M.D.F. (1975). A Classification of the Biogeographical Provinces of the World. International Union for Conservation of Nature and Natural Resources, Morges, Switzerland.

U.S. Soil Conservation Service, 1972. CN-SCS Method.

VENETO 2010 – La Grande alluvione. Commissario delegato per il superamento dell'emergenza derivante dagli eventi alluvionali che hanno colpito il territorio della regione Veneto nei giorni dal 31 ottobre al 2 novembre 2010. Ordinanza del Presidente del Consiglio dei Ministri n. 3906 del 13/11/2010.

Verstraeten, G.; Poesen, J. (1999). The nature of small-scale flooding, muddy floods and retention pond sedimentation in central Belgium. Geomorphology, 29, 275-292.

Vitousek, P.M.; Mooney, H.A.; Lubchenco, J.; Melillo, J.M. (1997). Human domination of Earth's ecosystems. Science 277: 494-99.

Vogel, H. J.; Roth, K. (2003). Moving through scales of flow and transport in soil. J. Hydrol.; 272, 95/106.

Voltz, M.; Andrieux, P.; Bouzigues, R.; Lennartz, B.; Louchart, X.; Moussa, R.; Ribolzi, O. (1998). Transport of water and matter in a farmed sedimentary soil system in the Mediterranean environment. In Proceedings of the 16th International Congress of Sol Science, Montpellier; 8 pp.

Watershed Plans of Eastern-Alps 2010. Brenta and Bacchiglione river basins.

Watkins, D. (2005). LiDAR Types and Uses: with a Case Study in Forestry. State College, PA, USA: Department of Geography, Pennsylvania State University.

Webster, T.L.; Dias, G. (2006). An automated GIS procedure for comparing GPS and proximal LiDAR elevations. Computers & Geosciences 32(6), 713-726.

Wehr, A.; Lohr, U. (1999). Airborne laser scanning - an introduction and overview. ISPRS Journal of Photogrammetry and Remote Sensing 54(4), 68-82.

Weitkamp, C. (2005). LiDAR: Introduction. In Fujii, T. and Fukuchi, T.; editors, Laser Remote Sensing, Boca Raton, London, New York and Singapore: Taylor & Francis, 1-36.

Wemple B.C.; Jones, J.A.; Grant, G.E. (1996). Channel network extension by logging roads in two basins, wester cascades, oregon, Water resources bulletin, 32(6), 1195-1207.

Widgren, M. (2010). Landscape research in a world of domesticated landscapes: The role of values, theory, and concepts. Elsevier, Quaternary International, LAC 2010. 1st International conference on Landscape Archaeology, Amsterdam.

Wilson, M.F.J.; O'Connel, B.; Brown, C.; Guinan, J.C.; Grehan, A.J. (2007). Multiscale terrain analysis of multibeam bathymetry data for habitat mapping on the continental slope. Marine Geodesy, 30, 3–35.

Wise, S. (1998). The effect of GIS interpolation errors on the use of digital elevation models in geomorphology. In: S.N. Lane, K.S. Richards and J.H. Chandler, Editors, Landform Monitoring, Modelling and Analysis, Wiley, New York, NY, 139–164.

Wood J.D. (1996). The Geomorphological Characterisation of Digital Elevation Models. Ph.D. Thesis, University of Leicester.

Wood J.D. (2009). Chapter 14 Geomorphometry in LandSerf, In: Tomislav Hengl and Hannes I. Reuter, Editor(s), Developments in Soil Science, Elsevier, 33, Geomorphometry - Concepts, Software, Applications, ISSN 0166-2481, ISBN 9780123743459, Doi: 10.1016/S0166-2481(08)00014-7, 333-349.

Yokoyama, R.; Sirasawa, M.; Pike, R. (2002). Visualizing topography by openness: A new application of image processing to digital elevation models. Photogrammetric Engineering & Remote Sensing, 68 (3), 257-265.

Young, R.A.; Voorhees, W.B. (1982). Soil erosion and runoff from planting to canopy development as influenced by tractor wheel-traffic. Trans. ASAE, 25, 708-712.

Zalasiewcz, J.; Williams, M.; Haywood, A.; Ellis, M. (2011). The Anthropocene: a new epoch of geological time? Phil. Trans. R. Soc. A, 369, 835-841, doi: 10.1098/rsta.2010.0339.

Zalasiewicz, J. et al. (2008). Are we now living in the Anthropocene? GSA Today 18, 4-8, doi: 10.1130/GSAT01802A.1.

Zevenbergen, L.W.; Thorne, C. (1987). Quantitative analysis of land surface topography. Earth Surface Processes and Landforms, 12, 47-56.

Ziadat, F.M. (2007). Effect of Contour Intervals and Grid Cell Size on the Accuracy of DEMs and Slop Derivatives. Transactions in GIS 11(1), 67-81.

Zimmerman, D.; Pavlik, C.; Ruggles, A.; Armstrong, M.P. (1999). An experimental comparison of ordinary and universal Kriging and inverse distance weighting. Mathematical Geology 31(4), 375- 389.

9 ACKNOWLEDGMENTS

I would like to thank Professor Paolo Tarolli because he gave me the possibility to carry out this work of thesis, always supporting and encouraging me.

A sincere thanks to my assistant supervisor Giulia Sofia who has always been very kind, patient and available for clarifying every doubt I might have ever had.

A really big and authentic thanks to my family because it has always supported me in any kind of choice I have ever made.

The last, but absolutely not the least thank, is turned to all my friends, either to those ones I have known since a long time ago and either to the "new ones". At this regard, I must spend a couple of words for the amazing "family" I had the fortune to meet at the Residenza Messori. We lived together for almost 2 years and, without any doubts, it has been one of the best experience of my life. Thanks Residenza!!